ANL-HEP-CP-13-48
FERMILAB-FN-0967-CMS-T

arXiv:1310.5189v1 [hep-ph] 19 Oct 2013

Working group report: QCD

Conveners: J. M. Campbell, K. Hatakeyama, J. Huston, F. Petriello

J. Andersen, L. Barzè, H. Beauchemin, T. Becher, M. Begel, A. Blondel, G. Bodwin, R. Boughezal, S. Carrazza, M. Chiesa, G. Dissertori, S. Dittmaier, G. Ferrera, S. Forte, N. Glover, T. Hapola, A. Huss, X.Garcia i Tormo, M. Grazzini, S. Höche, P. Janot, T. Kasprzik, M. Klein, U. Klein, D. Kosower, Y. Li, X. Liu, P. Mackenzie, D. Maitre, E. Meoni, K. Mishra, G. Montagna, M. Moretti, P. Nadolsky, O. Nicrosini, F. Piccinini, L. Reina, V. Radescu, J. Rojo, J. Russ, S. Sapeta, A. Schwartzman, P. Skands, J. Smillie, I. W. Stewart, F. J. Tackmann, F. Tramontano, R. Van de Water, J. R. Walsh, S. Zuberi

February 26, 2022

1.1 Executive summary

A quantitative description of Nature requires a detailed understanding of quantum chromodynamics (QCD) phenomenology. The success of Run 1 of the LHC relied upon advanced QCD simulation tools to support and guide experimental analyses, and the discovery of the Higgs boson illustrated the indispensable role of the QCD community in enabling discovery science. From parton distribution functions with robust errors, through calculations to the next-to-next-to-leading order and beyond in perturbative QCD, to the development of sophisticated Monte Carlo tools more faithful to the underlying hard dynamics, every advance from over a decade of research was needed to make this historic discovery possible. Run 2 of the LHC marks the beginning of the precision phase in our study of the mechanism of electroweak symmetry breaking. Quantitative QCD analyses will become ever more indispensable in unraveling the origin of what we have found.

In the nearly one decade since the previous Snowmass workshop, what was once considered impossible in the field of QCD has become commonplace. The technology in the area of next-to-leading order QCD computations has undergone an advancement so rapid as to invite comparison to the Industrial Revolution. We stand poised to enter a similar era for next-to-next-to-leading order calculations. Parton distribution function errors have become quantitative rather than qualitative, and parton showers matched with exact next-to-leading order matrix elements have become the default simulation tools for experimental studies. Any of these breakthroughs would have been considered unlikely at best if predicted at the time of the previous Snowmass workshop. It is therefore our difficult task to summarize the level of the tools that exist now, to extrapolate their advancement into the medium and long-term future, and to present a priority list as to the direction that the development of these tools should take.

Most of the efforts of the QCD working group concentrate on proton-proton colliders, at 14 TeV as planned for the next run of the LHC, and for 33 and 100 TeV, possible energies of the colliders that will be necessary to carry on the physics program started at 14 TeV. We also examine QCD predictions and measurements at lepton-lepton and lepton-hadron colliders, and in particular their ability to improve our knowledge of $\alpha_s(M_Z^2)$ (at both types of colliders) and our knowledge of parton distribution functions (PDFs) (at lepton-hadron colliders). Since the current world average of strong coupling measurements is dominated by the

determinations made using lattice gauge theory we also explore possible improvements to our knowledge of $\alpha_s(M_Z^2)$ from such extractions.

We summarize the main conclusions of this report below. A more detailed listing of the results of the QCD working group studies can be found in the conclusions.

- Improvement in our current understanding of PDFs is needed in both the 'precision region' relevant for Higgs boson studies and in the 'discovery region' of multi-TeV masses. The latter will be addressed by future LHC studies while the former is more difficult due to already-strong current constraints. A future electron-hadron collider, such as the LHeC, would be the ultimate machine to provide PDFs for precision proton-proton physics.
- Higher precision calculations are needed to fully realize the potential of the LHC and future hadron colliders. Further progress is required on fixed-order calculations to next-to-next-to leading order and beyond in the QCD coupling constant, and on the resummation of large logarithms that appear in observables where the available phase space is restricted. The inclusion of electroweak corrections into theoretical simulation programs is mandatory for physics studies in future high energy proton-proton collisions. Unravelling the identity of the Higgs boson requires further advances in our QCD calculational abilities.
- Theoretical predictions at the 1% level in QCD will require an understanding of numerous subtle conceptual issues, including the validity of the standard factorization approach and the universality of PDFs, power-suppressed contributions to cross sections, and perturbation theory in extreme kinematic configurations.
- The most recent lattice and continuum determinations of α_s, m_b and m_c could be used to immediately reduce the parametric uncertainties in predictions for Higgs boson decay rates. Future precision determinations from both the lattice and experiment could reduce the error on α_s to 0.1%.

1.2 Introduction

It is useful to recall the basic structure of a parton-level hadron collider cross section computed in perturbative QCD. The cross section can be written schematically as,

$$\sigma = \sum_{a,b} \int_0^1 \mathrm{d}x_1\, f_{a/A}(x_1,\mu_F^2) \int_0^1 \mathrm{d}x_2\, f_{b/B}(x_2,\mu_F^2) \Bigg\{ \int \mathrm{d}\hat{\sigma}_{ab}^{LO}\left(\alpha_s\right)\, \Theta_{\mathrm{obs}}^{(m)} + \alpha_s(\mu_R^2) \left[\int \left(\mathrm{d}\hat{\sigma}_{ab}^{V}\left(\alpha_s,\mu_R^2\right) + \mathrm{d}\hat{\sigma}_{ab}^{C}\left(\alpha_s,\mu_F^2\right)\right)\, \Theta_{\mathrm{obs}}^{(m)} + \int \mathrm{d}\hat{\sigma}_{ab}^{R}(\alpha_s)\, \Theta_{\mathrm{obs}}^{(m+1)} \right] \Bigg\} + \ldots \tag{1.1}$$

where we have sketched the terms that contribute up to the next-to-leading order (NLO) level in QCD. The first ingredients in the perturbative description are the PDFs, defined for a given species of parton a, b inside incoming hadrons A, B. The PDFs are functions of the parton momentum fractions x_1, x_2 and the factorization scale μ_F. The leading order prediction depends on the hard matrix elements, contained in the factor $\mathrm{d}\hat{\sigma}_{ab}^{LO}$, which in turn depend on the value of the strong coupling, α_s, for strongly-interacting final states. In this equation the quantity α_s is a shorthand notation since it must be evaluated at the renormalization scale μ_R, $\alpha_s \equiv \alpha_s(\mu_R^2)$. The hard matrix elements may also depend upon additional parameters in the Standard Model Lagrangian, such as the quark masses. The predicted cross section depends on the cuts that are applied to the m-parton configuration in order to define a suitable observable, $\Theta_{\mathrm{obs}}^{(m)}$. In the case of

cross sections for multi-jet processes this factor accounts for the jet definition that is required for infrared safety. Finally, there may be additional non-perturbative inputs required, such as fragmentation functions or the matrix elements needed for processes such as quarkonium production. At NLO there are further contributions, as indicated on the second line of the equation. The virtual diagrams contain an explicit dependence on the renormalization scale, $\mathrm{d}\hat{\sigma}^V_{ab}\left(\alpha_s, \mu_R^2\right)$ while the collinear counterterms that are necessary in order to provide an order-by-order definition of the PDFs introduce explicit factorization scale dependence, $\mathrm{d}\hat{\sigma}^C_{ab}\left(\alpha_s, \mu_F^2\right)$. The effects of real radiation, $\mathrm{d}\hat{\sigma}^R_{ab}(\alpha_s)$ now include a cut on the $(m+1)$-parton configuration. They may therefore be sensitive to kinematic effects that are not present in the m-parton case, for instance the effect of jet vetoes in electroweak processes. At next-to-next-to-leading order (NNLO) we would include terms in Eq. (1.1) that have an explicit factor of α_s^2 in addition to those present at leading order. In outline the extension is clear, with the introduction of configurations that contain m, $m+1$ and $m+2$ parton. As a result NNLO calculations may be even more sensitive to kinematic effects that are only approximately modeled, if at all, in lower orders. However, the interplay between soft and collinear divergences in each of these contributions greatly complicates the calculation of NNLO effects.

From this guiding equation it is clear that detailed QCD predictions require knowledge of:

- $\alpha_s(M_Z^2)$ and its uncertainty;
- PDFs and their uncertainties;
- higher order corrections to cross sections;
- the impacts of restrictions on phase space, such as jet vetoes;
- quark masses and other Standard Model parameters;
- possible additional non-perturbative inputs, such as fragmentation functions or quarkonium matrix elements.

Measurements at 14 TeV and higher will access a wide kinematic range, where PDF uncertainties and the impact of higher order corrections may be large. At scales large compared to the W mass, electroweak (EWK) corrections can be as important as those from higher order QCD; mixed QCD-EWK corrections also gain in importance. Higher energies also imply higher luminosities, which require the ability to isolate the physics of interest from the background of multiple interactions accompanying the higher luminosities. Much of the physics of interest will still involve the production of leptons, jets, etc at relatively low scales. Obtaining theoretical predictions in the presence of strict kinematic cuts, especially those involving high transverse momenta, masses, etc., can result in the creation of large logarithms of ratios of scales involved in the processes. All of these effects mean that, as the center-of-mass energy increases, both the perturbative and non-perturbative environments may make precision measurements of such objects more difficult.

In this contribution, we cannot hope for a comprehensive treatment of all of the above, but will try to summarize the most important aspects of QCD for future colliders.

1.3 The strong coupling from colliders

The strong coupling constant α_s is one of the fundamental parameters of QCD. The coupling constant itself is not a physical observable, but a quantity defined in the context of perturbation theory, which enters predictions for experimentally-measurable observables. The uncertainty on α_s is currently considered to

be one of the major contributors to the parametric uncertainties on the prediction for the $H \to b\bar{b}$ partial width. Reducing this uncertainty would enable a more precise measurement of both this partial width and the total width of the Higgs boson at future lepton colliders, where the experimental uncertainty no longer dominates [1]. The size of α_s is not given by theory, but can be extracted from experimental measurements at e^+e^-, ep, pp, and $p\bar{p}$ colliders, as well as from lattice QCD calculations.

A recent review on the determination of α_s may be found in the 2012 PDG review [2]. The current world average presented in the 2012 PDG review is:

$$\alpha_s(M_Z^2) = 0.1184 \pm 0.0007$$

which has 0.6% relative uncertainty and is summarized in Fig. 1-1. The quoted uncertainty is a factor of 4 better than the value in the PDG review in 1992 [3], showing a significant progress on the determination of α_s over the last two decades. As demonstrated in [2], the central value of the world average of $\alpha_s(M_Z^2)$ is rather stable against different inputs to this average. The result from lattice calculations, which has the smallest assigned uncertainty, agrees well with the exclusive average of the other results; however, it largely determines the size of the overall uncertainty.

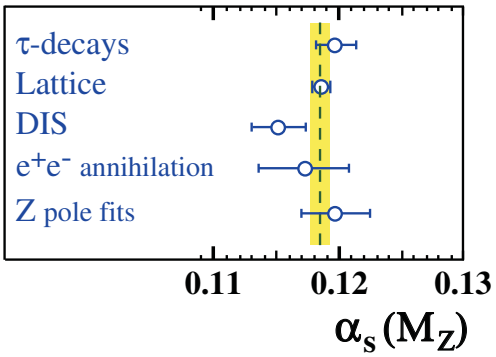


Figure 1-1. *Summary of values of $\alpha_s(M_Z^2)$ obtained for various sub-classes of measurements. The world average value of $\alpha_s(M_Z^2) = 0.1184 \pm 0.0007$ is indicated by the dashed line and the shaded band. Figure taken from [2].*

Below we discuss various approaches to determine α_s and future possibilities to further improve the determination of α_s with measurements at the LHC and future accelerator facilities and with lattice QCD calculations. Given the current $\alpha_s(M_Z^2)$ uncertainty, the main theme is to see if and/or how we can potentially reduce its uncertainty to the level of 0.1% relative or 0.0001 absolute [4].

1.3.1 Strong coupling from e^+e^- colliders

Various studies on α_s have been performed using e^+e^- annihilation data. They include the determination of α_s from hadronic τ decays, heavy quarkonia decays, event shapes, jet rates, and the hadronic Z decay rate. Future prospects with some of these approaches are discussed below.

1.3.1.1 Hadronic final states of e^+e^- annihilations

Jet rates and hadronic event shapes have a strong sensitivity to α_s, and they have been studied extensively in the past. For these observables, the theoretical predictions are calculated up to NNLO and the resummation is achieved up to NNLL or N^{3}LL.

The typical experimental uncertainty for these measurements is about 1%, and it is considered that improvements should be possible. The hadronization uncertainty estimated based on the difference between various hadronization models is typically around 1–2%. And, the theoretical uncertainties for the scale choice and variation, matching with resummed calculations, and quark mass effects are typically 1–3%. For a review of these determinations see for instance Ref. [5]. By the time the next generation of e^+e^- colliders come online, it is conceivable that both these theoretical and hadronization uncertainties have been reduced; however, going well below 1% appears to be quite challenging, if not impossible.

1.3.1.2 Hadronic W/Z decay widths from e^+e^- annihilations

An accurate determination of α_s may be obtained from the precise experimental measurement of hadronic Z decays. An advantage of using such inclusive observables is that the theoretical predictions are known to N^{3}LO and non-perturbative effects are strongly suppressed. The ratio R_Z of the partial width of the Z into hadrons to that to one massless charged lepton flavour may be written as:

$$R_Z \equiv R_l^0 \equiv \frac{\Gamma(Z \to \text{hadrons})}{\Gamma(Z \to \text{leptons})} = R_Z^{\text{EW}} N_C (1 + \delta_{\text{QCD}} + \delta_{\text{m}} + \delta_{\text{np}}), \tag{1.2}$$

$$\delta_{\text{QCD}} = \sum_{n=1}^{4} c_n \left(\frac{\alpha_s}{\pi}\right)^n + \mathcal{O}(\alpha_s^5), \quad c_1 = 1,\ c_2 = 0.76264,\ c_3 = -15.490, c_4 = -68.241,$$

$$\delta_{\text{m}} \sim \mathcal{O}\left(\frac{m_q^2}{M_Z^2}\right), \qquad \delta_{\text{np}} \sim \mathcal{O}\left(\frac{\Lambda^4}{M_Z^4}\right),$$

where the δ_{QCD}, δ_{m}, and δ_{np} terms are for the QCD, mass, and non-perturbative corrections, respectively.

The latest result from the LEP electroweak working group on R_l^0 is $R_l^0 = 20.767 \pm 0.025$ [6], whose relative uncertainty is 0.12%. Up to a few years ago, when only NNLO predictions were available, and the Higgs mass was still unknown, this measurement was translated to a value of $\alpha_s(M_Z^2)$ as (see eg. [7] and references therein):

$$\begin{aligned}\alpha_s(M_Z^2) \;=\; & 0.1226 \pm 0.0038(\text{exp}) \,{}^{+\,0.0028}_{-\,0.0005}(\mu = {}^{2}_{0.25} M_Z) \,{}^{+\,0.0033}_{-\,0.0}(M_H = {}^{900}_{100}\ \text{GeV}) \\ & \pm 0.0002(M_{\text{top}} = \pm 5\ \text{GeV}) \pm 0.0002(\text{renormal. schemes}) \\ =\; & 0.1226 \,{}^{+\,0.0058}_{-\,0.0038}.\end{aligned}$$

Since the uncertainty due to the Higgs mass dependence is no longer relevant, the top quark mass dependence is negligible, and the pQCD scale uncertainty from latest N^{3}LO calculations [8,9] is only 0.0002 on $\alpha_s(M_Z^2)$, the question comes down to if a future Z factory can measure R_l^0 with an absolute precision of ~ 0.001. Such a reduction in the experimental uncertainty, which dominates this $\alpha_s(M_Z^2)$ determination, will be necessary, since the relative uncertainty on $\alpha_s(M_Z^2)$ is about 25 times larger than the relative uncertainty on R_l^0, because $c_1 \alpha_s(M_Z^2)/\pi \sim 0.04 = \mathcal{O}(1/25)$ in Eq. (1.2).

The LEP measurement of $R_l^0 = 20.767 \pm 0.025$ [6] is mainly limited by lepton statistics. With $\sim 10^{12}$ Z event statistics expected from TLEP [10] and assuming the selection efficiency uncertainties scale with

statistics, one might expect a reduction of the uncertainty by a factor of ~ 200. At this level of precision, we will have to consider many subtle systematic uncertainties and a detailed analysis would be necessary. The R_l^0 measurement is sensitive to the electroweak vertex correction δ_b on the $Zb\bar{b}$ vertex which may be sensitive to possible new physics effects; however, it can be constrained by the direct extraction of $R_b = \Gamma(Z \to b\bar{b})/\Gamma(Z \to \text{hadrons})$, so this is not expected to be a limitation. As discussed above, in order to achieve the absolute 0.0001 uncertainty on $\alpha_s(M_Z^2)$, about a factor of 30 reduction in the uncertainty is necessary. This is challenging and will require a lot of work, but the TLEP target goal of the measurement of R_l^0 with a relative precision of $< 10^{-5}$ meets this requirement. This would be an interesting possibility to explore [10]. With the GigaZ running of the ILC, the Z event statistical error improves by a factor of about 7 compared to LEP. This may lead to an $\alpha_s(M_Z^2)$ determination with an absolute uncertainty of $\sim 0.0004 - 0.0006$ [11], which is an interesting possibility of ILC.

Another interesting possibility suggested is to use the W hadronic width, i.e. $B_h \equiv (\Gamma_{\text{had}}/\Gamma_{\text{tot}})_W$, which we can extract by measuring the branching fractions of WW events to the $l\nu\, l\nu$, $l\nu\, qq$, and $qq\, qq$ final states. The previous LEP measurement of $B_h = 67.41 \pm 0.27$ [12] was limited by WW event statistics of about 4×10^4 events. With 0.5×10^8 W pairs expected at TLEP and assuming that selection efficiency uncertainties scale with statistics, it may be possible to reduce the uncertainty on B_h by a factor ~ 70 and thus the absolute uncertainty on $\alpha_s(M_Z^2)$ to ~ 0.0002. This is an interesting possibility of the proposed TLEP facility.

1.3.1.3 Hadronic τ decay width from e^+e^- annihilations

The τ lepton is the only lepton that can decay hadronically. It provides an excellent testbed to study QCD at low energies and determine α_s. This channel may be considered even more inclusive than R_Z at the Z pole, as we are integrating over the hadronic invariant mass spectrum. One interesting advantage of the α_s determination from hadronic τ decays is the fact that the uncertainty δ on a measurement of $\alpha_s(Q^2)$ translates to an uncertainty $\delta' = (\alpha_s^2(M_Z^2)/\alpha_s^2(Q^2)) \cdot \delta$ on $\alpha_s(M_Z^2)$. Therefore, the relative uncertainty on $\alpha_s(M_Z^2)$ is about a factor 3 smaller than the relative uncertainty on $\alpha_s(M_\tau^2)$, when the $\alpha_s(M_\tau^2)$ measurement at the τ mass scale is transported to the Z scale using the QCD beta-function.

The ratio R_τ of the τ decay width into hadrons to that into an electron channel may be expressed by:

$$R_\tau \equiv \frac{\Gamma(\tau^- \to \nu_\tau + \text{hadrons})}{\Gamma(\tau^- \to \nu_\tau e^- \bar{\nu}_e)} = S_{\text{EW}} N_C (1 + \delta_{\text{QCD}} + \delta_{\text{np}}), \tag{1.3}$$

$$\delta_{\text{QCD}} = \sum_{n=1}^{4} c_n \left(\frac{\alpha_s}{\pi}\right)^n + \mathcal{O}(\alpha_s^5), \quad c_1 = 1,\ c_2 = 5.202,\ c_3 = 26.37.490, c_4 = 127.1,$$

$$\delta_{\text{np}} = \frac{\text{ZERO}}{m_\tau^2} + c_4 \cdot \frac{\langle O_4 \rangle}{m_\tau^4} + c_6 \cdot \frac{\langle O_6 \rangle}{m_\tau^6} + \cdots,$$

where the δ_{QCD} and δ_{np} terms are for the perturbative and non-perturbative QCD corrections, respectively, and the notation of ref. [13] for δ_{np} is adopted. The approach used at LEP was to fit simultaneously α_s and the non-perturbative coefficients by measuring various moments of the τ spectral function. Interestingly, the non-perturbative contributions turn out to be rather small, e.g. $\delta_{\text{np}} = -0.0059 \pm 0.0014$ [14]. It would be interesting to measure such moments again, with much improved precision, e.g. with an uncertainty on δ_{np} of < 0.0005. The challenge for a more precise $\alpha_s(M_Z^2)$ determination appears to be the fact that various methods of estimating the impacts of higher-order QCD terms lead to differences in $\alpha_s(M_\tau^2)$ of $\gtrsim 5\%$, which translates to $\gtrsim 1\%$ for $\alpha_s(M_Z^2)$ (see e.g. Refs. [13, 15]). Furthermore, also the importance of the "ZERO" term in the expansion for δ_{np} is subject of discussion [13]. Thus, it seems unlikely that the relative uncertainty on $\alpha_s(M_Z^2)$ using τ decays will be reduced well below the 1% level in the near future.

1.3.2 Strong coupling from hadron colliders

The strong coupling constant has been extracted from measurements at hadron colliders as well. The results on the strong coupling constant from hadron collider jet data are based on the p_T-dependence of the inclusive jet cross section measurements by the CDF [16], D0 [17], and ATLAS [18] Collaborations, the jet angular correlations by the D0 Collaboration [19], and the ratio of the inclusive 3-jet and 2-jet cross sections by the CMS Collaboration [20]. One of the complexities of the hadron-hadron environment is that it is hard to disentangle the extraction of the value of the strong coupling constant from the uncertainties in the gluon distribution, which can be significant in the relevant x-range. The most precise measurement to date, $\alpha_s(M_Z^2) = 0.1161^{+0.0041}_{-0.0048}$, is from the inclusive jet cross section measurement from D0. The uncertainty is dominated by the experimental uncertainties from the jet energy calibration, the p_T resolution, and the integrated luminosity, and as well as the uncertainties on non-perturbative corrections and the renormalization and factorization scales.

The recent result on $\alpha_s(M_Z^2)$ from CMS using the $t\bar{t}$ cross section [21] yielded $\alpha_s(M_Z^2) = 0.1178^{+0.0033}_{-0.0032}$ based on a full NNLO QCD calculation for the inclusive $t\bar{t}$ cross section. This is the first determination of the strong coupling constant from top-quark production and shows the best precision among hadron collider measurements.

There have been significant developments in measurements at hadron colliders in recent years, and we expect that future LHC measurements will improve the precision on α_s further. The α_s extraction from the jet data is also likely to benefit from recent progress towards a full NNLO QCD prediction for inclusive jet and dijet production [22] by the time of the next LHC running. However, given the currently-quoted scale uncertainty and the experimental systematic uncertainty, it will be challenging to achieve $< 1\%$ relative uncertainty on $\alpha_s(M_Z^2)$. The improved precision from hadron collider data at relatively high-Q^2 is still important for the robustness of α_s determinations, and testing the running of α_s and asymptotic freedom, as the current world average of $\alpha_s(M_Z^2)$ is driven by low-Q^2 measurements.

1.3.3 Strong coupling constant from *ep* colliders

Studies of deep-inelastic scattering by HERA experiments have led to a number of precise determinations of α_s. PDG quotes the average value of $\alpha_s = 0.1151 \pm 0.0022$ from deep-inelastic scattering (DIS) measurements [2].

One proposed future *ep* collider is the Large Hadron Electron Collider (LHeC) [23], which can provide improvements not only on PDFs but also on the determination of α_s. Using the intense, high energy hadron beams of the LHC, the LHeC would add a new electron beam of typically 60 GeV energy to construct a first TeV energy scale electron-proton and electron-ion collider.[1] As the first application of energy recovery techniques for high energy particle physics, the LHeC is designed to achieve a luminosity in excess [24, 25] of $10^{33}\,\mathrm{cm}^{-2}\mathrm{s}^{-1}$. Very high integrated *ep* luminosities of several hundreds of fb^{-1}, i.e. around 1000 times more than at HERA, can be collected by operating the new electron machine synchronously with the LHC. Such a huge luminosity enables measurements close to $x = 1$ and the exploitation of the full Q^2 range, up to $Q^2 \simeq 10^6\,\mathrm{GeV}^2$, exceeding the kinematic range of HERA by a factor of 20.

[1] As HERA never accelerated ions, nor deuterons, the kinematic range in lepton-nucleus (eA) DIS is extended with the LHeC by nearly four orders of magnitude in four-momentum squared Q^2 and towards low Bjorken x. This leads to a determination of the proton but also the neutron and nuclear PDFs in a hugely extended range and with unprecedented diversity, as is described in [23].

Two independent approaches have been undertaken in order to verify the potential of the LHeC to determine α_s. These analyses used a complete simulation of the experimental systematic errors of the neutral currents (NC) and charged currents (CC) pseudo-data with higher order QCD fit analysis techniques (see the LHeC conceptual design report (CDR) [23] for details). The total experimental uncertainty on α_s is estimated to be 0.2 % from the LHeC alone and 0.1 % when combined with HERA. The theoretical errors on this determination of α_s from LHeC will be of order 0.5 %, and will require a complete calculation of DIS to order N^{3}LO. Relying solely on inclusive DIS ep data at high Q^2, this determination is free of higher twist, hadronic and nuclear corrections, unlike any of the recent global QCD fit analyses. There are known further parametric uncertainties in DIS determinations of α_s. These will be much reduced with the LHeC as it resolves the full set of parton distributions, $u_v,\ d_v,\ \overline{u},\ \overline{d},\ s,\ \overline{s},\ c,\ b$ and xg for the first time, providing x and Q^2 dependent constraints that do not arise from the assumed functional forms of the PDFs.

1.3.4 Summary

We have reviewed the current status of α_s determinations using collider data and discussed future prospects with various approaches. These measurements are complementary and sensitive to α_s at different Q^2 values, thus providing a test of asymptotic freedom, the driving principle of QCD. Table 1-1 shows a summary of α_s determinations from both collider data and lattice QCD, together with target precisions for the next generations of experiments and calculations. The lattice QCD determination of α_s as well as quark masses are discussed in detail in section 1.4. The current world average of $\alpha_s(M_Z^2) = 0.1184 \pm 0.0007$ [2] is dominated by lattice QCD results. The lattice determination of $\alpha_s(M_Z^2)$ may improve to the level of an absolute uncertainty of 0.0004 in the next 5 years or so. The GigaZ running of ILC may also reduce the $\alpha_s(M_Z^2)$ uncertainty to a similar level [11], and the improvements from LHeC and TLEP could reduce the error on $\alpha_s(M_Z^2)$ to 0.1%.

We note that the α_s uncertainty used by the Higgs cross section working group [26] is three times larger than that of the world average from PDG which is dominated by the lattice determination. Given its important role in future Higgs coupling extractions, this uncertainty should be revisited in order to fully benefit from on-going and future improvements in α_s determinations. This is discussed in more detail in the following section.

1.4 Quark masses and strong coupling from lattice QCD

The single largest source of error in the theoretical calculation of the dominant Standard-Model Higgs decay mode $H \to b\overline{b}$ is the parametric uncertainty in the b-quark mass. Because this mode dominates the total Higgs width, this uncertainty is also significant for most of the other Higgs branching fractions. Parametric uncertainties in α_s and m_c also play important roles in many of the Higgs decay channels, and are the largest sources of uncertainty in the partial widths $H \to gg$ and $H \to c\overline{c}$, respectively. In this section, the determination of these quantities with lattice-QCD calculations is discussed.

The most precise way of obtaining m_c and m_b from experiment using continuum perturbation theory employs correlation functions of the quark's electromagnetic current [39]. Moments of these correlation functions have been calculated to third order in α_s. They can be determined experimental data in e^+e^- annihilation.

Such moments are also the most precise way known of determining the heavy-quark masses using lattice gauge theory, as well as a good way of obtaining α_s [35,40]. They can easily be calculated nonperturbatively in lattice simulations and then compared to the perturbative expressions to $\mathcal{O}(\alpha_s^3)$. Lattice calculations of correlators of quark bilinears offer several advantages over determination of these correlators from experiment.

Method	Current relative precision	Future relative precision
e^+e^- evt shapes	expt $\sim 1\%$ (LEP) thry $\sim$ 1–3% (NNLO+up to N^{3}LL, n.p. signif.) [27]	$< 1\%$ possible (ILC/TLEP) $\sim 1\%$ (control n.p. via Q^2-dep.)
e^+e^- jet rates	expt $\sim 2\%$ (LEP) thry $\sim 1\%$ (NNLO, n.p. moderate) [28]	$< 1\%$ possible (ILC/TLEP) $\sim 0.5\%$ (NLL missing)
precision EW	expt $\sim 3\%$ (R_Z, LEP) thry $\sim 0.5\%$ (N^{3}LO, n.p. small) [9, 29]	0.1% (TLEP [10]), 0.5% (ILC [11]) $\sim 0.3\%$ (N^{4}LO feasible, ~ 10 yrs)
τ decays	expt $\sim 0.5\%$ (LEP, B-factories) thry $\sim 2\%$ (N^{3}LO, n.p. small) [8]	$< 0.2\%$ possible (ILC/TLEP) $\sim 1\%$ (N^{4}LO feasible, ~ 10 yrs)
ep colliders	$\sim$ 1–2% (pdf fit dependent) [30, 31], (mostly theory, NNLO) [32, 33]	0.1% (LHeC + HERA [23]) $\sim 0.5\%$ (at least N^{3}LO required)
hadron colliders	$\sim 4\%$ (Tev. jets), $\sim 3\%$ (LHC $t\bar{t}$) (NLO jets, NNLO $t\bar{t}$, gluon uncert.) [17, 21, 34]	$< 1\%$ challenging (NNLO jets imminent [22])
lattice	$\sim 0.5\%$ (Wilson loops, correlators, ...) (limited by accuracy of pert. th.) [35–37]	$\sim 0.3\%$ (~ 5 yrs [38])

Table 1-1. *Summary of current uncertainties in extractions of $\alpha_s(M_Z^2)$ and targets for future ($5-25$ years) determinations. For the cases where theory uncertainties are considered separately, the theory uncertainties for future targets reflect a reduction by a factor of about two.*

For example, the numerical lattice data for correlators are much cleaner than the experimental data. Further, the lattice offers several choices of current operators and the most well-behaved one can be chosen for the determinations; in practice, this turns out to be the pseudoscalar current. The lattice calculations still need an input from experiment to set the overall energy scale, but this can be chosen in a way that also reduces final uncertainties. For example, if m_c is obtained from the pseudoscalar correlator, choosing m_{η_c} to set the energy scale reduces sensitivity to the tuning of the bare charm-quark mass. Using these methods, the HPQCD Collaboration obtains $m_c(m_c, n_f = 4) = 1.273(6)$ GeV in the $\overline{\rm MS}$ scheme [35]. By contrast, the Karlsruhe group obtains $m_c(m_c, n_f = 4) = 1.279(13)$ GeV from e^+e^- experimental data [39]. The most important reason for the greater precision of the lattice determination is that the data for the lattice correlation functions is much cleaner than the e^+e^- annihilation data. The uncertainty is dominated by continuum perturbation theory, and therefore may improve only modestly unless another order of perturbation theory is calculated. However, these charm correlation functions are very easy to calculate with lattice QCD. The lattice part of this determination will be checked by many lattice groups and should be very robust.

The b quark mass can also be obtained in this way, with the result $m_b(m_b, n_f = 5) = 4.164(23)$ GeV [35]. The sources of systematic uncertainty are completely different than for m_c. Perturbative uncertainties are tiny because $\alpha_s(m_b)^4 \ll \alpha_s(m_c)^4$. However, the method requires treating the b quark as a light quark, which is just barely working at lattice spacings used so far. Discretization errors dominate the current uncertainty, followed by statistical errors. The lattice result for m_b is not currently as precise as the result from e^+e^- experimental data, $m_b(m_b, n_f = 5) = 4.163(16)$ GeV [39]. Discretization and statistical errors should be straightforward to reduce by brute force computing power, and so are likely to come down by a factor of two in the next few years, perhaps to 0.011 GeV or better. Precisions of that order for m_b have already been claimed from e^+e^- data from reanalyses of the data and perturbation theory [39], and coming lattice calculations will be able to check these using the computing power expected in the next few years.

	Higgs X-section Working Group [26]	PDG [2]	Non-lattice	Lattice (2013)	Lattice (2018)	Targets of ILC/TLEP/LHeC
$\delta\alpha_s$	0.002	0.0007	0.0012 [2]	0.0006 [35]	0.0004	0.0001–0.0006 [10, 11, 23]
δm_c (GeV)	0.03	0.025	0.013 [39]	0.006 [35]	0.004	-
δm_b (GeV)	0.06	0.03	0.016 [39]	0.023 [35]	0.011	-

Table 1-2. *Projected future uncertainties in α_s, m_c, and m_b, compared with current uncertainties estimated from various sources.*

The strong coupling constant, α_s, is also an output of these lattice calculations. A very precise value of $\alpha_s(M_Z, n_f = 5) = 0.1183(7)$ has been obtained [35], with an uncertainty dominated by continuum perturbation theory. Unlike the heavy-quark masses, for which the correlation function methods give the most precise results at present, there are numerous good ways of obtaining α_s with both continuum and lattice methods. HPQCD has also obtained α_s from Wilson loops, obtaining $\alpha_s(M_Z^2) = 0.1184(6)$, comparable to their correlation function determination, but with completely independent methods and uncertainties. The Wilson loop determination makes heavy use of lattice perturbation theory, while the correlation function determination makes none. The precisions of both determinations are dominated by perturbation theory in one way or another. Several other quantities have been used to make good determinations α_s with lattice QCD, including the Adler function [36], the Schrödinger functional [41], and the ghost-gluon vertex [42]. All of the lattice determinations are consistent, and each is individually more precise than the most precise determination appearing in the 2012 world average [2] that does not use lattice QCD. The most precise current determination of α_s may improve only modestly over the next few years, since the error is dominated by perturbation theory. However, increasingly precise corroboration via an increasing number of quantities should continue.

Table 1-2 gives the current uncertainties in α_s, m_c, and m_b from both lattice and non-lattice methods, along with projections for the lattice errors in the next five years. For comparison, the uncertainties in these quantities estimated by the PDG and used by the LHC Higgs cross-section working group are also shown. The current uncertainties in α_s, m_c, and m_b from lattice QCD are all around a half a per cent. The lattice determinations of m_c and α_s are currently the most precise in the world. The charm correlation functions used to determine m_c are easy to calculate for many groups, and the uncertainty in m_c will be dominated by estimates of the uncalculated fourth and higher orders of perturbation theory, which may improve modestly. The same is true of α_s determined using charm correlation functions. For α_s, there should be more corroboration from an increasing number of physical quantities. The most precise lattice determination of m_b has uncertainties dominated by discretization and statistical errors, which should be reducible by perhaps a factor of two with the increasing amounts of computer power expected in the next few years.

1.5 Parton distribution functions

Parton distributions are an essential ingredient of present and future phenomenology at hadron colliders [43–45]. They are one of the dominant theoretical uncertainties for the characterization of the newly discovered Higgs-like boson at the LHC, they substantially affect the reach of searches for new physics at high final state masses and they limit the accuracy to which precision electroweak observables, like the W boson mass or the effective lepton mixing angle, can be extracted from LHC data [46].

1.5.1 Current knowledge and uncertainties

The determination of the parton distribution functions of the proton from a wide variety of experimental data has been the subject of intense activity in the last years. Various collaborations provide regular updates of their PDF sets. The latest releases from each group are ABM11 [31], CT10 [30], HERAPDF1.5 [47, 48], MSTW08 [49] and NNPDF2.3 [50]. A recent benchmark comparison of the most updated NNLO PDF sets was performed in Ref. [51], where similarities and differences between these five PDF sets above were discussed, and where W, Z and jet production data was used to quantify the level of agreement of the various PDF sets with the Tevatron and LHC measurements.

A snapshot of the comparisons between recent NNLO PDFs at the level of parton luminosities and cross section can be seen in Fig. 1-2, where we compare the gluon-gluon PDF luminosities between the five sets. We also show the predictions for the Higgs production cross section in the gluon-fusion channel and in WH associated production.[2] Results have been computed using the settings discussed in Ref. [51].

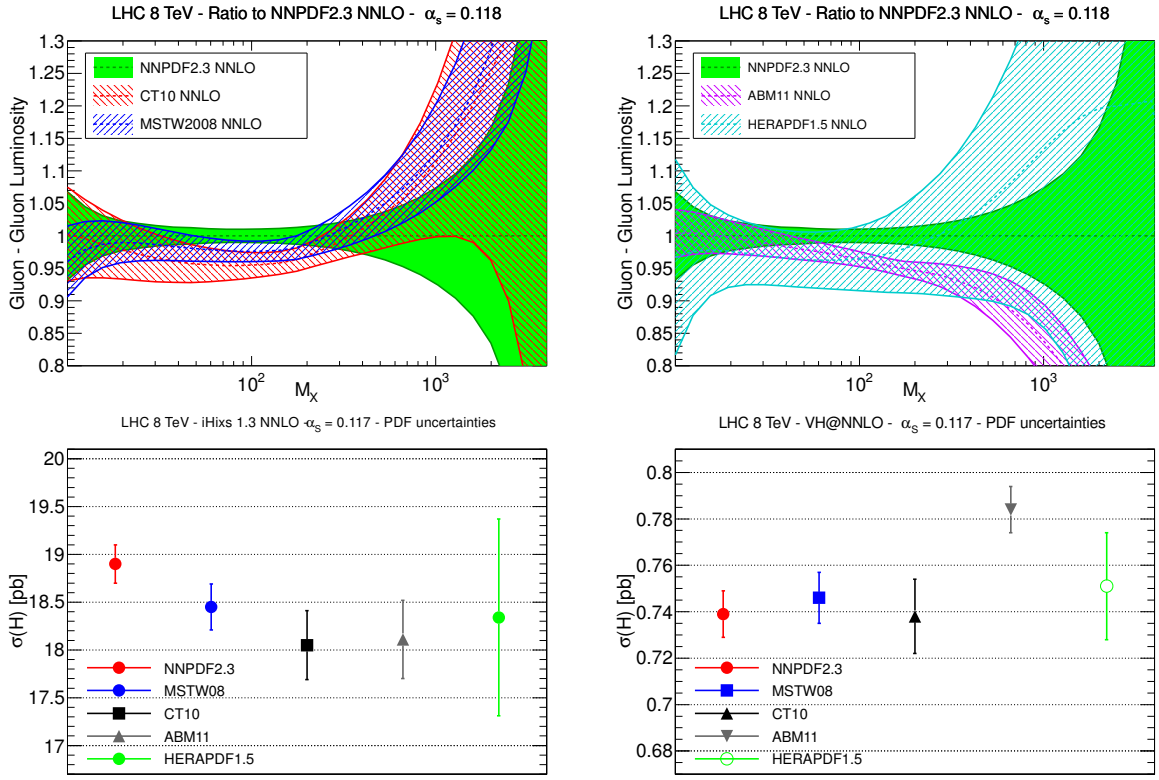


Figure 1-2. *Upper plots: Comparison of the gluon-gluon luminosity at the LHC 8 TeV as a function of the final state mass M_X between the ABM11, CT10, HERAPDF1.5, MSTW and NNPDF2.3 NNLO PDF sets. Lower plots: predictions for the Higgs production cross sections at LHC 8 TeV for the same PDF sets, in the gluon-fusion channel (left plot) and in the WH channel (right plot).*

[2] An extensive set of comparison plots for PDFs, parton luminosities, LHC total cross sections and differential distributions at NLO and NNLO and for different values of $\alpha_s(M_Z)$ can be found in `https://nnpdf.hepforge.org/html/pdfbench/catalog/`

In relation to previous comparisons, one of the main conclusions of the benchmark study [51] was that the agreement between the three global PDF sets, CT, MSTW and NNPDF has improved for most PDFs and ranges of Bjorken-x. On the other hand, there are still important differences that need to be understood, and that have substantial phenomenological impact. To begin with, the gluon luminosity for the three PDF sets differs maximally for $m_X \sim 125$ GeV, as can be seen from Fig. 1-2. It would be important to understand the source of these differences to improve the agreement of the three sets for the gluon-induced Higgs production cross sections. In addition, very large PDF uncertainties are present in the TeV range, affecting both the central values and the uncertainties for the production cross sections of massive particles. These large uncertainties at large masses degrade the prospects for eventual characterization of new BSM heavy particles. On top of this, there are theoretical uncertainties due to the choice of the heavy quark general-mass variable-flavor-number (GM-VFN) scheme, specific choices in the fitted dataset and methodological differences that still require further understanding to improve the agreement between the various PDF sets.

In the next subsection we discuss the prospects to obtain further constraints in PDFs from LHC data.

1.5.2 Parton distributions with QED corrections

Precision predictions for electroweak processes at hadron colliders require not only (N)NLO QCD corrections, but also the consistent inclusion of QED corrections to parton distributions and photon-initiated contributions. QED and electroweak corrections for various relevant collider processes have been computed in the last years in processes like inclusive W, Z production, vector boson pair production, $t\bar{t}$ and dijet production among many others. On the other hand, it is also known that a fully consistent treatment of electroweak corrections requires the use of parton distributions that also incorporate QED effects as well. QED effects on parton distributions have two main implications: first of all, the standard QCD DGLAP evolution equations are affected by $\mathcal{O}(\alpha)$ corrections and the associated breaking of isospin invariance, and, phenomenologically more important, the photon PDF needs to be determined from experimental data in parallel with the quark and gluon PDFs.

Until recently, only one PDF set with QED corrections was available, the MRST2004QED set [52], where the photon PDF was determined based on a model assumption. However, now the NNPDF framework has also been extended to provide PDF sets with QED corrections [53–55], and NNPDF2.3 QED is available in the NNPDF `HepForge` website.[3] NNPDF2.3 QED avoids any model assumption on the photon PDF and derives $\gamma(x, Q^2)$ and its associated uncertainties from a global fit to DIS and LHC data, where in the latter case neutral current and charged current vector boson production data provide stringent constraints on the shape and normalization of $\gamma(x, Q^2)$.

Electroweak corrections to parton distribution functions have important phenomenological implications, in particular for the electroweak production of high invariant mass final states. These include the measurement of the W mass, searches for W' and Z' resonances in the tails of the W and Z distributions and vector boson pair production among many others. The main effect is that the substantial uncertainties on the large-x photon PDF (that stem from the lack of available experimental constraints) translates into very large uncertainties from photon-initiated contributions that can be as large as a factor 100%.

As an illustration of these phenomenological consequences, in Fig. 1-3 we have computed the predictions of the NNPDF2.3 QED set for WW production at the LHC for various center of mass energies, compared with the results of the reference NNPDF2.3 set, as well as with the predictions from MRST2004QED. The computation has been done at leading order in the electroweak coupling but including photon-initiated

[3] `https://nnpdf.hepforge.org/html/nnpdf23qed/nnpdf23qed.html`

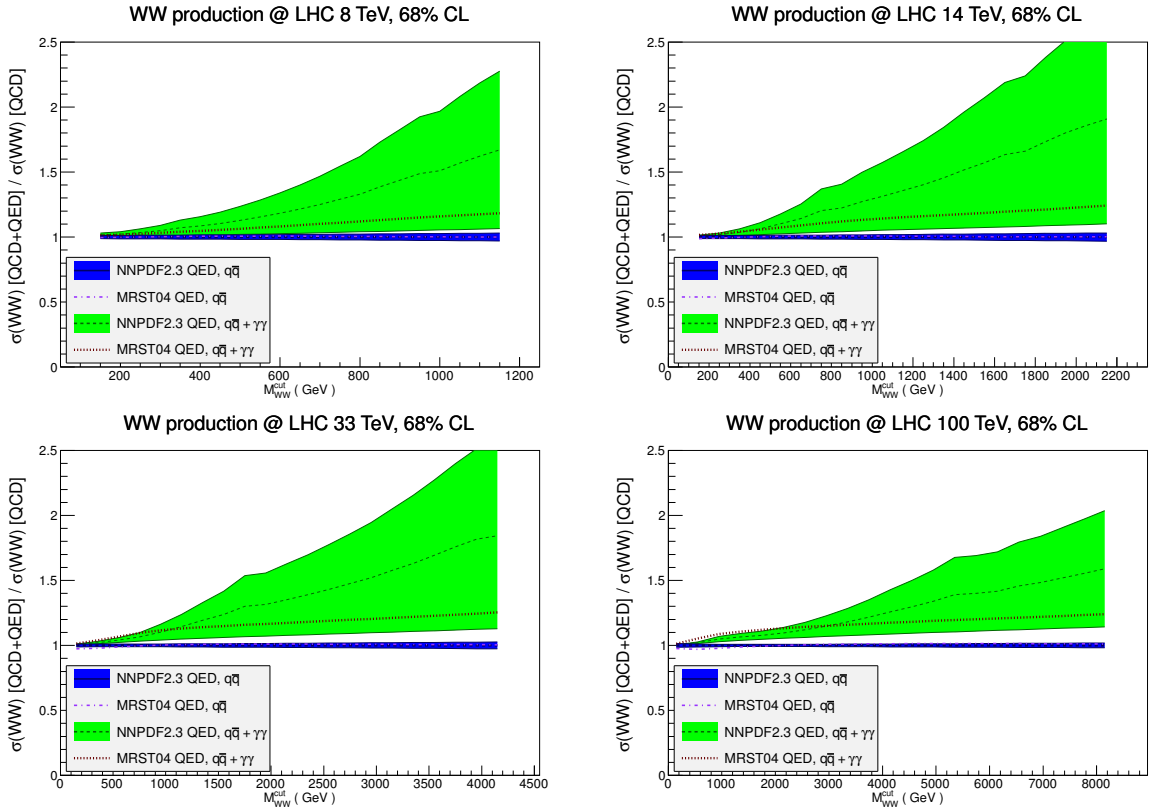


Figure 1-3. *The predictions of the NNPDF2.3 QED set for WW production at the LHC for various center of mass energies, compared with the results of the reference NNPDF2.3 set, as well as with the predictions from MRST2004QED. We show the total cross section as a function of the cut in the $M_{\rm WW}$ invariant mass, for 8, 14, 33 and 100 TeV energies. See text for more details.*

diagrams, using the same settings as in Ref. [56]. We show the total cross section as a function of the cut in the $M_{\rm WW}$ invariant mass, for 8, 14, 33 and 100 TeV energies.[4] It is clear that the QED-induced theoretical uncertainties are substantial and do degrade the constraining power of BSM searches in this channel, for example, searches for heavy resonances that decay into WW pairs. These effects are more severe the higher the cut in the invariant mass of the WW pair. As the energy is increased, for a given value of M_{WW} the PDF uncertainties decrease, but they are still very substantial at the highest available masses in each case, a factor 2 at least.

In summary, the development of parton distributions with QED corrections is an important ingredient of fully consistent theoretical predictions of hadron collider processes that include both higher order corrections in the QCD and EW couplings. On the other hand, the same analysis reveal the urgent need for more experimental data to constrain the photon PDF $\gamma(x, Q^2)$, and thus to reduce the currently large QED-induced uncertainties that affect high mass electroweak production at the LHC.

[4] We thank T. Kasprzick for providing us with these results.

1.5.3 PDF constraints from future LHC data

The excellent performance of the Large Hadron Collider is substantially increasing the range of processes that can be used to constrain PDFs in a global analysis. The traditional processes at hadron colliders that have been used for PDF constraints are inclusive jet production and W, Z production. Inclusive jet and dijet data are now available up to the TeV region from ATLAS and CMS [57, 58], and provide important constrains on the poorly known large-x quarks and gluons. In addition, ATLAS has presented the measurement the ratio of inclusive jet cross sections between 2.76 TeV and 7 TeV [59]. Such ratios between different center of mass energies [60] increase the PDF sensitivity of data taken at a single energy, since on the one hand many experimental uncertainties cancel in a dedicated measurement of a cross section ratio, and on the other hand several theory systematics, like scale variations, cancel as well. In the x-range currently dominated by HERA data ($x < 0.1$ for quarks and $x < 0.05$ for gluons), it will be difficult for hadron collider measurements to match the theoretical and experimental precision achieved at HERA. However, the HERA data provides little constraint in the high mass regions relevant for BSM searches. It is here where hadron collider measurements at high luminosity, at 14 TeV and at higher energies, can greatly contribute to improvements in the PDF uncertainties for both quarks and gluons. In this respect, recent progress towards the full NNLO QCD corrections for inclusive and dijet production [22] should make it feasible to achieve a few per-cent theoretical accuracy from scale dependence on these observables by the time of the 13 TeV data taking. Although improving, it may be difficult for the expected experimental precision to match the expected theoretical precision.

The precision measurements of W and Z boson production at hadron colliders provide important information on quark flavor separation, and in addition reduce systematic uncertainties of important observables like the W boson mass [46]. While the Z rapidity distribution and the W lepton asymmetry from the Tevatron and the LHC have been by now available for some time, recently the range of available processes has been extended by the measurement of the off-peak neutral current Drell-Yan process by ATLAS, CMS and LHCb. High-mass measurements of the Drell-Yan process provide useful information on the large-x quarks and antiquarks. Low-mass measurements provide information on the small-x gluons and possible departures from linear DGLAP evolution. Particularly striking signatures have been predicted for the LHCb kinematics. Future measurements at higher energies will benefit from an increased coverage in the dilepton invariant mass, allowing probes of very large-x antiquarks, which are effected by very large PDF uncertainties. Measurements in the peak region will benefit from reduced systematics and by negligible statistical uncertainties. To date, DGLAP evolution appears to be sufficient to describe the LHC data, but runs at higher energies may demonstrate the presence of BFKL-like effects [61]. On the theoretical side, the NNLO QCD corrections to fully-differential W and Z production have been known for several years [62–64]. Recently, the NNLO QCD and NLO electroweak corrections to neutral-current dilepton production have been consistently combined [65], and several combinations of NLO QCD, NLO electroweak and parton-shower effects for both W and Z production have appeared [66, 67].

In addition to the traditional processes discussed above, many new collider observables have recently become available for the first time for use in PDF fits. The recent calculation of the full NNLO top quark production cross section [34] makes possible for the first time the inclusion of top quark data into a NNLO analysis to constrain the large-x gluon PDF [68]. This is an important result since top production is currently the only hadronic observable which is both directly sensitive to the gluon and can be included in a NNLO global fit without any approximation. In turn, the more accurate gluon PDF will translate into an improvement of the theory predictions for various high-mass BSM processes driven by the gluon luminosity.

Future precision measurements of differential distributions in top quark pair production will allow more precision constraints on the gluon distribution and an ability to enlarge the range of Bjorken-x where the gluon PDF is being probed, especially once the NNLO calculation of [34] is extended to the fully differential

case. In addition to top quark data, the use of LHC isolated photon data and photon+jet data has also been advocated in order to pin down the gluon PDF [69, 70], though this process is affected by missing higher order and non-perturbative uncertainties.

Turning to the constraints on the quark distributions, the production of W and Z bosons in association with jets, for high p_T values of the electroweak boson, is a clean probe at the LHC of both quark flavor separation and of the gluon PDF [71]. In particular, ratios of W and Z distributions at large p_T provide constraints on quarks and antiquarks while benefiting from substantial cancellations of experimental and theory uncertainties. This is a good example of a process currently limited by statistics, and future LHC data will offer a much increased constraining power. Another important source of information on the quark PDFs is W production in association with charm, which is directly sensitive to the strange PDF [72], the worst known of all the light quark flavors. Measurements for this important process have been recently reported by both ATLAS [73] and CMS [74]. Interestingly, the two measurements seem to pull the strange PDF in different directions, with CMS showing good agreement with the strangeness suppression of global PDF fits derived from the neutrino DIS charm production data, and ATLAS preferring a symmetric strange sea, as previously derived from their inclusive W and Z data. Including all of these datasets into the global PDF fits is necessary to determine the optimal strange PDF which accounts for all experimental constraints.

Putting everything together, it is clear that the LHC will provide in the next years a plethora of new measurements that will be used to improve our knowledge of parton distributions. Quantitative projections in this respect are difficult since the precision measurements used in PDF analyses are dominated by systematic errors, which are notoriously difficult to predict. In addition, correcting for pile-up in the high-luminosity phase of the LHC might render such analyses even more complicated. However, there are good prospects that in the next years PDFs will be determined with increasingly better accuracy, in turn improving the theory predictions needed for Higgs boson characterization and for new physics searches.

1.5.4 Luminosities and uncertainties for 14, 33 and 100 TeV

As discussed above, in order to assess similarities and differences between PDF sets, it is useful to compare parton luminosities for different channels as a function of the final state mass M_X of the produced system, for different values of the hadronic collider energy. In the following we will redo the comparisons presented in Ref. [51], but this time for higher energy incarnations of the LHC: 14 TeV, 33 TeV and 100 TeV. This comparison is shown in Fig. 1-4, where we compare the quark-quark, quark-antiquark and gluon-gluon luminosities between the most updated CT, MSTW and NNPDF NNLO PDF sets at these three center of mass energies.

While in general we observe reasonable agreement between the three sets, there are also some cases where the agreement is marginal, e.g. for the gluon-gluon luminosity, or even non-existing, e.g. for the very high mass range for the quark-quark luminosity at 100 TeV. The quark-antiquark luminosities for the three PDFs in the W/Z mass range agree well at 14 TeV, and even better at 7 and 8 TeV. For 33 and 100 TeV energies, the uncertainties in that mass range rapidly increase as smaller quark x-values not well-constrained by HERA are probed.

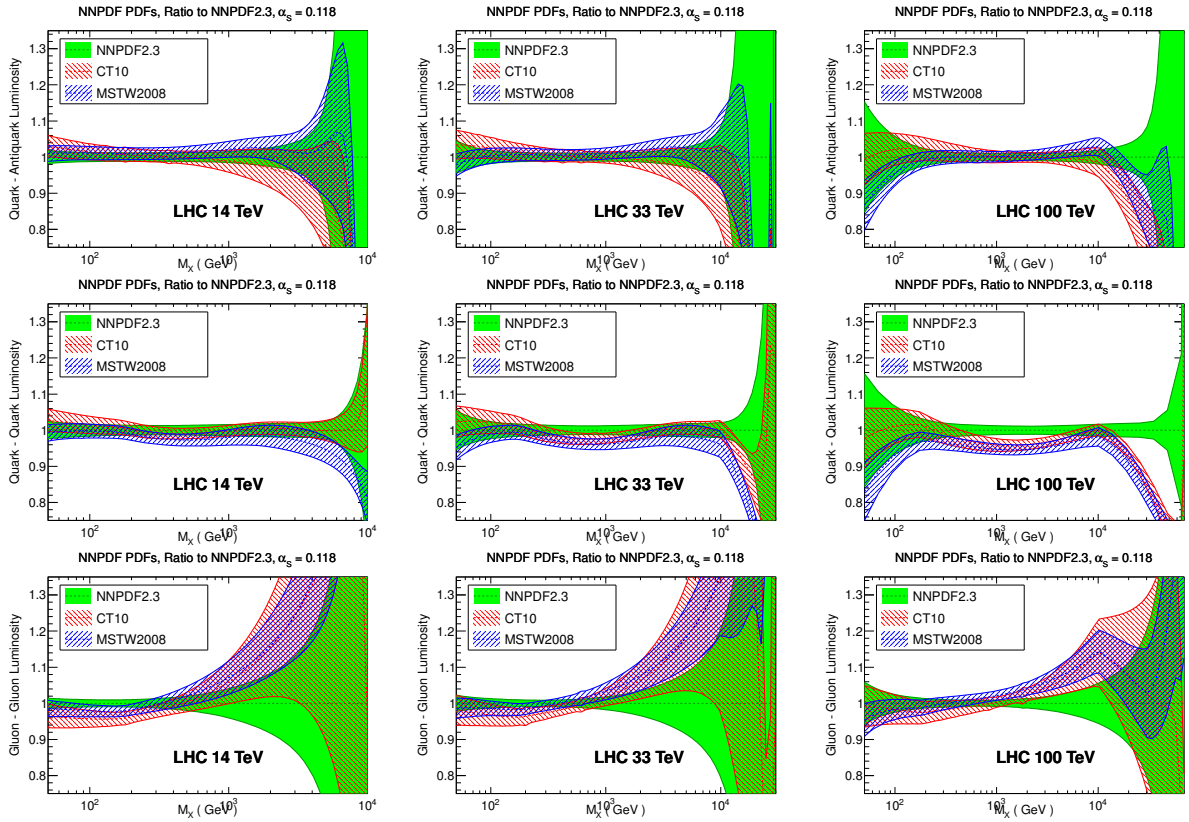


Figure 1-4. *Comparison of the partonic luminosities at 14, 33 and 100 TeV between the CT10, MSTW and NNPDF2.3 NNLO PDF sets. From top to bottom: quark-antiquark luminosity, quark-quark luminosity, and the gluon-gluon luminosity.*

1.5.5 Improvements from LHeC

With the LHeC, very precise measurements of charged currents (CC) and the exploitation of Z exchange in neutral currents (NC) become possible, in addition to extending photon exchange NC to extremely low x. The question of gluon saturation at low x can be expected to be settled with precision measurements of the structure functions F_2 and also F_L down to $x \geq 10^{-6}$ [23] while the large x determination of xg is crucial for the LHC Higgs and BSM program [24,25]. The LHeC, combined with HERA to fill in the medium Q^2-larger x region, provides a unique and complete DIS data set. With unprecedented precision there will be for the first time a determination possible of *all* PDFs, u_v, d_v, $\bar{u}$, $\bar{d}$, s, $\bar{s}$, c, b and even t, in furthermore a hugely extended kinematic range. To explore this, a full set of NC and CC cross section measurements has been simulated and a QCD fit analysis been applied in order to study the potential for the determination of the parton distribution functions in the proton.

As detailed in [23], the strange quark distribution will be measured in an accurate way with charm tagging of W fusion in CC scattering. Precise measurements of the charm and the beauty quark distributions would be possible, from Q^2 values below the quark masses squared up to $\sim 10^5\,\mathrm{GeV}^2$, based on the small beam spot size of $\sim 7\,\mu\mathrm{m}^2$ and a high resolution silicon detector of large acceptance. This, for example, will determine the charm mass with the experimental error of 3 MeV [23], an order of magnitude improved as compared

to HERA, and similarly for the bottom mass. Such high precision input will certainly provide a new basis for higher order tests of the treatment of heavy quarks in the Q^2 evolution, which currently is a significant source of uncertainty in the understanding of PDFs and in predictions for the LHC.

Monte Carlo data were simulated for NC and CC scattering assuming $e^{\pm}p$ luminosities of $10\,\mathrm{fb}^{-1}$ and a 40 % polarization. Using the HERAFitter framework [75–77] with settings based on the HERAPDF NLO QCD fit analysis, a set of PDFs has been generated (and is available on LHAPDF) for estimates of future measurement potentials. An example is the prediction of the $gg \to H$ cross section at the LHC, which will have an uncertainty from PDFs and α_s of only about 0.4 % and thus be sensitive to determinations of M_H via the cross section [25]. Another example is the importance of knowing xg for high mass searches of SUSY particles as has also been recently studied [24, 78].

The procedure used has been adopted from the HERA QCD fit procedure [75] with a minimum Q^2 cut of $3.5\,\mathrm{GeV}^2$ and a starting scale $Q_0^2 = 1.9\ \mathrm{GeV}^2$, chosen to be below the charm mass threshold. The fits have been extended to very low values of x for systematic uncertainty studies, even when at such low x values non-linear effects are expected to appear, eventually altering the evolution laws.

The parameterized PDFs are the valence distributions xu_v and xd_v, the gluon distribution xg, and the $x\bar{U}$ and $x\bar{D}$ distributions, where $x\bar{U} = x\bar{u}$, $x\bar{D} = x\bar{d} + x\bar{s}$. This ansatz is natural to the extent that the NC and CC inclusive cross sections determine the sums of up and down quark distributions, and their antiquark distributions, as the four independent sets of PDFs, which may be transformed to the ones chosen if one assumes $u_v = U - \overline{U}$ and $d_v = D - \overline{D}$, i.e. the equality of anti- and sea quark distributions of given flavor. The following standard functional form is used to parameterize the PDFs:

$$xf(x) = Ax^B(1-x)^C(1 + Dx + Ex^2), \tag{1.4}$$

where the normalization parameters (A_{uv}, A_{dv}, A_g) are constrained by quark counting and momentum sum rules. The parameters $B_{\bar{U}}$ and $B_{\bar{D}}$ are set equal, $B_{\bar{U}} = B_{\bar{D}}$, such that there is a single B parameter for the sea distributions. The strange quark distribution at the starting scale is assumed to be a constant fraction of $\bar{D}$, $x\bar{s} = f_s x\bar{D}$, chosen to be $f_s = 0.5$ such that $\overline{s} = \overline{d}$. In addition, to ensure that $x\bar{u} \to x\bar{d}$ as $x \to 0$, $A_{\bar{U}} = A_{\bar{D}}(1 - f_s)$. The D and E are introduced one-by-one until no further improvement in χ^2 is found. The best fit resulted in a total of 12 free parameters, specifically fitting B_g, C_g, D_g, B_{uv}, C_{uv}, E_{uv}, B_{dv}, C_{dv}, $C_{\overline{U}}$, $A_{\overline{D}}$, $B_{\overline{D}}$, $C_{\overline{D}}$. While the LHeC NC, CC real data, and the inclusion of further information, as of s, c, b and F_L, will certainly lead to quite a different parameterization, it has been checked that with a more flexible set of 15 parameters very similar results to the PDF uncertainties found here are obtained.

The PDFs are evolved using DGLAP evolution equations at NLO in the $\overline{\mathrm{MS}}$ scheme with the renormalization and factorization scales set to Q^2 using standard sets of parameters, such as for $\alpha_s(M_Z)$. These, as well as the exact treatment of the heavy quark thresholds, have no significant influence on the estimates of the PDF uncertainties. The experimental uncertainties on the PDFs are determined using the $\Delta\chi^2 = 1$ criterion. The LHeC Design Report [23] contains a very detailed presentation of the results of the present analysis for valence and sea quarks with many remarkable features as the determination of the u/d ratio or the measurement of the valence quarks down to low $x \simeq 10^{-4}$.

1.5.5.1 Determination of the Gluon Distribution at the LHeC

The result for the gluon distribution is presented in Fig. 1-5. In the left panel, recent gluon distribution determinations and their uncertainties are shown plotted as a ratio to MSTW08. Below $x \simeq 10^{-3}$ the HERA data have vanishing constraining power due to kinematic range limitations, and the gluon is just not determined at low x. At large $x \geq 0.3$ the gluon distribution becomes very small and large variations

differing by orders of magnitude appear in its determination. This is related to uncertainties in jet data, theory uncertainties and the fact that HERA had not enough luminosity to cover the high x region. Moreover, the sensitivity to xg at HERA diminishes, as the valence quark evolution is insensitive to it. The larger x situation can be expected to improve with LHC jet data and possibly top data and the HERA II data. The right panel shows the experimental uncertainty of xg based on the LHeC, on HERA alone and in various combinations with further data; see the LHeC design report [23] for more details. At small x a few per cent precision becomes possible, as can be seen by comparing the right and left panels. Note that the non-LHeC low x uncertainty bands (right) remain narrow below $x \simeq 10^{-3}$, as an artifact due to the parameterization of xg.

It is for the LHeC to discover whether xg saturates or not and whether indeed the DGLAP equations need to be replaced by non-linear parton evolution equations such as BFKL. This is important not only for QCD but also for super high energy neutrino physics and low x physics at the LHC. In the region of the Higgs data at the LHC, $x \sim 0.02$, the LHeC will pin down the gluon extremely accurately and the $gg \to H$ cross section uncertainties will essentially be removed as has been discussed in [25]. At large values of e.g. $x = 0.6$ the LHeC can be expected to determine xg to $5 - 10\,\%$ precision (inner blue band). This is crucial for when the LHC operates at maximum luminosity and the searches approach the few TeV mass region, as in $gg \to \tilde{g}\tilde{g}$ [78]. It is also important for testing QCD, as factorization and scales, as well as electroweak effects at large x in a future critical comparison of such ep with LHC pp data as for jets, see also [24]. Similarly, surprises may result from comparisons with inclusive LHeC jet data, not considered here. PDF physics rests on controlling and testing the underlying theory.

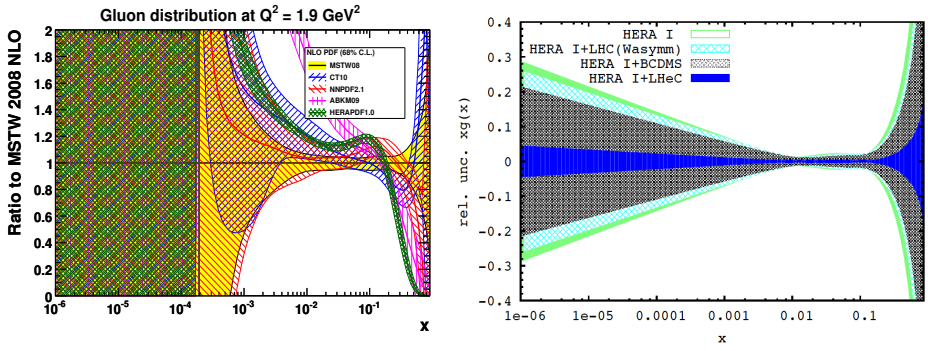


Figure 1-5. *Uncertainty of the gluon distribution at $Q^2 = 1.9\,GeV^2$ as a function of Bjorken x, see text. The LHeC PDF set, corresponding to the inner blue error band, is available on LHAPDF.*

1.5.5.2 Final Remark

It is important to emphasize that while the PDF analysis presented here serves as a valid starting point for comparison with existing PDFs, the LHeC has a unique potential to release the underlying simplifying assumptions and to provide a radically different and novel way to determine the PDFs. With the consideration of the direct measurements of the strange, charm and beauty PDFs, and perhaps even the top PDF, and with the addition of tagged eD data, it will be possible to analyze the behavior of not just 4 suitable combinations of PDFs but to determine the full set for the first time with crucial direct input. For example, the valence quarks at high x will be determined by high statistics CC data, and at low x they will be measured with electroweak structure functions. Light quarks can be determined independently of each other using ep and en and CC data. The LHeC the will radically change the world of PDFs. The present study of uncertainties

to this extent is an illustration only and initially rather narrow in scope. It yet becomes evident that with the LHeC the development of QCD will hugely progress and the LH(e)C can be turned into a precision Higgs facility. Electromagnetic substructure of the heaviest elementary particles may also be revealed. Finally, the anticipated investment into the highest LHC luminosity will be underpinned by the necessary precision QCD and PDF measurements by the LHeC without which highest mass limits must remain weaker and interpretations of subtle new features possibly uncertain. The LHeC appears as an important upgrade to the LHC with which the symmetry between pp, ep and may be e^+e^- can be restored at TeV energies. This fruitful symmetry allowed the Tevatron, HERA and LEP/SLC to eventually establish the Standard Model of particle physics.

1.6 Higher-order corrections

The implementation of higher-order corrections in parton-level predictions and Monte Carlo generators is essential for maximizing the potential of future experiments. This section presents a wide survey of both current tools and directions of future development, with applications to LHC operations at 14 TeV and to proton-proton collisions at 33 and 100 TeV. The section concludes with an overview of the highest-priority perturbative calculations, ones that could feasibly be tackled in the next 5–10 years.

1.6.1 NLO cross sections at 14, 33 and 100 TeV

As a first step towards investigating the physics potential of future proton-proton colliders, it is interesting to investigate the center-of-mass energy dependence of notable cross-sections at such machines. Figure 1-6 shows the predicted cross sections for a selection of basic processes, ranging over twelve orders of magnitude from the total inelastic proton-proton cross section to Higgs boson pair-production. For inclusive jet and direct photon production, 50 GeV transverse momentum cuts are applied to the jet and the photon respectively. The cross sections presented in this figure have been calculated at next-to-leading order in QCD using the MCFM program [79,80], or taken from the European Strategy report [81] (in the case of Higgs cross sections).

The growth of the cross-sections with $\sqrt{s}$ largely reflects the behavior of the underlying partonic luminosities. For instance, the top pair cross section is dominated by the partonic process $gg \to t\bar{t}$ and the gluon-gluon luminosity rises significantly at higher values of $\sqrt{s}$. The same holds true for the Higgs production channel $t\bar{t}H$ but, in contrast, the associated production channels are dominated by quark-antiquark contributions and rise much more slowly. The different behavior means that, unlike at current LHC operating energies, the $t\bar{t}H$ channel becomes the third-largest Higgs production cross section at 33 TeV and above. As a figure of merit for estimating the difficulty of observing the Higgs pair production process it is not unreasonable to consider the ratio of its cross section to the top pair cross section. In many of the possible Higgs boson decays the final states receive significant background contributions from the top pair process. The fact that both processes are predominantly gluon-gluon induced means that this measure is approximately constant across the range of energies considered. It is therefore not clear that the prospects for extracting essential information from the Higgs-pair process would be significantly easier at a higher-energy hadron-collider, even though the rates increase dramatically.

A different sort of contribution to event rates can also be estimated from this figure. The contribution of double parton scattering (DPS) – where a single proton-proton collision is responsible for two hard events –

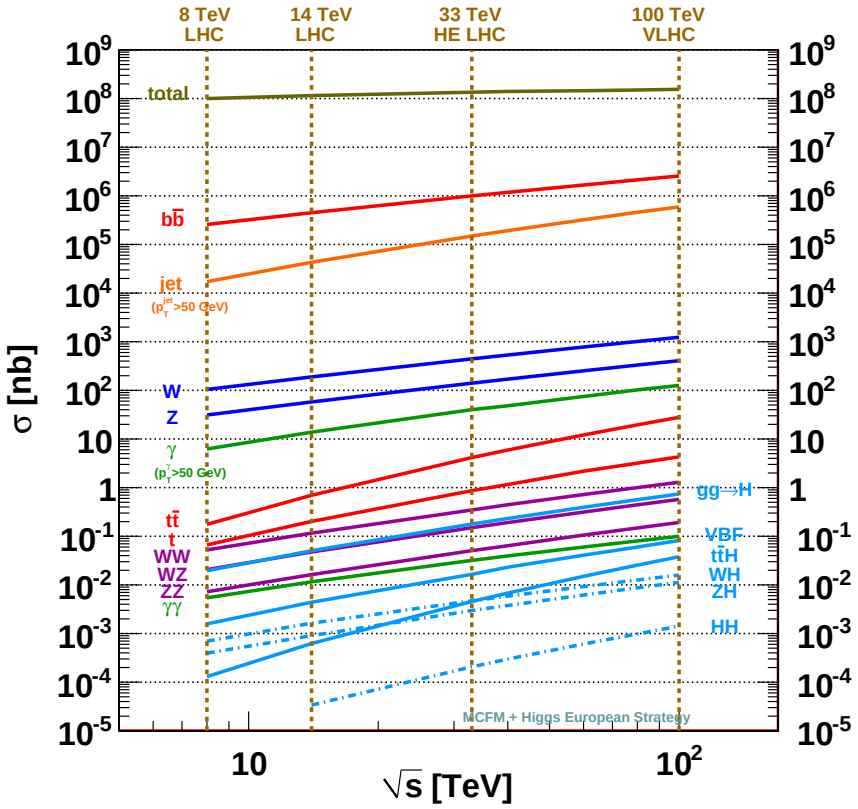


Figure 1-6. *Cross section predictions at proton-proton colliders as a function of center-of-mass operating energy, $\sqrt{s}$.*

can be estimated by,

$$\sigma_{XY}^{\rm DPS} \approx \frac{\sigma_X \sigma_Y}{15 \text{ mb}} \,. \tag{1.5}$$

In this equation the DPS contribution for the final state XY is related to the usual cross sections for individually producing final states X and Y dividing by an effective DPS cross section. This cross section appears to be approximately independent of energy up to 8 TeV and is approximately 15 mb (for example, see Ref. [82] for a recent measurement at 7 TeV). Of course the uncertainty on the effective cross section, and indeed on the accuracy of Eq. (1.5) itself, is such that this should be considered an order-of-magnitude estimate only. A particularly simple application of this is the estimation of the fraction of events for a given final state in which there is an additional DPS contribution containing a pair of b-quarks. This fraction is clearly given by the ratio, $\sigma_{b\bar{b}}/(15 \text{ mb})$. From the figure this fraction ranges from a manageably-small 2% effect at 8 TeV to a much more significant 20% at 100 TeV. More study would clearly be required in order to obtain a true estimate of the impact of such events on the physics that could be studied at higher energies, but these simplified arguments can at least give some idea of the potentially troublesome issues.

As an example of the behavior of less-inclusive cross sections at higher energies, Fig. 1-7 shows predictions for $H + n$ jets $+ X$ cross sections at various values of $\sqrt{s}$ and as a function of the minimum jet transverse momentum. The cross sections are all normalized to the inclusive Higgs production cross section, so that

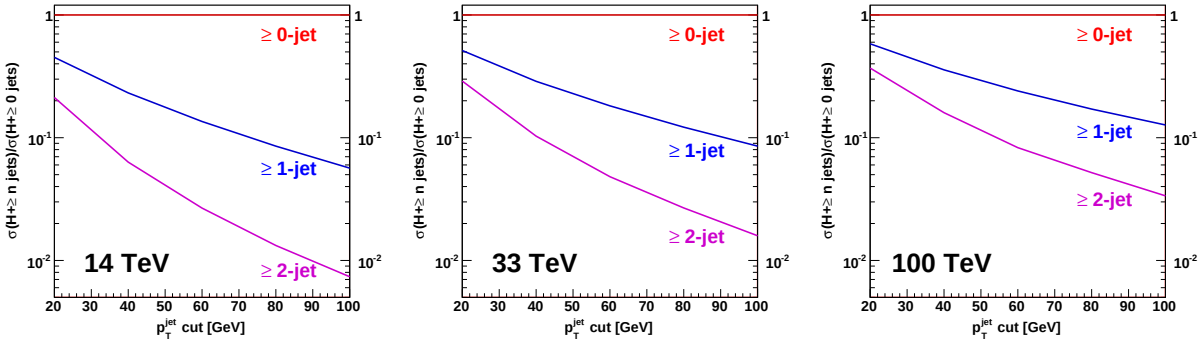


Figure 1-7. *Cross sections for the production of a Higgs boson produced in association with n or more jets, for $n = 0, 1, 2$, normalized to the inclusive Higgs cross section ($n = 0$). Cross sections are shown as a function of the minimum jet p_T and are displayed for a proton-proton collider operating at 14 TeV (left), 33 TeV (center) and 100 TeV (right).*

the plots indicate the fraction of Higgs events that contain at least the given number of jets. The inclusive Higgs cross section includes NNLO QCD corrections, while the 1- and 2-jet rates are computed at NLO in QCD.

The extent to which additional jets are expected in Higgs events is strongly dependent on how the jet cuts must scale with the machine operating energy. For instance, consider a jet cut of 40 GeV at 14 TeV, a value in line with current analysis projections. For this cut, approximately 20% of all Higgs boson events produced through gluon fusion should contain at least one jet. The fraction with two or more jets is expected to be around 5%. To retain approximately the same jet compositions at 33 and 100 TeV requires only a modest increase in the jet cut to 60 and 80 GeV respectively.

At higher operating energies it is especially interesting to compare predictions produced using the standard perturbative expansion, here at NLO, with alternative formalisms that directly appeal to the high energy limit. One such formalism is encoded in the program HEJ ("High Energy Jets") [83, 84] that implements a resummation scheme based on the factorization of scattering amplitudes in the high energy limit. For this study we investigate predictions for $H + 2$ jet events, with particular interest in the region where two of the jets are separated by a large rapidity span. As well as being relevant for separating the gluon fusion and vector boson fusion processes, this region is expected to be particularly sensitive to differences between the predictions of NLO QCD and HEJ [85]. Jets are reconstructed using the k_T algorithm with $D = 0.6$ and $|y| < 5$. In the first scenario we consider a minimum transverse momentum cut of 40 GeV for operating energies of 14, 33 and 100 TeV. In the second scenario the jet cut is doubled to 80 GeV at 33 TeV and again to 160 GeV at 100 TeV.

The results of this study are shown in Fig. 1-8. Predictions are shown for the ratio of inclusive 3-jet to inclusive 2-jet events, as a function of the rapidity difference between the two most widely-separated jets. The uncertainty band is obtained by varying the scale choice by a factor of two about the central value ($H_T/2$, where H_T is the sum of the total transverse momentum of all objects in the final state). The predictions for ratios of cross sections from HEJ are very stable against variations in the factorisation and renormalisation scales. This is because both numerator and denominator are resummed predictions, with virtual corrections counter-acting the renormalisation scale dependence of the born level predictions. The NLO MCFM results are much more sensitive to changes in the scale, as can be seen from the wider uncertainty bands. This is further illustrated in the first plot (for collider energy 14 TeV and jet $p_T > 40$ GeV) where the additional

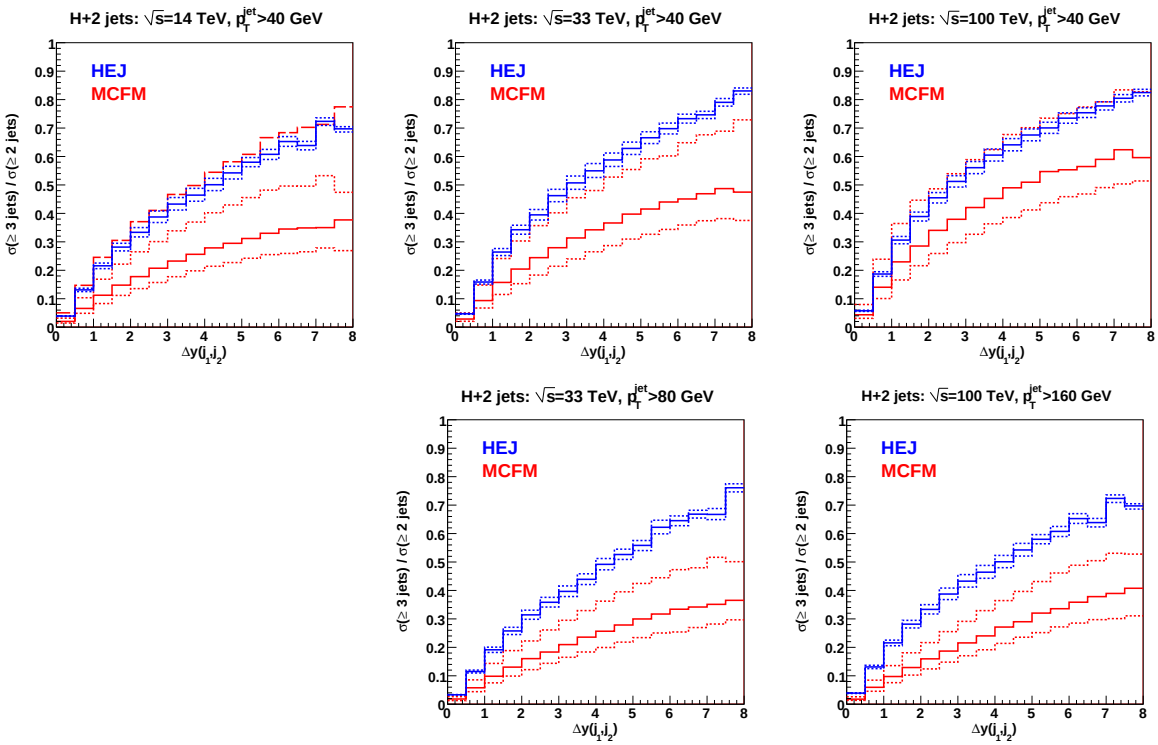


Figure 1-8. *The ratio of number of events that contain at least three jets to the number that contain at least two jets, as a function of the rapidity difference between the two most widely-separated jets. Predictions are obtained using the NLO calculation of the $H + 2$ jet process and are shown at three operating energies. The jet transverse momentum cut is at 40 GeV (top), or scales with the operating energy (bottom).*

dashed line shows the MCFM result for an even lower scale choice of $H_T/6$. A typical H_T value for these events is around 250 GeV, so this choice is closer to the scale of the jet p_T. The prediction for this choice is very close to the HEJ prediction throughout the range.

In all five scenarios, the predictions from HEJ for the ratio of 3-jet to 2-jet events rise faster and reach a higher value than the predictions from the NLO calculation as the rapidity span of the event increases. This is the region where the higher-order corrections included in HEJ become significant. As the collider energy is increased while the jet p_T cut is kept constant the phase space for the production of higher numbers of jets increases. This is illustrated in the top row of Fig. 1-8, where it can be seen that the value of the ratio increases in both descriptions. As the energy of the collider increases, the difference between the HEJ and MCFM descriptions is reduced. As a results, at $\sqrt{s} = 100$ TeV, the HEJ curve practically coincides with the MCFM prediction using $H_T/4$.

In the cases where the jet p_T cut is also increased (bottom row), the predictions are rather similar across energies. However the higher p_T cuts mean that the central scale is much larger in the MCFM calculation and, as a result, the scale dependence band is smaller than in the case of a fixed cut. This leads to a larger difference in the predictions of HEJ and MCFM using our default scale variation, although once again the HEJ curves could be mimicked by choosing a slightly smaller scale of $H_T/6$ in MCFM.

1.6.2 Extrapolation from existing NLO results

The progress within the last 5 years in the calculation of NLO corrections for complex final states has been truly impressive, as witnessed for example by the calculation of $W + 5$ jets by the Blackhat+Sherpa Collaboration [86]. Of course, there is a limit, as increasing the number of partons in the final state by definition increases the complexity of the calculation, while the physics reward (typically) decreases. Within a matrix-element + parton shower framework, additional jets can be added either at leading order or through the parton shower. In addition, there are heuristic tools that can be developed to extrapolate cross sections for higher jet multiplicity based on the patterns observed at lower jet multiplicity. For instance, known results for $W + 2$ through $W + 5$ jet production can be used to assess the scaling behavior of the $W + n$ jet cross sections [5] Defining the quantity $R^{\pm} = \sigma(W^{\pm} + n \text{ jets})/\sigma(W^{\pm} + n - 1 \text{ jets})$, Blackhat+Sherpa have developed predictions for this ratio for $n \geq 3$, in pp collisions at 7 TeV, for jets with $p_T > 25$ GeV. The predictions are:

$$R^{+}_{\text{NLO}} = 0.263 \pm 0.009 - (0.009 \pm 0.003)\, n,$$
$$R^{-}_{\text{NLO}} = 0.248 \pm 0.008 - (0.009 \pm 0.002)\, n.$$

From these formulae, the cross sections at NLO for $W + 6$ or 7 jets can be predicted, without any actual calculation. Of course, such scaling formulae are strongly dependent on the kinematic regions being considered, but can easily be re-assessed for different cuts or center-of-mass energies. However, there seems to be no a priori reasons why similar predictions would not be possible for other final states for which n-jet cross sections are known.

There also exist other techniques for approximating NNLO (or higher) contributions to hard cross sections. One such technique is LoopSim [87]. The LoopSim method allows for the merging of NLO Monte Carlo samples of different jet multiplicities in order to obtain approximate NNLO predictions, and has been applied to processes such as W and Z + jets [88] and WZ production [89]. The LoopSim method makes use of any existing virtual matrix elements in the merged samples, and where these are not available, determines exactly the singular (or logarithmic) terms of the loop diagrams, which, by construction, match precisely the corresponding singular terms of the real diagrams with one extra parton. The approximate NNLO cross section thus constructed differs from the complete NNLO cross section only by the constant terms. In some sense, this technique makes use of matrix element information from a number of multi-leg NLO calculations in a way similar to that carried out by a matrix element-parton shower combination such as MEPS@NLO [90]. This technique can potentially be very powerful when new sub-processes at higher jet multiplicities result in substantial additional contributions to the cross section. One example is the production of a W boson with 1 or more jets at the LHC (7 TeV). In Fig. 1-9, the p_T distribution for the leading jet (left) and for the $H_{T,tot}$ distribution (the sum of the transverse momenta of all of the jets and W boson decay products) (right) are shown, with predictions at LO, NLO and approximate NNLO ($\bar{n}$NLO) [88]. There are sizable NLO QCD corrections for the leading jet p_T distribution, increasing with the jet transverse momentum, and a considerable scale dependence even at NLO. Both result from the addition of new topologies where the W boson is soft or collinear. At $\bar{n}$NLO, there is a modest increase in the cross section (within the NLO uncertainty band), but a considerable reduction in the scale dependence. In contrast, the $H_{T,tot}$ distribution receives large corrections at $\bar{n}$NLO (outside of the NLO scale uncertainty band) with a smaller relative reduction in the scale dependence. The increase results from the inclusion of a third jet in the $W+ \geq 1$ jet cross section calculation; even though the third jet will be relatively soft, its inclusion in a steeply falling distribution results in sizable effects for the $H_{T,tot}$ cross section. This technique can also be applied to produce approximate NNNLO cross sections.

[5] $W + 1$ jet behaves differently because of missing production channels and kinematic differences.

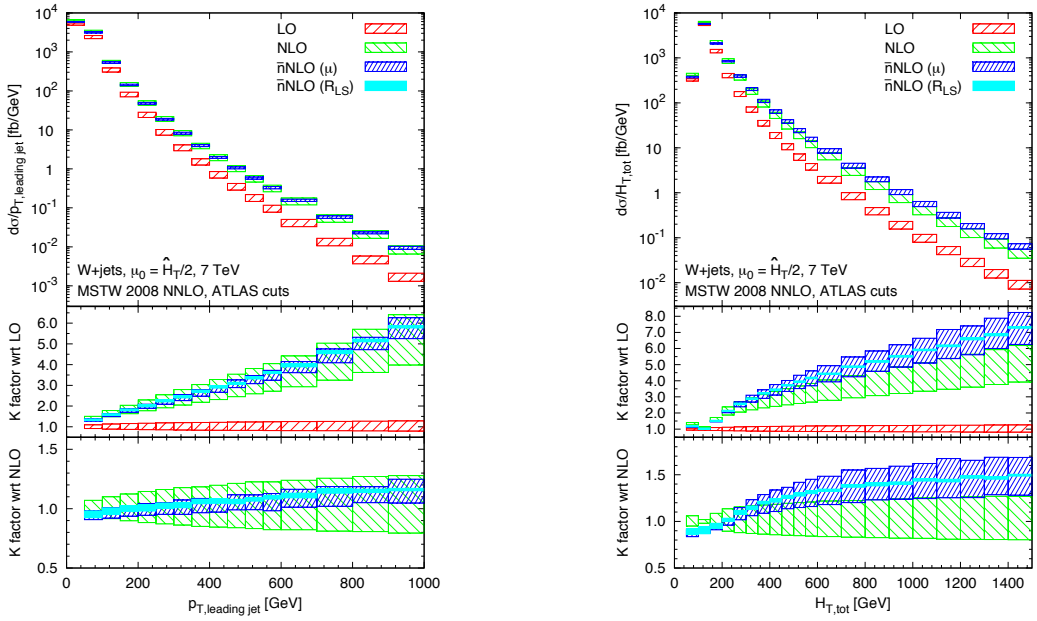


Figure 1-9. *The differential cross sections and K-factors for $p_{T,leading\ jet}$ and $H_{T,tot}$ at parton level at LO, NLO and $\bar{n}$NLO. The bands correspond to varying $\mu_R = \mu_F$ by factors of 0.5 and 2.0 around the central value.*

1.6.3 Computational complexity

The advances of NLO and NNLO multi-leg calculations have resulted in programs that are (1) very complex and (2) very time-consuming to run using the resources available to a typical user. It can thus be difficult for a full dissemination of the theoretical results to the experimental community. The Blackhat+Sherpa Collaboration has partially addressed these issues by releasing results for $W/Z + n$ jets in ROOT ntuple format, with all information needed for calculation of physical cross sections with a variety of jet parameters and cuts. In addition, the results can be re-weighted for different scales and different PDFs. The cost is the presence of very large outputs, but subdivided into files of a few GB that are ideal for parallel processing. Ntuples are probably not practical, though, for some of the more complex NNLO calculations, such as inclusive jet production, where the number of files needed would be prohibitive. Making the resultant program user-friendly, though, can take a great deal of time.

An alternative is to make such complex programs available to the user on high performance computing platforms, which inherently have much greater processing and storage capabilities; in addition, the programs may be pre-compiled by the authors insuring that the calculation is run correctly. Initial tests of HPC platforms have been successfully carried out during the Snowmass workshop. We have shown weak scaling up to 16000 cores on IBM BlueGene/Q, up to 8192 cores on CRAY XK7, and strong scaling up to 1024 cores on CRAY XK7 using Sherpa. Another possibility for large-scale production runs may be the Open

Science Grid. More details on the use of HPC resources in high energy theoretical research can be found in Ref. [91].

1.6.4 Improvements to matrix element and parton shower matching

General-purpose event generators have been undergoing tremendous development over the past years. Both the fixed-order and logarithmic accuracy underpinning their simulations of perturbative QCD have been improved in order to match increased precision needs in the experiments.

The basis for the these developments was established by the MC@NLO technique [92], which matches NLO QCD calculations to parton showers, such that fully differential events can be generated at the particle level. The POWHEG [93, 94] method was later introduced to eliminate negative weights from simulations.

Parton-shower matched predictions have been provided for some of the most challenging NLO calculations to date, including, for example, $pp \to W + 3$ jets [95] and $pp \to t\bar{t}+$ jet [96]. The current limitation in matching to even higher multiplicity processes is not of algorithmic nature, but purely computational, and it is related to the memory consumption of executables. Fixed-order calculations benefit from the fact that they can be split into different parts, corresponding to Born, virtual correction, integrated infrared subtractions and real-emission correction minus real subtraction. Due to the intricate interplay between real and virtual corrections in MC@NLO and POWHEG, such a splitting is harder to achieve when matching to a parton shower.

Different proposals were made to combine MC@NLO simulations of varying jet multiplicity into inclusive event samples [90, 97]. They are natural extensions of the CKKW(-L) [98, 99] and MLM [100] leading-order merging schemes to the next-to-leading order, respectively. Another, entirely independent method was introduced earlier, which relies on a different subtraction scheme [101, 102]. The simulations provided by these new techniques can be used to obtain NLO-accurate predictions for different jet multiplicities at the same time.

Achieving this level of fixed-order accuracy has been a priority in the development of Monte-Carlo event generators for more than a decade. The current technology has undoubtedly benefited greatly from the advances in computing fixed-order NLO QCD corrections at large jet multiplicity in a fully automated manner. These calculations provide the parton-level input for the new merging methods.

NLO-merged predictions have been provided for $pp \to W/Z+$ jets with up to two jets described at NLO accuracy [90], $pp \to H+$ jets in gluon fusion, with up to one jet at NLO accuracy [97, 102] and $pp \to t\bar{t}+$jets with up to one jet at NLO accuracy [97, 103]. All related implementations are fully automated and can, in principle, be used for any type of reaction. However, because MC@NLO parton-level predictions are needed as an input, the current limitations are identical to those for MC@NLO. They are not due to algorithmic deficiencies, but mostly due to memory constraints on production systems and restrict the usage of the methods to processes with fewer than four light jets in the final state computed at NLO.

It is conceivable that working techniques for matching NNLO fixed-order calculations to parton-shower simulations will be constructed in the near to mid-term future. Such a matching, which could be dubbed 'MC@NNLO', would further stabilize predictions for the differential cross section at lowest multiplicity, and eliminate the unitarity violation observed in most NLO merging methods in a natural way.

An alternative technique already exists, which does not rely on a modified subtraction scheme to construct counterterms for fixed-order calculations, but on constructing counterterms for the parton shower, at the

order at which the shower is to be matched [101]. This is very easy to achieve. The method has been used as proof of principle to provide NNLO matched predictions for $e^+e^- \to$ jets production [101].

At the same time that matching to fixed-order NNLO calculations is being developed, the logarithmic accuracy of parton shower simulations must be improved systematically, in order not to degrade the precision of the fixed-order result after matching. This involves two developments.

Firstly, corrections which are sub-leading in the number of colors, N_c, must be included. A proposal to do this was formulated some time ago [104], but first steps to implementation were taken only recently [105,106]. The importance of sub-leading N_c corrections in processes with non-trivial color structure at Born level was observed in an analysis of the $t\bar{t}$ forward-backward asymmetry [103]. Respecting the full color structure during parton evolution will allow to include all next-to-leading logarithmic effects in the parton shower, in a manner that is independent of the actual evolution variable, and therefore does not rely on angular ordering.

Secondly, it will be beneficial to systematically extend parton-showers to higher logarithmic accuracy, for example by including higher-point splitting functions. An alternative approach, based on the matching of parton showers to analytic calculations at higher logarithmic accuracy also seems promising. Such an approach was used already to generate predictions for the thrust distribution and several event shapes in $e^+e^- \to$ jets [107]. First results for $pp \to e^+e^-$ have been reported [108].

Logarithmic enhancements of the cross section at high energy, which are resummed in the HEJ framework [83,84] could be crucial to understanding the structure of multi-jet events at the LHC. Including these contributions in event generators may become important [109].

1.6.5 Beyond NNLO: Higgs boson production

Small x "BFKL" (or high-energy) resummation and large x "Sudakov" (or threshold/soft-gluon) resummation provide information on the all-order behavior of a wide class of hadron collider observables in two opposite kinematic limits. Because the Mellin transform of a partonic cross section $\sigma(N, \alpha_s(M^2))$ is an analytic function of the variable N which is conjugate to the longitudinal momentum scaling variable (usually called x or τ), this information provides powerful constraints on the unknown higher order perturbative corrections to the cross-section.

The use of resummation to determine approximate higher order perturbative corrections has a long history, and, in particular, approximate NNLO jet cross sections determined using results from threshold resummation [110] are routinely used in PDF fits. Recently, in Ref. [111], it was suggested that especially accurate results can be obtained if maximal use is made of analyticity constraints, by not only combining information from different kinds of resummation, but also by making sure that the known all-order analytic properties of the cross section are reproduced as much as possible. So, for instance, while as $N \to \infty$ $\sigma(N, \alpha_s(M^2)) \sim \sum_k (\alpha_s(Q^2) \ln^2 N)^k$, the cross section is expected to have poles and not cuts when $N = 0$. Indeed, a more detailed analysis reveals that the logarithmic behaviour of the cross section only arises through functions such as $\psi_0(N)$, which indeed has a simple pole at $N = 0$ even though $\psi_0(N) \sim \ln N$ as $N \to \infty$.

In Ref. [111] it was shown that indeed this approach leads to a very good approximation to the known NLO and NNLO expressions for the total cross section for Higgs production in gluon fusion with finite m_t. An approximate expression for the N^{3}LO correction to the cross section was then constructed.

The full N^{3}LO Higgs production cross section at the LHC at $\sqrt{s} = 8$ TeV, with $m_H = 125$ GeV was found to be

$$\begin{aligned}\sigma^{\mathrm{N^3LO}}_{\mathrm{approx}}(\tau, m_H^2) &= \sigma^{(0)}(\tau, m_H^2)\left[\sum_{ij}\left(\delta_{ig}\delta_{jg} + \alpha_s K^{(1)}_{ij} + \alpha_s^2 K^{(2)}_{ij}\right) + \alpha_s^3 K^{(3)}_{gg,\mathrm{approx}}\right] \\ &= \left(22.61 \pm 0.27 + 0.91 \cdot 10^{-2}\bar{g}_{0,3}\right)\ \mathrm{pb} \qquad \text{for } \mu_R = m_H \\ &= \left(24.03 \pm 0.45 + 1.55 \cdot 10^{-2}\bar{g}_{0,3}\right)\ \mathrm{pb} \qquad \text{for } \mu_R = m_H/2,\end{aligned} \tag{1.6}$$

using the NNPDF2.1 PDF set with $\alpha_s(M_z) = 0.119$, where the error shown is an estimate of the uncertainty in the approximation procedure, and the coefficient $\bar{g}_{0,3}$ is unknown. The known perturbative behaviour of the coefficients $g_{0,i}$, which provide constant corrections to the cross section (i.e. neither logarithmically enhanced nor power-suppressed as $N \to \infty$) suggests that $\bar{g}_{0,3}$ is possibly of order ten. The renormalization scale dependence of the contribution from the gluon-gluon channel to the cross section is shown in Fig. 1-10 for various choices of the collider energy (red band), and compared to the exact LO, NLO, and NNLO results, and also to the a different soft approximation and its collinear improvement (see below). Note that the factorization scale dependence of the result is known to be essentially negligible even at LO, more so at NLO and NNLO.

The main features of this approximate result are the following:

- The perturbative expansion converges quite slowly: in particular, it is clear that at each order the next-order result is not contained within the range found varying the scale by a factor two about either m_H or $m_H/2$.
- The perturbative expansion converges better as the collider energy increases. The reason for this can be understood by computing the value of N which dominates the cross-section [112], which is fully determined by the collider energy and the Higgs mass, and then studying the perturbative behavior of the cross section for the given value of N (see Fig. 1-11).
- For all collider energies, the scale dependence is considerably reduced by the inclusion of the N^{3}LO corrections.
- The central prediction of Ref. [111], Eq. (1.6), amounts to a rather substantial correction, of order of 17% for $\mu_R = m_H$ at LHC 8 TeV.
- The N^{3}LO truncation of the resummed result of Ref. [113], together with its collinear improvement according to Ref. [114] would predict a rather smaller correction to the NNLO result, of order of 6% for $\mu_R = m_H$.
- The whole NNLL correction to the NNLO result from Ref. [113] modifies the NNLO result by about 8%, 6% of which, as mentioned, comes from the N^{3}LO, and the remaining 2% or so from higher orders. This means that the resummation is perturbative in this region. It mostly amounts to a prediction for the N^{3}LO correction.
- The discrepancy between the prediction of a 6% correction N^{3}LO (expanding out the resummation of Ref. [113]) and a a 17% correction (using the approximation of Ref. [111]) is partly due to the choice of the value for the constant $\bar{g}_{0,3}$. In fact, using the value of the constant which is implicit in the resummed result of Ref. [113] reduces the N^{3}LO correction of Eq. (1.6) from about 17% to about 12%. The remaining difference is due to the (allegedly more accurate) approximation of Ref. [111].

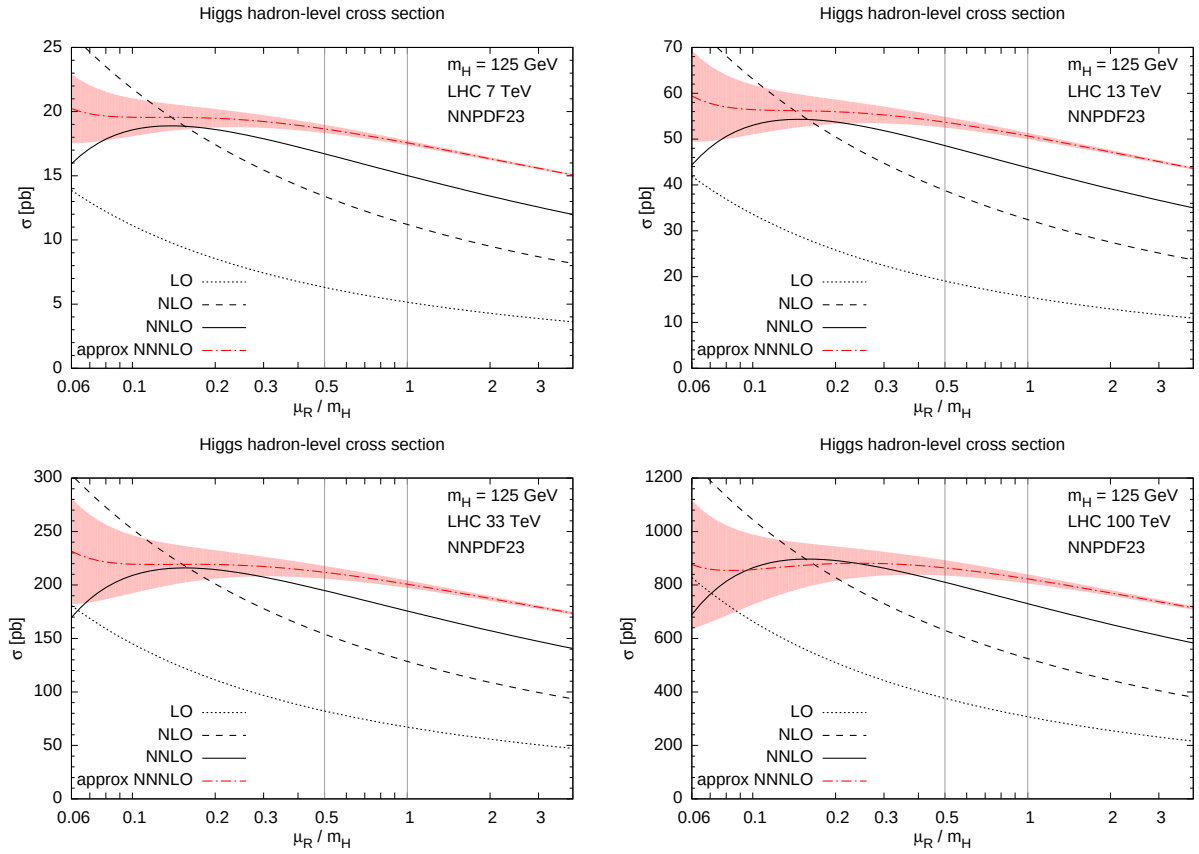


Figure 1-10. *Dependence on the renormalization scale of the LO, NLO, NNLO and approximate N^3LO contribution from the gluon-gluon channel to the total cross section for Higgs production at a proton-proton collider with four different values of the collider energy. The results shown are obtained using the NNPDF2.3 PDF set with $\alpha_s(M_Z^2) = 0.118$*

- The difference between the approximation of Ref. [111] and the expansion of the resummed result is mostly due to the fact that the soft approximation in Ref. [111] is designed to preserve the small N singularity structure. The explicit inclusion of the correct small N terms from the "BFKL" resummation stabilized somewhat the scale dependence at the very lowest edge $\mu_R/m_H < 0.1$ of the scale variation range of Fig. 1-10, but it otherwise has a small impact.
- The scale dependence of the N^{3}LO result was also determined in Ref. [115] as a function of the value of the cross-section at the reference scale $\mu_R = m_H/2$. It was found that if this value is such that the scale dependence of the N^{3}LO is smaller than that of the NNLO, then the N^{3}LO is in the same ballpark as found in Ref. [111].

There are ongoing efforts to complete a full N^{3}LO calculation of the $gg \to H$ cross section, i.e. to provide the value of the coefficient $\bar{g}_{0,3}$ in Eq. 1.6. Given the slow convergence of the perturbative series for this process, a full calculation to this order may be necessary to achieve the needed theoretical precision for Higgs production, both for 14 TeV and for still higher energies. An extraction of PDFs at N^{3}LO is strictly needed in order to have a complete prediction for a hadron-collider cross section at N^{3}LO. In particular, the DGLAP kernels which control the Q^2 evolution of the PDFs would need to be computed to one higher

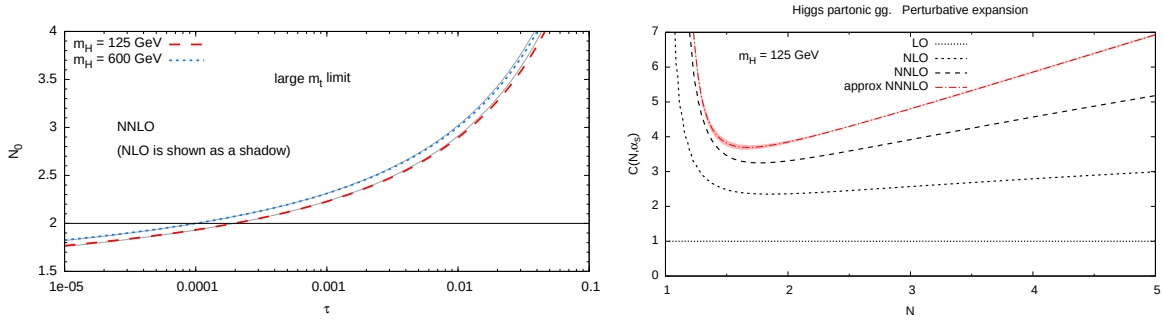


Figure 1-11. *Position of the saddle-point value of N which dominates the Mellin-space cross section for production of a 125 GeV Higgs boson in gluon fusion as a function of the collider energy (left), and perturbative expansion of the cross-section (right)*

order than currently known. This calculation is unlikely to be performed soon. However, it is easy to check that the shifts in predicted Higgs cross sections upon changing from NLO to NNLO PDFs is much smaller than the change induced by going from NLO to NNLO in the coefficient function, once the value of α_s is fixed [116]. This mismatch in the order of perturbation theory and the PDF order is therefore likely not a major phenomenological obstacle.

1.6.6 Wishlist for higher order QCD and EW corrections

The Les Houches NLO wish list, consisting of calculations that were phenomenologically important for LHC physics, and were feasible but difficult to calculate at NLO in perturbative QCD, was started in 2005. After being incremented in 2007 and 2009 it was terminated in 2011. By 2011, every calculation on the wish list had been completed, and technology had advanced far enough that any reasonable multi-parton calculation could be carried out at NLO using semi-automated technology. In 2013, the NLO QCD wish list was replaced by one focussing on NNLO and the combination of QCD and EW corrections, the new calculational frontier. The inclusion of electroweak corrections is vital given the precision inherent at NNLO. The new wish list [6] is shown in Tables 1-3, 1-4 and 1-5, giving the level to which the current calculation is known, and the level which is desired for full exploitation of physics at the LHC and higher energy hadron-hadron colliders. For the Higgs boson processes listed in Table 1-3 the improved calculations will enable more accurate extractions of Higgs couplings. The processes involving heavy quarks and jets, Table 1-4, will predominantly provide better extractions of PDFs. The vector boson processes given in Table 1-5 will be essential in investigating the precise nature of electroweak symmetry breaking, by providing more accurate predictions for channels that are sensitive to vector boson scattering at high energy and to anomalous cubic and quartic gauge boson couplings.

Until recently, the state-of-the-art for NNLO was the calculation of $2 \to 1$ processes. Within the last few years, several calculations of $2 \to 2$ processes have been completed. Indeed, the year 2013 has seen the completion of a number of landmark calculations at NNLO, namely the total cross section for top pair production [34] and first approximations of jet production [22] and the Higgs + jet process [117]. It is noteworthy that the wish list even contains $2 \to 3$ processes at NNLO. Adding to the complexity is the need for the inclusion of decays for many of the massive final state particles. Given the recent progress in the

[6] To appear in the 2013 Les Houches proceedings.

field, it is difficult to speculate as to what length of time will be needed for the completion of this new list, but a period of 10 years may be a reasonable estimate.

Note that for many processes the higher order QCD and the higher order EW corrections are currently known separately, while the desire is to have combined corrections, often at NNLO in QCD and NLO in EW. One of the ambiguities in situations where the corrections are known separately is whether the two corrections are multiplicative or additive, i.e., whether the EW corrections are affected by the (often) large QCD corrections. The degree to which the corrections are multiplicative or additive no doubt depends on the particular process and even on the observable within that process. The joint calculations posited here will resolve this ambiguity.

1.7 Electroweak corrections and Sudakov logarithms

At future high-energy collider experiments the electroweak (EW) radiative corrections are generally expected to become more important due to the fact that they include terms of the form, $\alpha_{\rm w} \ln^2\left(Q^2/M_{\rm W}^2\right)$, where Q denotes the energy scale of the hard-scattering process, $M_{\rm W}$ is the W-boson mass, and $\alpha_{\rm w} = \alpha/\sin^2\theta_{\rm w} = e^2/(4\pi\sin^2\theta_{\rm w})$ with $\theta_{\rm w}$ denoting the weak mixing angle. The corrections that contain such terms, called Sudakov logs, are generated by diagrams in which virtual and real gauge bosons are radiated by external leg particles. They correspond to the soft and collinear singularities appearing in QED and QCD, i.e. when massless gauge bosons are involved. At variance with this latter case, the weak boson masses act as a physical cutoff on these "singularities", so that virtual and real weak bosons corrections can be considered separately. Experimentally the radiation of real weak bosons is in principle detectable and event selections can me made such that it is not included. In this case the physical effect of virtual corrections is singled out and can amount to several tens of per cent, or more. The one-loop Sudakov logs are naturally included in any complete calculation of NLO EW radiative corrections to a given process.

Often, including only the effect of double and single Sudakov logs can be a reasonable approximation to the full NLO electroweak corrections for a process. This approach misses finite contributions of order α, but can work very well in the Sudakov regime, where s and $|t|$ are both large ($\gg m_W^2$). This type of approach is well-suited to implementation by process-independent methods in Monte Carlo event generators.

For many of the interesting kinematic regions at both the LHC, and at higher energy colliders, there can be simultaneously large QCD corrections and large electroweak corrections. In the absence of a calculation that accounts for the presence of both corrections simultaneously, one can provide an interim solution by either multiplying or adding together the separate QCD and EW corrections. These two possibilities lead to cross sections of the schematic forms

$$\begin{aligned} \sigma_{add} &\sim \sigma_0\left[1 + \mathcal{O}(\alpha_s) + \mathcal{O}(\alpha_{EW})\right], \\ \sigma_{mult} &\sim \sigma_0\left[1 + \mathcal{O}(\alpha_s)\right] \times \left[1 + \mathcal{O}(\alpha_{EW})\right], \end{aligned} \tag{1.7}$$

where the combinations are denoted by σ_{add} and σ_{mult}, and the Born-level cross section by σ_0. Expanding the product of brackets in σ_{mult} shows that these two prescriptions differ by terms of order $\mathcal{O}(\alpha_s\alpha_{EW})$. Only a complete calculation of these mixed corrections can determine whether either of these prescriptions provides an accurate description of the perturbative expansion. Even in current data, this ambiguity can result in significant uncertainties in the comparison of standard model predictions to the data. The relative $\mathcal{O}(\alpha_s\alpha_{EW})$ corrections have been calculated for inclusive Higgs production, in a tractable parametric limit [118]. And recently, the relative $\mathcal{O}(\alpha_s\alpha_{EW})$ corrections have also been calculated for W and Z production, using a resonance expansion around the W/Z pole [119]. While both results suggest that the multiplicative combination is a good approximation, this conclusion is not necessarily applicable to other processes.

Process	known	desired	details
H	dσ @ NNLO QCD dσ @ NLO EW finite quark mass effects @ NLO	dσ @ NNNLO QCD + NLO EW MC@NNLO finite quark mass effects @ NNLO	H branching ratios and couplings
H + j	dσ @ NNLO QCD (g only) dσ @ NLO EW finite quark mass effects @ LO	dσ @ NNLO QCD + NLO EW finite quark mass effects @ NLO	H p_T
H + 2j	σ_{tot}(VBF) @ NNLO(DIS) QCD dσ(gg) @ NLO QCD dσ(VBF) @ NLO EW	dσ @ NNLO QCD + NLO EW	H couplings
H + V	dσ @ NNLO QCD dσ @ NLO EW	with $H \to b\bar{b}$ @ same accuracy	H couplings
t$\bar{t}$H	dσ(stable tops) @ NLO QCD	dσ(top decays) @ NLO QCD + NLO EW	top Yukawa coupling
HH	dσ @ LO QCD (full m_t dependence) dσ @ NLO QCD (infinite m_t limit)	dσ @ NLO QCD (full m_t dependence) dσ @ NNLO QCD (infinite m_t limit)	Higgs self coupling

Table 1-3. *Wishlist part 1 – Higgs (*V = W, Z*).*

Process	known	desired	details
t$\bar{t}$	σ_{tot} @ NNLO QCD dσ(top decays) @ NLO QCD dσ(stable tops) @ NLO EW	dσ(top decays) @ NNLO QCD + NLO EW	precision top/QCD, gluon PDF, effect of extra radiation at high rapidity, top asymmetries
t$\bar{t}$ + j	dσ(NWA top decays) @ NLO QCD	dσ(NWA top decays) @ NNLO QCD + NLO EW	precision top/QCD top asymmetries
single-top	dσ(NWA top decays) @ NLO QCD	dσ(NWA top decays) @ NNLO QCD (t channel)	precision top/QCD, V_{tb}
dijet	dσ @ NNLO QCD (g only) dσ @ NLO weak	dσ @ NNLO QCD + NLO EW	Obs.: incl. jets, dijet mass $\to$ PDF fits (gluon at high x) $\to \alpha_s$
3j	dσ @ NLO QCD	dσ @ NNLO QCD + NLO EW	Obs.: $R3/2$ or similar $\to \alpha_s$ at high scales dom. uncertainty: scales
γ + j	dσ @ NLO QCD dσ @ NLO EW	dσ @ NNLO QCD +NLO EW	gluon PDF γ + b for bottom PDF

Table 1-4. *Wishlist part 2 – jets and heavy quarks.*

Process	known	desired	details
V	dσ(lept. V decay) @ NNLO QCD dσ(lept. V decay) @ NLO EW	dσ(lept. V decay) @ NNNLO QCD + NLO EW MC@NNLO	precision EW, PDFs
V + j	dσ(lept. V decay) @ NLO QCD dσ(lept. V decay) @ NLO EW	dσ(lept. V decay) @ NNLO QCD + NLO EW	Z + j for gluon PDF W + c for strange PDF
V + jj	dσ(lept. V decay) @ NLO QCD	dσ(lept. V decay) @ NNLO QCD + NLO EW	study of systematics of H + jj final state
VV$'$	dσ(V decays) @ NLO QCD dσ(stable V) @ NLO EW	dσ(V decays) @ NNLO QCD + NLO EW	off-shell leptonic decays TGCs
gg $\to$ VV	dσ(V decays) @ LO QCD	dσ(V decays) @ NLO QCD	bkg. to $H \to VV$ TGCs
Vγ	dσ(V decay) @ NLO QCD dσ(PA, V decay) @ NLO EW	dσ(V decay) @ NNLO QCD + NLO EW	TGCs
Vb$\bar{\text{b}}$	dσ(lept. V decay) @ NLO QCD massive b	dσ(lept. V decay) @ NNLO QCD massless b	bkg. for VH $\to$ b$\bar{\text{b}}$
VV$'\gamma$	dσ(V decays) @ NLO QCD	dσ(V decays) @ NLO QCD + NLO EW	QGCs
VV$'$V$''$	dσ(V decays) @ NLO QCD	dσ(V decays) @ NLO QCD + NLO EW	QGCs, EWSB
VV$'$ + j	dσ(V decays) @ NLO QCD	dσ(V decays) @ NLO QCD + NLO EW	bkg. to H, BSM searches
VV$'$ + jj	dσ(V decays) @ NLO QCD	dσ(V decays) @ NLO QCD + NLO EW	QGCs, EWSB
$\gamma\gamma$	dσ @ NNLO QCD		bkg to $H \to \gamma\gamma$

Table 1-5. *Wishlist part 3 – EW gauge bosons* (V = W, Z).

In the following each of these issues will be discussed in turn. Also, the whitepaper by K. Mishra *et al.* [120] presents a nice summary of implications of electroweak corrections at high energies.

1.7.1 Importance of Sudakov logarithms for basic processes

Dijet production The inclusive production of two jets (dijets) allows for a detailed study of QCD at TeV energies. It is also the main background for searches of new heavy particles from Beyond Standard Model (BSM) physics decaying into dijet signatures. Inclusive jet and dijet production have been analyzed by the ATLAS [57] and CMS [121] Collaborations at $\sqrt{s} = 7$ and 8 TeV showing sensitivity to dijet invariant masses of up to 5 TeV and jet transverse momenta of up to 2 TeV at the LHC. At the current level of experimental and theoretical accuracy, the SM is able to describe data well. However, the size of the EW correction [122] is comparable to the experimental uncertainty for the highest p_T bins, as shown in Fig. 1-12. Given this sensitivity we thus say that the dijet measurement at $\sqrt{s} = 8$ TeV has already started probing the "Sudakov zone". The electroweak corrections in Ref. [122] comprise NLO corrections through order $\alpha_s^2\alpha$ as well as

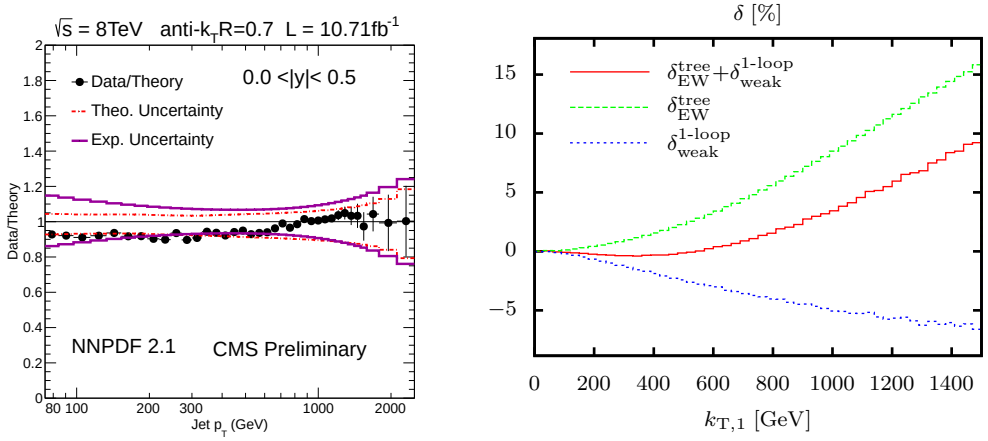


Figure 1-12. *The uncertainties in the jet transverse momentum measured in 8 TeV pp collisions [121] (left) and the relative magnitude of electroweak corrections in pp collisions at 8 TeV [122] (right).*

additional tree-level contributions of order $\mathcal{O}\left(\alpha_s\alpha,\, \alpha^2\right)$. The tree-level contributions arise through diagrams such as the ones shown in Fig. 1-13 and correspond to $|d_1 + d_2|^2$ and the interference $(d_1 + d_2)d_3^*$. [7] The tree-level contributions are typically of the same size as the loop corrections at $\sqrt{s} = 8$ TeV. The total correction to the integrated cross section is negligible, typically staying below the per-cent level. However, the Sudakov logarithms affect the tails of the distributions in the dijet invariant mass and in the transverse momenta of the two jets. The magnitude of the corrections at $\sqrt{s} = 8$ TeV and 14 TeV were found to be similar in Ref. [122].

Results for the same same observable at $\sqrt{s} = 33$ and 100 TeV are shown in Fig. 1-14. The 1-loop virtual corrections do not depend strongly on the collider energy, while the tree-level corrections decrease with $\sqrt{s}$. The latter effect can be explained by the fact that the tree-level contributions do not depend on the gluon distribution and are therefore relatively less important. The cancellation between the loop and tree contributions is therefore less perfect and, as a result, the virtual negative corrections dominate in the

[7] The contribution $|d_3|^2$ is of course part of the leading order QCD result.

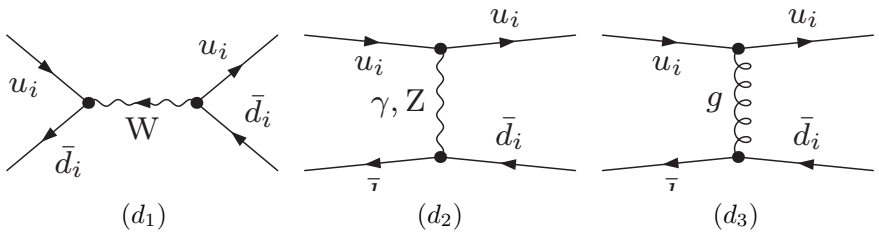


Figure 1-13. *Representative tree-level diagrams that enter the calculation of EW corrections to dijet production presented in Ref. [122].*

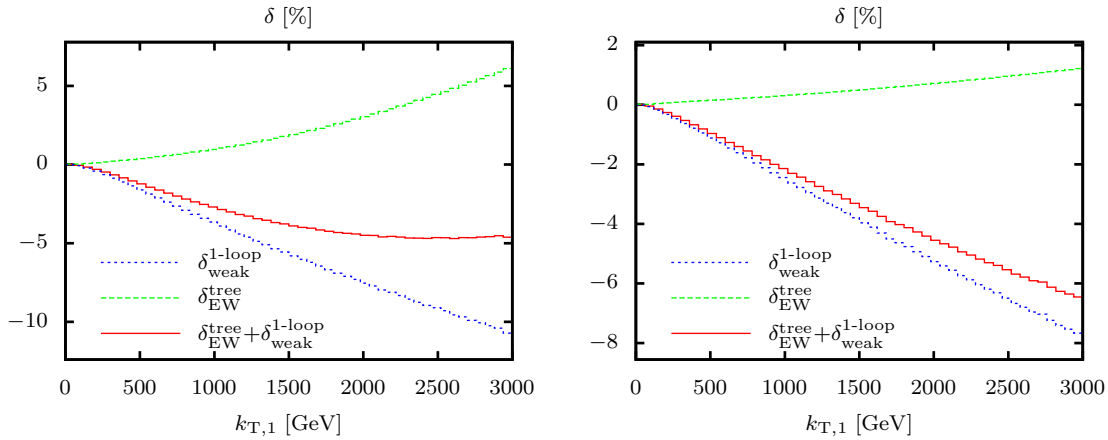


Figure 1-14. *The relative magnitude of electroweak corrections on the leading jet transverse momentum [122] in pp collisions at 33 TeV (left) and 100 TeV (right).*

kinematic tails at large $\sqrt{s}$. Since the kinematic reach becomes larger as $\sqrt{s}$ increases, these corrections will become progressively more important.

Inclusive vector boson production The production of a single electroweak boson is one of the basic hard-scattering processes at the LHC and constitutes major background for BSM searches like $W' \to \ell\nu$ and $Z' \to \ell\ell$ and important SM measurements like $H \to ZZ^* \to 4\ell$. Like in the diboson case, the virtual corrections due to electroweak-boson exchanges can become quite significant. Since we are considering single electroweak-boson production, without additional radiation of soft or collinear W or Z bosons, the cross section will contain Sudakov logarithms that can be as large as 20% for boson $p_T \sim 1$ TeV at the LHC. These effects need to be included for precise prediction of kinematic distribution in the region $p_T \gg M_{\mathrm{V}}$. Inclusive W and Z spectra have been analyzed by the ATLAS [123] and CMS [124] collaborations at $\sqrt{s} = 8$ TeV showing sensitivity to invariant masses of up to 2 TeV and boson transverse momenta of up to 800 GeV. The current experimental uncertainty for invariant masses above 1 TeV is somewhat larger than the size of the EW corrections computed in Ref. [125]. However, the same measurements at 14 TeV will be sensitive to probing the Sudakov zone. Studies of these effects up to 100 TeV indicate that the relative corrections depend only on p_T and are are essentially independent of $\sqrt{s}$. However, since the kinematic reach naturally increases, these corrections will become progressively more important [120].

Vector boson production in association with jets The production of a W or Z boson in association with jets has played a special role in collider physics. It was the dominant background to top-quark pair production at the Tevatron. At the LHC it remains an important background for processes involving lepton, missing energy, and jets. Prominent examples are measurements of top quarks, Higgs boson, and multi-boson production and BSM searches for supersymmetry signatures. Such measurements also permit stringent tests of the predictions of the Standard Model. Measurements of W and Z boson production in association with multiple jets have been made by the ATLAS [126–128] and CMS [129–131] collaborations at $\sqrt{s} = 7$ and 8 TeV, showing sensitivity to boson and leading jet transverse momenta of up to about 500 GeV at the LHC.

The full NLO EW corrections for W + 1-jet production have been computed for the final state containing a charged lepton, a neutrino, and a hard jet [132]. The full NLO EW corrections for Z + 1-jet production have also been computed for the final state containing two charged leptons and a hard jet [133], and for the monojet scenario, where the Z decays into two undetected neutrinos [134]. The overall magnitude of these corrections as a function of boson p_T is similar to the inclusive W/Z case. As in that case, the current experimental uncertainty for the highest p_T bins is somewhat larger than the size of the EW corrections. The same measurements at 14 TeV will be sensitive to probing the Sudakov zone.

Results from repeating the same calculation as in Ref. [133] for Z + 1-jet events at $\sqrt{s} = 100$ TeV are listed in Table 1-6 as a function of the leading jet p_T. The relative corrections show very weak dependence on $\sqrt{s}$ and depend more strongly on the leading jet p_T. A similar statement holds for the dependence of the corrections on the invariant mass of the boson system. As the kinematic reach increases with increase in $\sqrt{s}$ these corrections will become progressively more important.

Vector-boson pair production Vector-boson pair production is among the most important SM benchmark processes at the LHC, because of its connection to the electroweak symmetry breaking. It is a probe of Higgs boson production in $gg/q\bar{q} \to H \to WW^*$, ZZ^*, $\gamma\gamma$ processes, and of gauge boson self interactions. Diboson production can also help to gain a deeper understanding of the electroweak interaction in general, and to test the validity of the SM at highest energies.

The case of WW production at large invariant masses or large W p_T is the kinematic regime of high interest. It can be subject to large EW corrections. This kinematic regime has recently been analyzed by the ATLAS [135] and CMS [136] collaborations at $\sqrt{s} = 8$ TeV, showing sensitivity to invariant masses of up to 1 TeV and boson transverse momenta of up to 500 GeV. The size of the experimental uncertainty for the highest kinematic end points is comparable with the full one-loop EW corrections to on-shell WW production [56, 137]. As noted in Ref. [56], the corrections due to photon-induced channels can be large at high energies, while radiation of additional massive vector bosons does not influence the results significantly. Results from repeating the exact same calculation for $\sqrt{s} = 33$ TeV and 100 TeV are shown in Fig. 1-15. While the relative NLO EW corrections hardly depend on the collider energy, the relative photon-induced contributions are suppressed at to larger values of $\sqrt{s}$. As a result, the overall corrections show very little dependence on $\sqrt{s}$. However, as in the case of other processes described earlier, the EW corrections will become progressively more important with increase in $\sqrt{s}$ due to the extended kinematic reach.

Summary The above discussion represents a survey of the most abundant processes at LHC for sensitivity to electroweak corrections at various proton-proton collision energies relevant for LHC and future hadron colliders. The observations are summarized in Table 1-7. For most processes, the overall electroweak corrections do not change much as the collider energy increases. However, the corrections become more important at high collider energies simply because of the increase in kinematic reach at high $\sqrt{s}$, where the corrections are inherently large.

$pp \to \ell^+\ell^-$ jet $+ X$ at $\sqrt{s} = 100\,\text{TeV}$

$p_{\text{T,jet}}$/ GeV	$100 - \infty$	$200 - \infty$	$400 - \infty$	$800 - \infty$	$2000 - \infty$	$4000 - \infty$
$\sigma^{\mu=M_Z}_{\text{Born}}$/ pb	114.29(1)	23.772(3)	3.5452(4)	0.42003(4)	0.017238(1)	0.00094403(9)
$\sigma^{\text{var}}_{\text{Born}}$/ pb	118.30(1)	23.762(3)	3.1922(3)	0.31583(3)	0.0091290(9)	0.00035205(3)
$\delta^{\mu=M_Z}_{\text{EW}}$/%	−5.62(1)	−9.57(1)	−16.86(2)	−27.11(8)	−43.5(1)	−58.8(1)
$\delta^{\text{rec},\mu=M_Z}_{\text{EW}}$/%	−4.65(3)	−8.72(2)	−16.08(2)	−26.29(4)	−43.15(7)	−58.5(2)
$\delta^{\text{var}}_{\text{EW}}$/%	−5.50(1)	−9.29(1)	−16.38(3)	−26.36(4)	−43.2(2)	−57.5(1)
$\delta^{\text{rec,var}}_{\text{EW}}$/%	−4.48(2)	−8.52(2)	−15.62(2)	−25.64(4)	−42.21(7)	−56.8(1)
$\delta^{\mu=M_Z}_{\text{QCD}}$/%	97.4(2)	146.0(1)	215.2(2)	288.7(2)	378.0(3)	472.6(5)
$\delta^{\text{var}}_{\text{QCD}}$/%	85.4(2)	130.0(2)	201.7(1)	298.8(2)	487.9(3)	769.0(7)
$\delta^{\mu=M_Z}_{\text{QCD,veto}}$/%	35.7(2)	54.2(1)	66.7(1)	61.3(1)	13.2(2)	−43.1(1)
$\delta^{\text{var}}_{\text{QCD,veto}}$/%	29.6(2)	47.4(1)	65.5(1)	76.4(3)	65.6(2)	51.5(1)
$\delta^{\mu=M_Z}_{\gamma,\text{Born}}$/%	0.1218(3)	0.1400(4)	0.1681(5)	0.2114(7)	0.291(1)	0.382(1)
$\delta^{\text{var}}_{\gamma,\text{Born}}$/%	0.1407(3)	0.1799(5)	0.2482(7)	0.365(1)	0.630(2)	1.006(5)
$\sigma^{\text{var}}_{\text{full,veto}}$/ pb/%	147.0(2)	32.86(4)	4.767(4)	0.475(1)	0.01124(2)	0.0003343(7)

Table 1-6. *Z + 1-jet production: Integrated cross sections for different cuts on the p_T of the leading jet (jet with highest p_T) at a proton-proton collider with $\sqrt{s} = 100$ TeV. The LO results are shown both for a variable and for a constant scale. The relative EW corrections δ_{EW} are given with and without lepton-photon recombination. The QCD corrections δ_{QCD} are presented for a fixed as well as a for variable scale and with or without employing a veto on a second hard jet. The EW corrections and the corrections due to photon-induced processes, δ_γ, are presented for the variable scale. Finally, the last row shows the full NLO cross section $\sigma^{\text{var}}_{\text{full,veto}}$. The error from the Monte Carlo integration for the last digit(s) is given in parenthesis as far as significant. See Ref. [133] for details.*

Table 1-7. *Are we in the Sudakov zone yet?*

Process	$\sqrt{s} = 8$ TeV	$\sqrt{s} = 14$ TeV	$\sqrt{s} = 33, 100$ TeV
Inclusive jet, dijet	Yes	Yes	Yes
Inclusive W/Z tail	$\sim$ Yes	Yes	Yes
Wγ, Zγ tail ($\ell\nu\gamma, \ell\ell\gamma$)	No	$\sim$ Yes	Yes
W/Z + jets tail	$\sim$ Yes	Yes	Yes
WW leptonic	Close	$\sim$ Yes	Yes
WZ, ZZ leptonic	No	No	Yes
WW, WZ, ZZ semileptonic	$\sim$ Yes	Yes	Yes

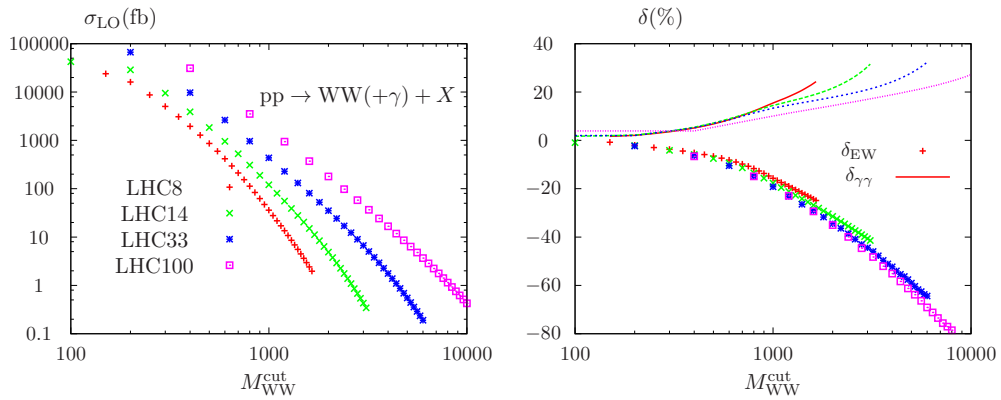


Figure 1-15. *WW production: Total cross sections for W-pair production for different cuts on WW invariant mass evaluated at pp collision energies of 8, 14, 33, and 100 TeV. Left: absolute predictions; right: relative electroweak corrections ($\delta_{\rm EW}$) and relative contributions from the $\gamma\gamma$-induced process ($\delta_{\gamma\gamma}$).*

1.7.2 Interplay of electroweak and QCD corrections in Drell-Yan production

The effects of electroweak Sudakov logarithms on more differential quantities, and their interplay with higher-order QCD corrections, have been studied for the example case of lepton-pair production via the Drell-Yan mechanism at a 33 TeV pp collider. The results shown are obtained with the numerical program FEWZ [62, 63, 65], which additively combines higher-order QCD and electroweak corrections. MSTW PDFs at the appropriate order in QCD perturbation theory are used. Shown first in Fig. 1-16 is the lepton-pair invariant mass distribution, with minimal acceptance cuts imposed on the transverse momenta and pseudorapidities of the leptons. The shift due to NLO QCD corrections alone is shown, as is the result of combining the full NLO electroweak correction with the QCD one. Both shifts are normalized to the leading-order prediction. Over a broad range of invariant masses, the QCD corrections increase the cross section by $20 - 30\%$. The electroweak corrections grow in importance with invariant mass, and lead to a decrease in the cross section. The electroweak corrections begin to overtake the QCD ones at $M_{ll} \approx 5$ TeV, and the reduction in the cross section from the combined corrections reaches 30% at invariant masses of 15 TeV.

The shifts induced by the combined QCD and electroweak corrections on the lepton differential distributions are considered next. The cross section is first divided into the following invariant mass bins: $M_{ll} \in [500\,\text{GeV}, 1\,\text{TeV}]$, $M_{ll} \in [1\,\text{TeV}, 5\,\text{TeV}]$, and $M_{ll} \in [5\,\text{TeV}, 20\,\text{TeV}]$. The lepton transverse momenta and pseudorapidity distributions in each bin are then studied. The results are shown in Figs. 1-17, 1-18, and 1-19. The QCD and electroweak corrections have the same shape as a function of lepton p_T. The dips appearing in the corrections at half the lower bin edge, and the rise at the upper bin edge, are artifacts produced by the Jacobian peaks present in the leading-order result. An interesting feature emerges in the lepton η distributions at higher invariant masses. The electroweak corrections act more strongly for central pseudorapidities, leading to a dip in the combined corrections that is quite large for the highest invariant mass bin.

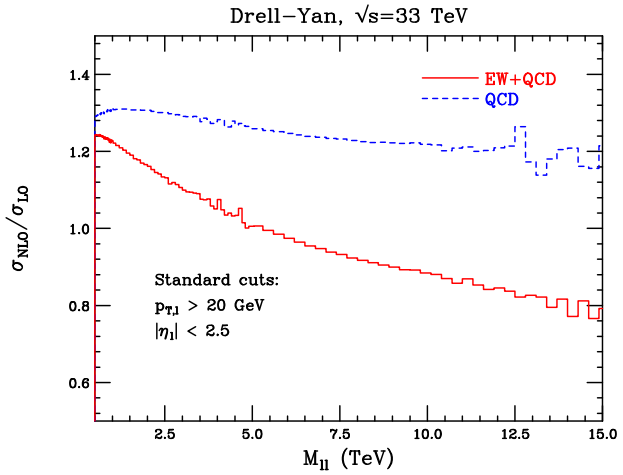


Figure 1-16. *QCD corrections and combined electroweak-QCD corrections to lepton-pair production as a function of the lepton-pair invariant mass, at a 33 TeV pp collider.*

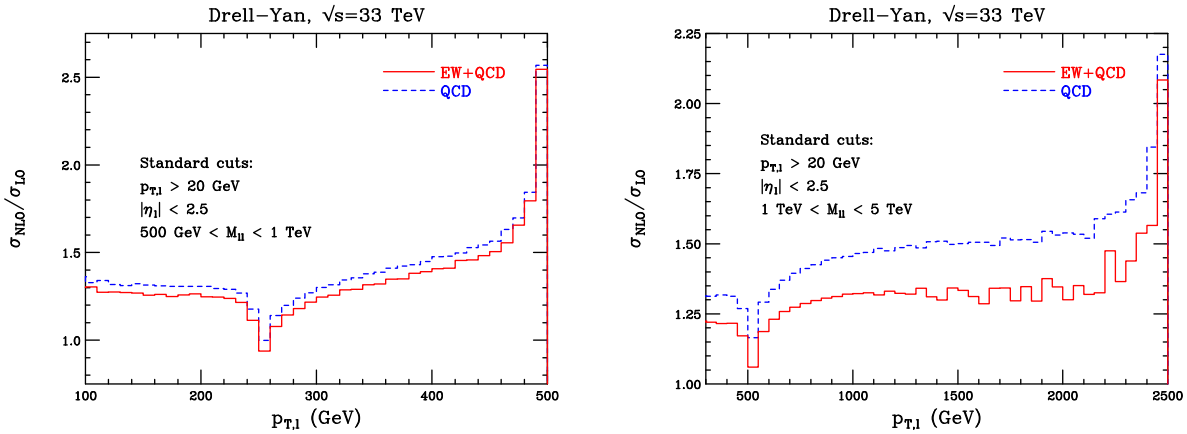


Figure 1-17. *QCD corrections and combined electroweak-QCD corrections to lepton-pair production as a function of the lepton transverse momentum, at a 33 TeV pp collider. Results for two bins of lepton-pair invariant mass, $M_{ll} \in [500\,\text{GeV}, 1\,\text{TeV}]$, and $M_{ll} \in [1\,\text{TeV}, 5\,\text{TeV}]$, are shown.*

1.7.3 Electroweak corrections to $Z + 2$ and $Z + 3$ jets hadroproduction in the Sudakov zone

Important searches for new physics (NP) beyond the Standard Model (SM) at present and future proton-proton (pp) colliders are based on the analysis of events with jets and missing transverse momentum ($\not{p}_T$). The main SM backgrounds to this signature are given by the production of weak bosons accompanied by jets ($W/Z + n$ jets), pure QCD multiple jet events and $t\bar{t}$ production. Among these processes only $Z + n$ jets (in particular with $Z \to \nu\bar{\nu}$) constitutes an irreducible background and is particularly relevant for final states with 2 and 3 jets.

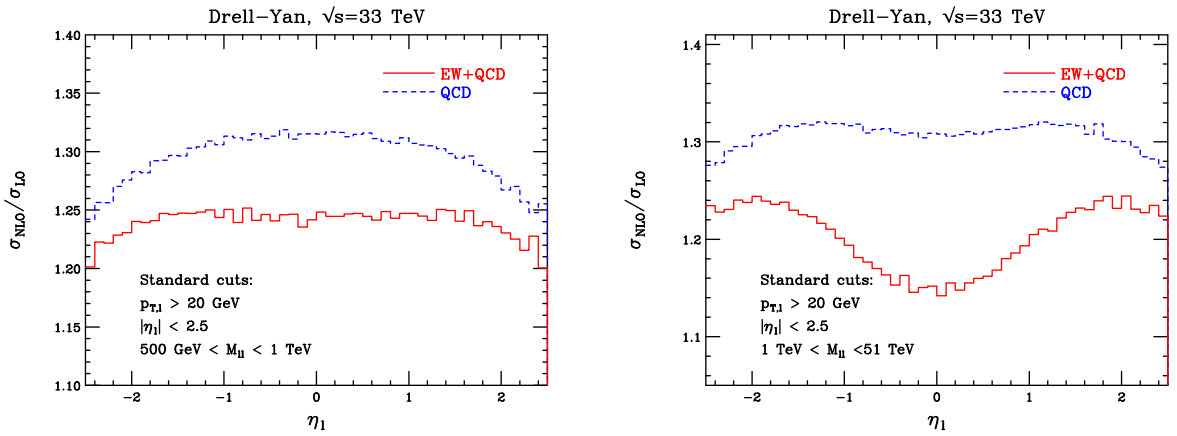


Figure 1-18. *QCD corrections and combined electroweak-QCD corrections to lepton-pair production as a function of the lepton pseudorapidity, at a 33 TeV pp collider. Results for two bins of lepton-pair invariant mass $M_{ll} \in [500\,\text{GeV}, 1\,\text{TeV}]$, and $M_{ll} \in [1\,\text{TeV}, 5\,\text{TeV}]$, are shown.*

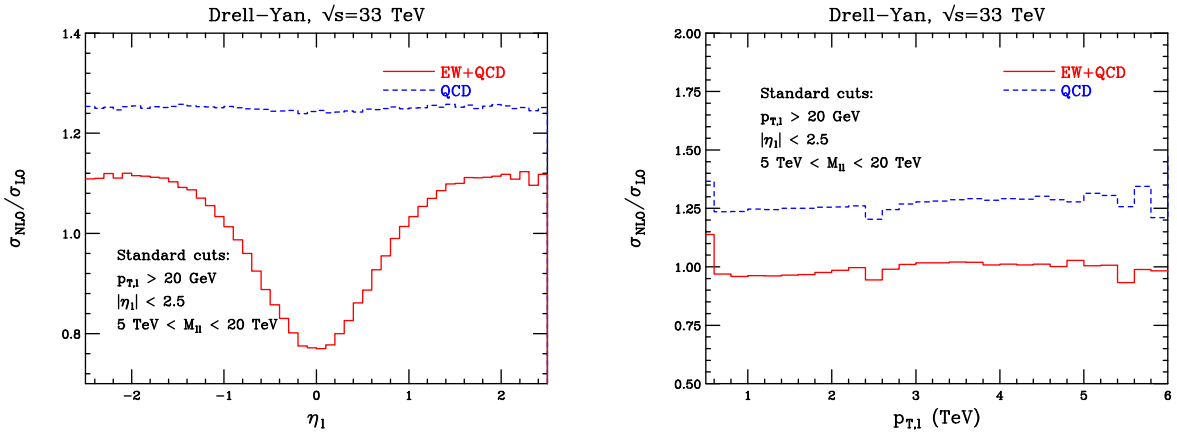


Figure 1-19. *QCD corrections and combined electroweak-QCD corrections to lepton-pair production as a function of the lepton pseudorapidity and transverse momentum, at a 33 TeV pp collider. Results for the bin of lepton-pair invariant mass $M_{ll} \in [5\,\text{TeV}, 20\,\text{TeV}]$ are shown*

The one-loop Sudakov logs are naturally included in any complete calculation of NLO EW radiative corrections to a given process. Up to now, these calculations are available for a limited class of $2 \to 2$ and $2 \to 3$ processes, see for instance [122, 132–134, 138–143], many of which have already been discussed in Section 1.7.1. On the other hand, by virtue of their universality, the Sudakov logarithmic contributions can be accounted for by means of process-independent methods, as shown in Ref. [144–154]. In particular, Denner and Pozzorini presented a method to single out the double and single Sudakov log contributions, as detailed in [149,150]. The generality of this algorithm has been recently combined [155] with the leading order matrix element event generator `ALPGEN v2.1.4` [156], to obtain a tool able to calculate NLO EW Sudakov corrections to processes involving multijet final states. Phenomenological results have been presented in Ref. [155] for the production processes $Z(\to \nu\bar{\nu}) + 2(3)$ jets in pp collisions at $\sqrt{s} = 7, 14$ TeV.

The considered processes are, at the leading order $\alpha_s^{\text{njets}}\alpha$, of neutral current type, so the EW contributions can be separated into purely weak corrections (which contain the Sudakov logs and are the subject of the

present contribution) and QED corrections. The latter can be treated separately together with their real counterparts and, for sufficiently inclusive event selections, they give rise to rather moderate corrections.

In this section, the focus is on the virtual EW Sudakov corrections to $Z+2$ and $Z+3$ jets hadroproduction, studying their scaling with the center-of-mass energy of proton-proton collisions from 14 TeV to 33 and 100 TeV. The event selections and considered observables are those of Ref. [155]. The parameters and PDF setting are the `ALPGEN` defaults. In particular, for $Z+2$ jets, the observable/cuts are those presently adopted by ATLAS [157], namely

$$\begin{aligned} & m_{\rm eff} > 1 \text{ TeV} \qquad \not{E}_T/m_{\rm eff} > 0.3 \\ & p_T^{j_1} > 130 \text{ GeV} \qquad p_T^{j_2} > 40 \text{ GeV} \quad |\eta_j| < 2.8 \\ & \Delta\phi(\vec{p}_T^{\,j},\vec{\not{E}}_T) > 0.4 \quad \Delta R_{(j_1,j_2)} > 0.4 \end{aligned} \tag{1.8}$$

where j_1 and j_2 are the leading and next-to-leading p_T jets. For the $Z+3$ jets final state the observables/cuts used by CMS [158, 159] are considered, namely

$$\begin{aligned} & H_T > 500 \text{ GeV} \qquad |\vec{\not{H}}_T| > 200 \text{ GeV} \\ & p_T^j > 50 \text{ GeV} \qquad |\eta_j| < 2.5 \quad \Delta R_{(j_i,j_k)} > 0.5 \\ & \Delta\phi(\vec{p}_T^{\,j_1,j_2},\vec{\not{H}}_T) > 0.5 \qquad \Delta\phi(\vec{p}_T^{\,j_3},\vec{\not{H}}_T) > 0.3\,, \end{aligned} \tag{1.9}$$

where $H_T = \sum_i p_{T,i}$ and $\vec{\not{H}}_T = -\sum_i \vec{p}_{T,i}$.

In Ref. [155] it has been shown that Sudakov virtual corrections to $Z+2$ and $Z+3$ jets production are negative and can be as large as about -40% at $\sqrt{s} = 7, 14$ TeV. Here that analysis is extended to c.m. energies of future hadronic colliders, namely 33 and 100 TeV. For the sake of reference, we report here some partial results from Ref. [155] corresponding to the c.m. energy of 14 TeV. Fig. 1-20 shows the effect of the Sudakov logs on the effective mass distribution in the process $Z+2$ jets according to the event selection of Eq. (1.8). All plots start from $m_{\rm eff} = 1$ TeV and have different upper limits: 5 TeV for $\sqrt{s} = 14$ TeV, 10 TeV for $\sqrt{s} = 33$ TeV and 18 TeV for $\sqrt{s} = 100$ TeV. The upper panels display the effective mass distribution at LO (blue, solid) and including the approximate NLO virtual corrections (red, dotted) due to weak bosons in the Sudakov zone as calculated with `ALPGEN`, according to Ref. [155], respectively. The lower panels show the relative corrections due to virtual weak corrections. As can be seen, the negative correction due to Sudakov logs is of the order of some tens of percent, increasing to about 40% (60%, 80%) in the extreme regions at $\sqrt{s} = 14$ (33, 100) TeV, respectively. As can be naively expected, for a given bin of the $m_{\rm eff}$ distribution, the relative EW corrections is practically the same, independently of the collider c.m. energy. It is interesting to study whether and how the effects on the $m_{\rm eff}$ distribution change when adopting acceptance cuts scaled with the c.m. energy w.r.t. the case $\sqrt{s} = 14$ TeV (for simplicity the geometrical acceptance cuts are kept fixed). Figure 1-21 shows the predictions for

$$\begin{aligned} & m_{\rm eff} > 2(7) \text{ TeV}\,, \ (\sqrt{s} = 33(100) \text{ TeV})\,, \\ & p_T^{j_1} > 260(910) \text{ GeV}\,, \ (\sqrt{s} = 33(100) \text{ TeV})\,, \\ & p_T^{j_2} > 80(280) \text{ GeV}, \ (\sqrt{s} = 33(100) \text{ TeV})\,, \end{aligned}$$

with the rest of the cuts unchanged w.r.t. Eq. (1.8). The effects of the tighter acceptance cuts are very mild, the leading effect being given by the $m_{\rm eff}$ cut.

Fig. 1-22 shows the effect of the Sudakov logs on the observable $|\vec{\not{H}}_T|$ in the process $Z+3$ jets according to the event selection of Eq. (1.9). All plots start from $|\vec{\not{H}}_T| = 0.2$ TeV and have different upper limits: 2.2 TeV for $\sqrt{s} = 14$ TeV, 4 TeV for $\sqrt{s} = 33$ TeV and 6 TeV for $\sqrt{s} = 100$ TeV. As for the $Z+2$ jets effective mass distributions, the effect of NLO weak corrections on $|\vec{\not{H}}_T|$ is large and negative, raising to about 40% (60%,

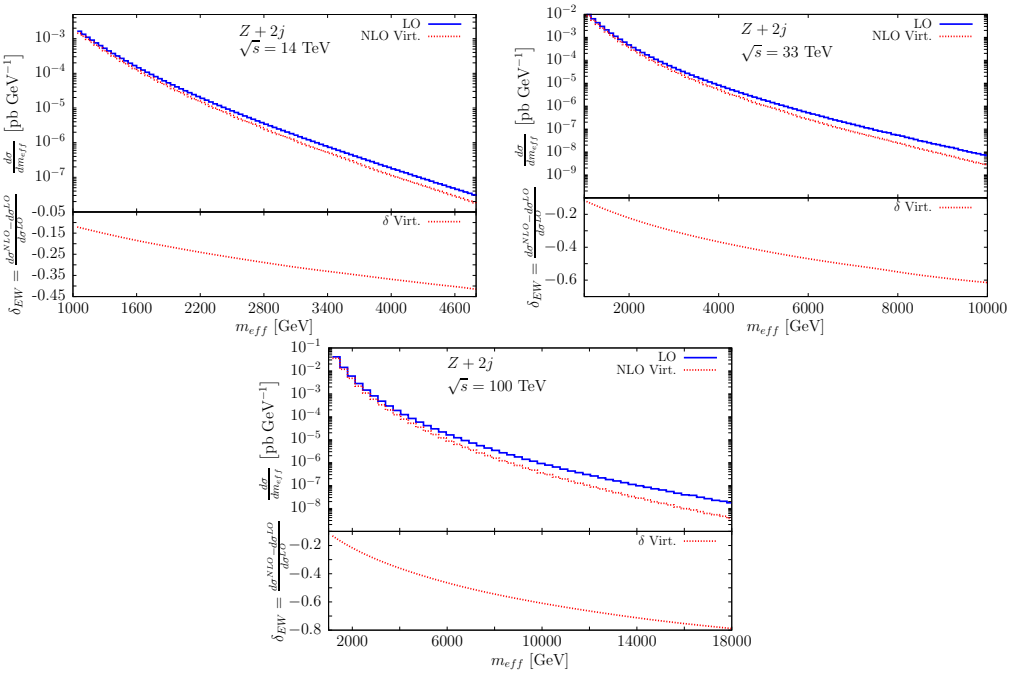


Figure 1-20. *$Z+2$ jets: ATLAS $m_{\rm eff}$ and EW correction at $\sqrt{s}=14$, 33 and 100 TeV.*

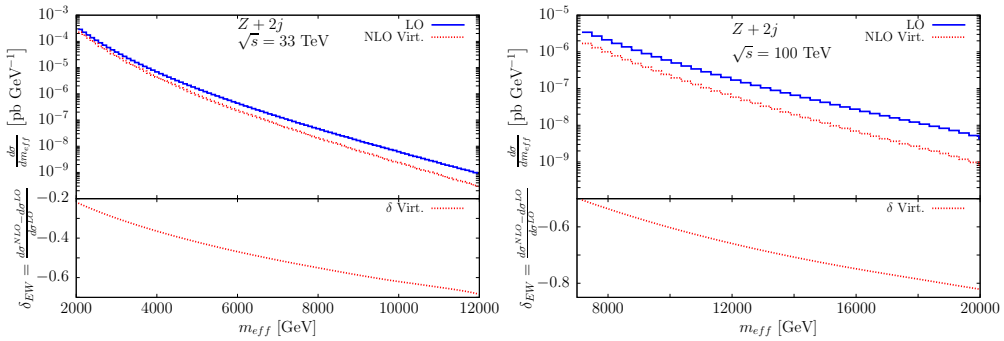


Figure 1-21. *The same as Fig. 1-20 with rescaled cuts at 33 and 100 TeV, as described in the text.*

70%) in the extreme regions at $\sqrt{s}=14$ (33, 100) TeV, respectively. For a chosen $|\vec{\not{H}}_T|$ bin, the relative effects of the corrections are quite insensitive to the change of the collider energy and of the acceptance cuts. Figure 1-23 shows the $|\vec{\not{H}}_T|$ with scaled acceptance cuts:

$$\begin{aligned} &H_T > 1(3.5)\ \text{TeV}\,,\ (\sqrt{s}=33(100)\ \text{TeV}) \\ &|\vec{\not{H}}_T| > 0.4(1.4)\ \text{TeV}\,,\ (\sqrt{s}=33(100)\ \text{TeV}) \\ &p_T^j > 100(350)\ \text{GeV}\,,\ (\sqrt{s}=33(100)\ \text{TeV})\,, \end{aligned} \tag{1.10}$$

with the rest of the cuts unchanged w.r.t. Eq. (1.9). The changes in slope in the $|\vec{\not{H}}_T|$ distributions are due to the presence of the cuts on the variable H_T.

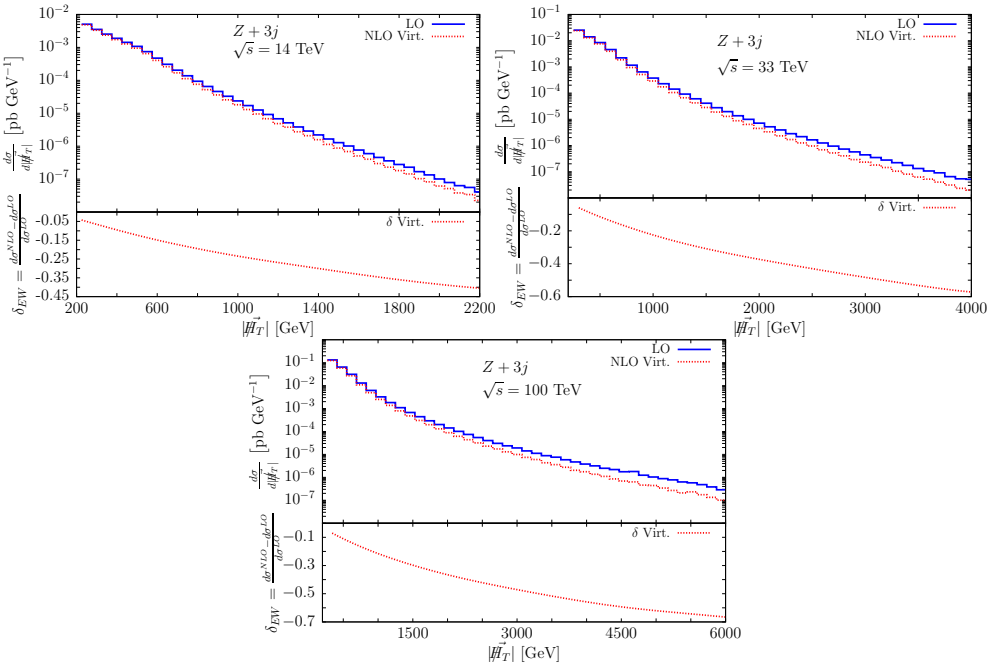


Figure 1-22. *$Z + 3$ jets: CMS $|\vec{\not{H}}_T|$ and EW correction at $\sqrt{s} = 14$, 33 and 100 TeV.*

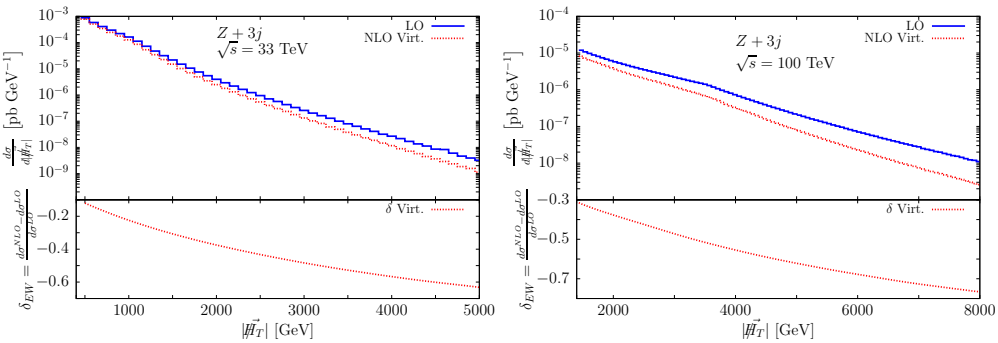


Figure 1-23. *The same as Fig. 1-22 with rescaled cuts at 33 and 100 TeV, as described in the text.*

Summary The NLO EW Sudakov corrections to $Z + n$ jets, $n = 2, 3$ have been computed using `ALPGEN`, for two key observables, m_{eff} and $|\vec{\not{H}}_T|$, that are used in NP searches at the LHC. The relative corrections do not show sensitivity to the collider energy for c.m. energies up to 100 TeV. The corrections are negative and become very large (more than 50% in absolute value) for extreme kinematically accessible values of the observables. With such large negative effects, also the possible compensation of real heavy gauge boson radiation and the higher-order contributions (beyond one-loop) requires further investigation.

1.8 Jet vetoes and exclusive jet binning

The prediction of cross sections in bins of exclusive jet multiplicity poses an interesting theoretical challenge. The distribution for an observable τ in QCD perturbation theory has the structure shown in Fig. 1-24. This form of the distribution follows from the presence of Sudakov double logarithms, $\alpha_s/\pi \times \ln^2(Q/\tau_{cut})$, appearing in the perturbative expansion for the cross section, where Q denotes the hard scale of the process such as the partonic center-of-momentum scattering energy, and τ_{cut} denotes some experimental constraint τ. For the cross section for the production of a fixed number of jets, τ_{cut} would denote the restriction on the transverse momentum of potential additional jets. When τ is relatively unconstrained and $\tau_{cut} \sim Q$, as in the tail region of Fig. 1-24, these logarithms are of order unity, and fixed-order QCD perturbation theory can be applied to predict the distribution. When $\tau_{cut} \ll Q$ in the peak region, the Sudakov logarithms overwhelm the α_s suppression, and the perturbative expansion must be resummed to all orders to ensure that the distribution does not diverge as $\tau_{cut} \to 0$. However, techniques exist to perform this resummation, and the higher-order corrections in fixed-order perturbation theory give only small corrections in the peak region. The transition region is the theoretically most intricate region to predict. The logarithms are large enough that resummation must be performed, but not so large that the fixed-order corrections are negligible. Progress on both resummation and fixed-order calculations are needed to accurately describe such observables. Higgs production at the LHC in exclusive jet bins is an example of an observable in the transition region. For Higgs plus jets observables, $Q \sim m_H$ and $\tau_{cut} \sim p_T^{cut} = 25 - 30\,\text{GeV}$, where p_T^{cut} denotes the transverse momentum cut used to define a jet. Both higher-order corrections and resummation are needed to accurately predict the rates and distributions for Higgs plus jets. Since the hard scale Q grows with the partonic scattering energy, the high-p_T jet region accessible at potential future 33 TeV and 100 TeV colliders will potentially exhibit quite different behavior in QCD perturbation theory. This Section discusses predictions for Higgs production in both the gluon-fusion and associated production modes for 14 TeV, 33 TeV, and 100 TeV pp collisions, focusing on issues and uncertainties that arise because of the imposition of jet vetoes.

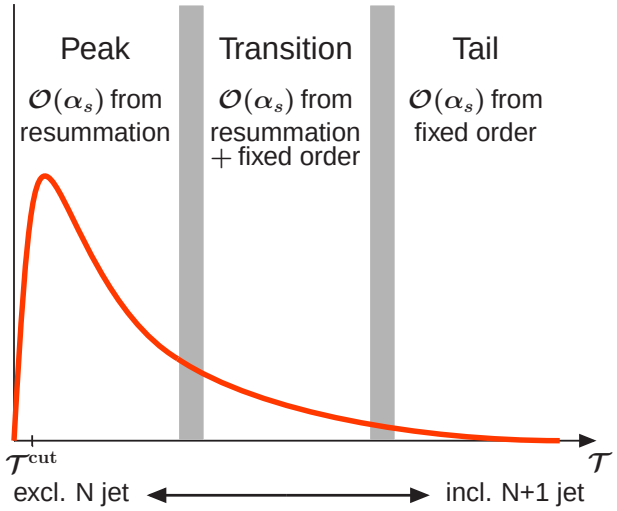


Figure 1-24. *Generic distribution for a variable τ obtained in QCD perturbation theory, taken from Ref. [107].*

1.8.1 Higgs production in gluon fusion

The discovery of the Higgs boson by the ATLAS and CMS collaborations has dominated the field of high energy physics during the past year. A large component of the future worldwide effort in particle physics will be devoted to measuring the properties of this state in order to determine the underlying theory from which it arises. Theoretical uncertainties from missing higher-order corrections are quickly becoming a limiting factor in this program. In the W^+W^- final state, the theoretical uncertainties are already a dominant systematic error [160,161]. The reasons for this are two-fold. The perturbative expansion for inclusive Higgs boson production is slowly convergent, and indeed even corrections beyond NNLO change the prediction in a significant way, as described in Section 1.6.5 of this report. In addition, and most importantly for this Section, significant cuts are imposed on the phase space of the hadronic radiation produced in association with the Higgs. This is required because the background composition to this signal changes as a function of jet multiplicity. In the zero-jet bin the background is dominated by continuum WW production, while in the one-jet and two-jet bins, top-pair production becomes increasingly important. The optimization of this search requires cuts dependent on the number of jets observed, and therefore also on theoretical predictions for exclusive jet multiplicities.

We present first a discussion of the NNLO QCD calculation for Higgs plus one-or-more jets, for which initial results for the gluon channel have recently been reported [117], and attempt to provide questions and guidance for phenomenological studies at future colliders when the full result is available. The cross section for inclusive Higgs plus one-or-more jets enters the prediction for the exclusive one-jet bin through the relation $\sigma_1 = \sigma_{\geq 1} - \sigma_{\geq 2}$, where the subscript denote the number of final-state jets produced in addition to the Higgs. We show the hadronic cross section for the production of the Higgs boson in association with one or more jets at the 8 TeV LHC through NNLO in perturbative QCD. Jets are reconstructed using the $k_\perp$-algorithm with $R = 0.5$ and $p_T^{cut} = 30$ GeV. The Higgs mass is taken to be $m_H = 125$ GeV, and NNPDF parton distributions are used [50]. The central renormalization and factorization scales are set to be $\mu_R = \mu_F = m_H$.

Fig. 1-25 shows the partonic cross section for $gg \to H + j$ multiplied by the gluon luminosity through NNLO in perturbative QCD:

$$\beta \frac{\mathrm{d}\sigma_{\rm had}}{\mathrm{d}\sqrt{s}} = \beta \frac{\mathrm{d}\sigma(s, \alpha_s, \mu_R, \mu_F)}{d\sqrt{s}} \times \mathcal{L}(\frac{s}{s_{\rm had}}, \mu_F), \tag{1.11}$$

where β measures the distance from the partonic threshold,

$$\beta = \sqrt{1 - \frac{E_{th}^2}{s}}, \qquad E_{th} = \sqrt{m_H^2 + p_{\perp,j}^2} + p_{\perp,j} \approx 158.55 \text{ GeV}. \tag{1.12}$$

It follows from Fig. 1-25 that NNLO QCD corrections are significant in the region $\sqrt{s} < 500$ GeV. In particular, close to partonic threshold $\sqrt{s} \sim E_{th}$, radiative corrections are enhanced by threshold logarithms $\ln \beta$ that originate from the incomplete cancellation of virtual and real corrections. There seems to be no significant enhancement of these corrections at higher energies, where the NNLO QCD prediction for the partonic cross section becomes almost indistinguishable from the NLO QCD one. This suggests that QCD corrections to inclusive Higgs plus one-jet production will be milder at potential future 33 TeV and 100 TeV pp colliders. Since more phase space for harder gluon emission will be available, the threshold region will contribute a smaller fraction of the cross section at these higher-energy machines, reducing the effect of $\ln \beta$ terms. This is consistent with the pattern for inclusive Higgs production reported in Section 1.6.5. It would be interesting to study $\mathrm{d}\sigma_{\rm had}/\mathrm{d}\sqrt{s}$ at higher-energy pp machines upon completion of the full calculation.

Discussed next is the resummation of jet-veto induced logarithms in exclusive jet bins. This has been the subject of intense discussion during the 7 TeV and 8 TeV LHC runs. Results combining resummation and

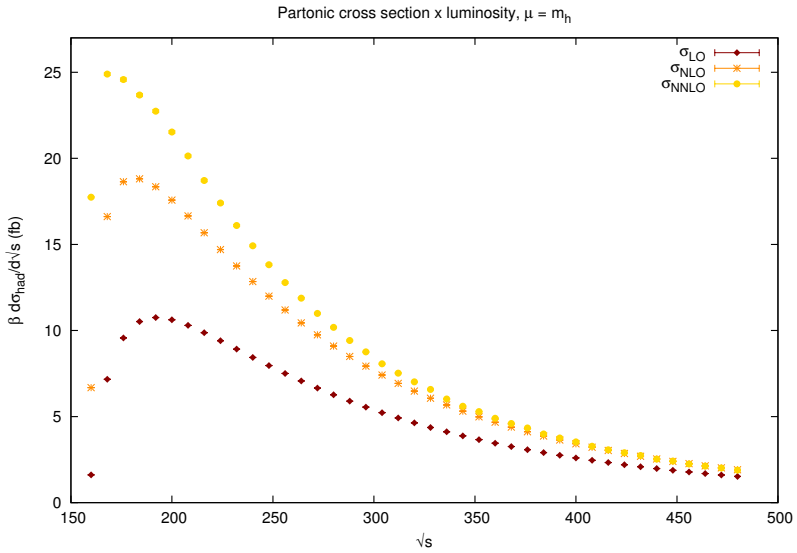


Figure 1-25. *Results for the product of partonic cross sections $gg \to H +$ jet and parton luminosities in consecutive orders in perturbative QCD for an 8 TeV LHC at $\mu_R = \mu_F = m_h = 125$ GeV. The x-axis gives the value of partonic center-of-momentum frame energy. See the text for further explanation.*

fixed-order are now available for the zero-jet [162–167] and one-jet [168, 169] bins. The resummation of large logarithms significantly reduces the theoretical uncertainties for the signal cross sections, and has a moderate impact on their central values. Given the continued importance of analyses utilizing exclusive jet bins during the 14 TeV run of the LHC and it potential future higher-energy colliders, it is important to study how predictions scale with increasing collider energy. For the exclusive Higgs plus one-jet bin in the gluon-fusion channel, the parametric form of the large logarithmic corrections is $\ln(\sqrt{s}/p_T^{cut})$, where $\sqrt{s}$ denotes the partonic center-of-momentum energy. As the collider energy increases, more events with large $\sqrt{s}$ contribute. The impact of the large logs and the resummation is expected to increase at higher-energy machines, if the transverse momentum cut p_T^{cut} remains the same.

Shown below in Table 1-8 are cross sections for the parameter choices $m_H = 125$ GeV, $|\eta_J| < 4.5$, and using MSTW 2008 PDFs [49]. A fixed transverse momentum cut $p_T^{cut} = 30$ GeV is assumed, and the central scale choice $\mu = m_H/2$ is chosen for the fixed order predictions. Uncertainties are computed as described in Ref. [169], where the central values for the resummation are also discussed. Also shown is the K-factor describing the change in the prediction as the resummation is added. Results are presented at the NLO in fixed-order perturbation theory, and at NLL$'$ + NLO in resummed perturbation theory (the order-counting of resummed perturbation theory used here is described in Ref. [170]). The usefulness of the resummation in decreasing the theoretical uncertainties is clear. The fixed-order uncertainties grow with collider energy, reaching nearly 100% at 100 TeV. In contrast, they remain between $20\% - 25\%$ when the resummation is implemented. In 14 TeV and 33 TeV pp collisions, the effect of resummation is to slightly decrease the central value of the prediction, by up to 5%. This behavior changes significantly at 100 TeV, where instead a nearly 30% increase in the cross section is found. This is likely caused by the fixed-order perturbative expansion entirely breaking down and heading to negative values for such a large hierarchy between the hard scale and p_T^{cut}. This is suggested by the large uncertainty present in the NLO result. Resummation cures this behavior, and leads to an increase in the cross section. However, it is likely that the minimum jet transverse momentum would have to be increased at future facilities, due to the increased energy deposited by the underlying soft physics. We model this by increasing the minimum jet transverse momentum to 60

	14 TeV	33 TeV	100 TeV
NLO	$12.48^{+34\%}_{-46\%}$	$40.17^{+54\%}_{-41\%}$	$131.3^{+72\%}_{-98\%}$
NLL′ + NLO	$11.73^{+27\%}_{-27\%}$	$39.71^{+24\%}_{-24\%}$	$166.9^{+22\%}_{-22\%}$
$K_{(\mathrm{NLL'+NLO})\mathrm{NLO}}$	0.940	0.989	1.27

Table 1-8. *Cross section central values and uncertainties for the exclusive Higgs plus one-jet bin for a fixed transverse momentum cut $p_T^{cut} = 30$ GeV. The results are shown in picobarns.*

	14 TeV	33 TeV	100 TeV
NLO	$12.48^{+34\%}_{-46\%}$	$26.90^{+30\%}_{-39\%}$	$91.23^{+38\%}_{-46\%}$
NLL′ + NLO	$11.73^{+27\%}_{-27\%}$	$27.44^{+24\%}_{-24\%}$	$103.0^{+24\%}_{-24\%}$
$K_{(\mathrm{NLL'+NLO})\mathrm{NLO}}$	0.940	1.02	1.13

Table 1-9. *Cross section central values and uncertainties for the exclusive Higgs plus one-jet bin, for the following transverse momentum cuts: $p_T^{cut} = 30$ GeV at 14 TeV, $p_T^{cut} = 60$ GeV at 33 TeV, and $p_T^{cut} = 80$ GeV at 100 TeV . The results are shown in picobarns.*

GeV in 33 TeV collisions, and to 80 GeV in 100 TeV collisions. The results are shown in Table 1-9. The change in K-factor as the collider energy is increased is ameliorated; a less than 15% increase in the cross section is found at 100 TeV.

Studied next is the cross section for Higgs production via gluon-fusion in the exclusive zero-jet bin. This cross section has been studied through NNLL′ + NNLO in resummed perturbation theory in Ref. [167]. A careful study of clustering contributions of the form $\ln \mathrm{R}$, where R denotes the anti-k_T jet-radius parameter, was also performed in this reference. Numerical results for the Higgs plus zero-jet cross section at the NNLL′+NNLO order are presented in Table 1-10 for pp collisions at 14, 33, and 100 TeV. Also shown is ϵ_0, the fraction of events which fall into the zero-jet bin. A fixed transverse momentum cut $p_T^{cut} = 30$ GeV is assumed. The most notable effect upon increasing collider energy is the significant reduction of the fraction of events in the zero-jet bin, from 60% at 14 TeV to 44% at 100 TeV. The range of Bjorken-x becomes larger as the collider energy is increased, leading to a larger probability for additional radiation and consequently reducing the number of zero-jet events. A small reduction of scale uncertainty is found when going from 14 TeV collisions to higher energies, similar to what was found for the one-jet cross section in Table 1-8.

	14 TeV	33 TeV	100 TeV
$\sigma_{\mathrm{NNLL'+NNLO}}$	$33.25^{+5.5\%}_{-5.5\%}$	$104.2^{+3.9\%}_{-3.9\%}$	$364.2^{+4.4\%}_{-4.4\%}$
$\epsilon_0^{\mathrm{NNLL'+NNLO}}$	$0.596^{+4.4\%}_{-4.4\%}$	$0.522^{+4.9\%}_{-4.9\%}$	$0.438^{+4.4\%}_{-4.4\%}$

Table 1-10. *Central values and uncertainties for the exclusive Higgs plus zero-jet bin cross section and zero-jet event fraction, for a fixed transverse momentum cut $p_T^{cut} = 30$ GeV. The results are shown in picobarns.*

1.8.2 *WH* production at NNLO

Sometimes it is experimentally necessary to require an exclusive final state, for example by restricting the number of jets allowed to be present. This is true for some current LHC analyses and will no doubt continue to be true for higher energies. This requirement of an exclusive final state can result in the presence of large logarithms due to the unbalancing of the cancellation between positive real emission terms and negative virtual corrections, thus affecting the convergence and reliability of the perturbative series. As an example, consider searches for Higgs boson production in the associated mode (VH). While this has been the major Higgs boson search channel at the Tevatron, at the LHC it suffers from large backgrounds. A precise measurement in this channel (with the Higgs decaying into a $b\bar{b}$ pair) can still be very useful in the years following the Higgs boson discovery in order to understand the Higgs coupling to b-quarks. A relative reduction in the background at the LHC can be achieved by requiring the vector boson and the Higgs boson to be at large transverse momentum, with no additional jets present greater than some threshold. While the impact of higher order QCD corrections is mild for the inclusive measurement, such restrictions can greatly affect the size of the higher order corrections and thus the convergence of the perturbative series. In this context, the issue was first raised in the original exclusive NNLO calculation of WH production [171].

In this report we address the extent to which this issue is exacerbated in predictions for higher energy proton-proton colliders. For the following study the transverse momentum of the W boson is required to be greater than 200 GeV. The Higgs boson decays into a $b\bar{b}$ pair that is reconstructed as a "fat jet" using the Cambridge-Aachen algorithm with $R = 1.2$. This fat jet must also be at large transverse momentum, greater than 200 GeV. In addition to these cuts, any additional jets were required have transverse momenta below 40 GeV. The study was repeated at 14, 33 and 100 TeV, with the results shown in Fig. 1-26 (left). The cross section is plotted as a function of the transverse momentum of the fat (Higgs) jet. As the center-of-mass energy increases, the effect of such stringent cuts increases. There are large negative corrections when going from LO to NLO, resulting in a NLO K-factor (NLO/LO) as low as 0.3 (for 100 TeV). The corrections from NLO to NNLO by comparison are modest, but the strong reduction from LO to NLO indicates that the fixed order prediction may be unreliable, and a resummed cross section is necessary to achieve a reliable prediction. As alternative scenarios at higher energies, Fig. 1-26 (right) shows the effect of raising the jet threshold to 60 GeV (at 33 TeV) and 80 GeV (at 100 TeV). In these cases, the effect of allowing additional phase space results in a better-behaved perturbative series, and cross sections that behave order-by-order in a manner that is more similar to the pattern observed for a 40 GeV veto at 14 TeV.

1.9 Quarkonium physics at future colliders

A detailed account of issues in quarkonium production at the Energy Frontier can be found in "Quarkonium at the Frontiers of High Energy Physics: A Snowmass White Paper" [172] and references therein.

The production of heavy quarkonia at large transverse momentum p_T is an aspect of quarkonium physics in which dramatic progress can be expected through the interaction of theory with experiments at the energy frontier. Quarkonium production is an aspect of QCD that is not yet fully understood and it can serve as a theoretical laboratory for QCD in which powerful effective-field theory tools can be brought into play. Quarkonium production can be used to test and to extend our understanding of factorization theorems, which are the theoretical foundation for all perturbative calculations in QCD, and to develop new theoretical concepts for controlling large higher-order corrections that could have wider applicability in the calculation of high-energy cross sections. Quarkonium production is also useful as a laboratory for exploring experimental techniques within a setting in which experimental signatures are very clean and very high statistics can be accumulated. Quarkonium production processes can be used to measure Higgs couplings, and so to probe

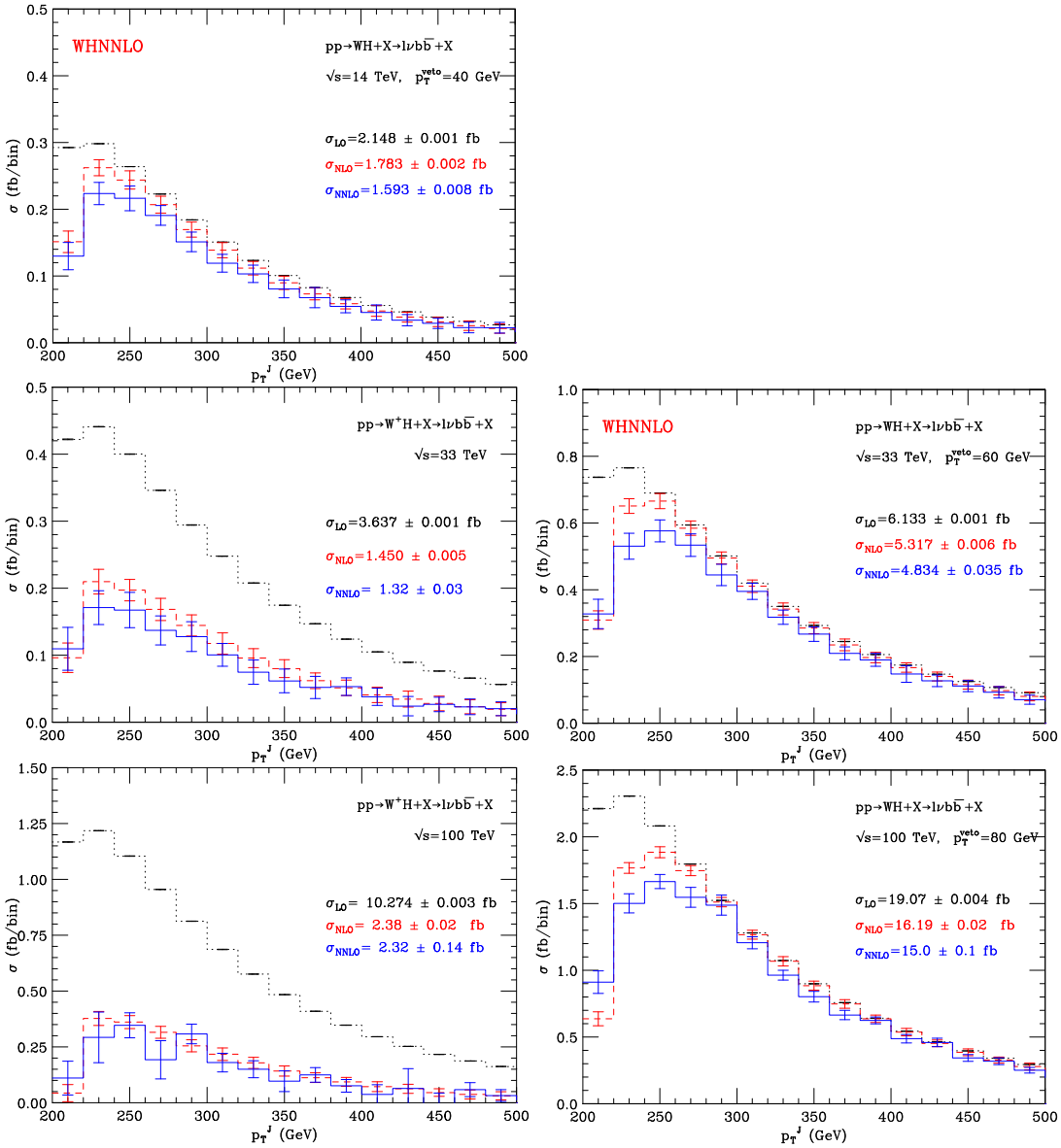


Figure 1-26. *The transverse momentum of the fat jet in WH production, at* 14 *TeV (top),* 33 *TeV (middle) and* 100 *TeV (bottom). In the left-hand column additional jets with transverse momenta above* 40 *GeV are vetoed, while in the right this veto is raised to* 60 *GeV at* 33 *TeV and* 80 *GeV at* 100 *TeV.*

for physics beyond the standard model. If new physics involves nonrelativistic bound states, then techniques that have been developed for understanding quarkonium production will be directly applicable.

The current standard method for calculating quarkonium production rates is the nonrelativistic QCD (NRQCD) factorization approach, which is based on the effective field theory NRQCD. In this approach, production rates are expressed as perturbatively-calculable partonic cross sections multiplied by nonperturbative constants called NRQCD matrix elements. Some of the NRQCD matrix elements must be determined through fits of NRQCD factorization predictions to experimental data. The universality feature of NRQCD factorization then allows one to make predictions for other quarkonium production processes—predictions that should be tested for as many processes as possible. The NRQCD factorization approach is a conjecture that has not been proven to all orders in α_s. Therefore, experimental tests take on an added importance. Standard methods for proving factorization suggest that, if NRQCD factorization is correct, then it holds only for p_T much larger than the quarkonium mass. Hence, high-p_T, high-statistics measurements of quarkonium production are key tests of factorization.

NRQCD factorization predictions have now been computed at next-to-leading order in α_s for many production processes. In general, these predictions agree with the experimental data from pp, $p\bar{p}$, ep, and e^+e^- colliders for the production of quarkonia at large p_T. The most notable exception is the polarization of the J/ψ, $\psi(2S)$, and $\Upsilon(nS)$ $(n = 1, 2, 3)$ at the Tevatron and at the LHC. This serious discrepancy between theory and experiment deserves further investigation from both the theoretical and experimental sides. Feeddown from quarkonium states of higher mass to the J/ψ and $\Upsilon(1S)$ states blurs the comparisons between theory and experiment. Future experiments could sharpen these comparisons by measuring direct-production rates of quarkonia.

At the frontiers of high-energy physics, there are many opportunities for further interesting work on quarkonium production. In Run 2 of the LHC, the extension of the energy frontier to 13 TeV and the increase in luminosity in comparison with Run I will make it possible to extend the p_T reach of quarkonium studies. Such high-p_T measurement are crucial tests of NRQCD factorization. Measurements of production and polarization for the χ_{cJ} and χ_{bJ} states and for new processes, such as associated production with W or Z bosons, would provide valuable additional tests of the theory.

The LHC luminosity upgrade would afford the opportunity to push studies of $b\bar{b}$ states to still higher values of p_T. The $b\bar{b}$ systems are particularly important tests of the validity of NRQCD because they are more nonrelativistic than the $c\bar{c}$ systems. However, tests of factorization for these systems will require that challenging measurements be made at values of p_T that are much larger than the bottomonium mass.

A future high-energy e^+e^- collider will allow studies of quarkonium production in two-photon collisions. In a Higgs factory mode, it would afford new opportunities to make precision measurements of the Higgs couplings to Standard Model particles. The decay modes $H \to J/\psi + \gamma$, $H \to J/\psi + Z$, and $H \to \Upsilon + Z$ might be particularly useful in this regard.

1.10 Jet and missing E_T performance at HL-LHC

Both the precision and the discovery physics programs at the 14 TeV LHC and at future colliders require high instantaneous luminosities. This will result in the presence of a large number of additional interactions for every crossing, and the subsequent difficulties in triggering on interesting physics and then in removing the effects of the pileup to recover the original physics. Pileup is one of the main challenges for jets and missing transverse energy, with both the presence of additional energy (offset) as well as the creation of additional fake jets due to local fluctuations in the energy density. Thus, it is important to develop the tools

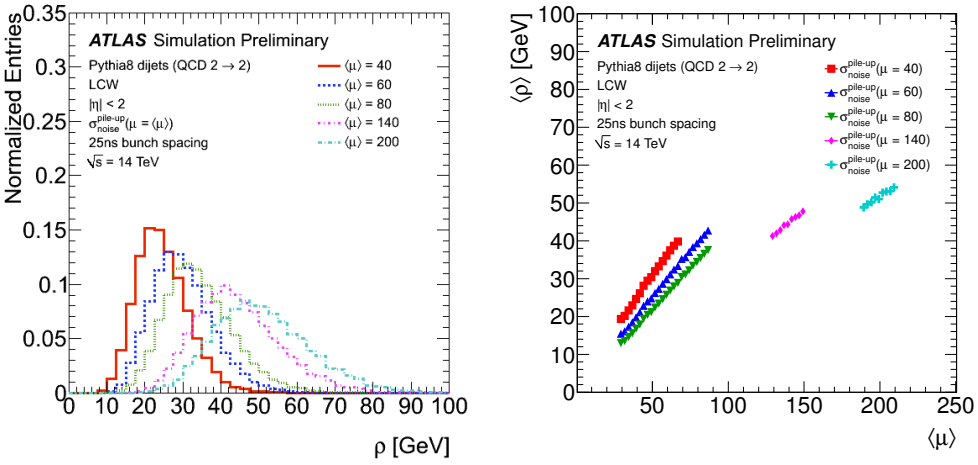


Figure 1-27. *Distributions of the event-by-event median p_T density (ρ) for different values of the mean number of interactions per bunch crossing $\langle\mu\rangle$ (left) and the dependence of ρ on the mean number of interactions per bunch crossing (right).*

needed for removing the effects of pileup in order to insure that precise measurements can still be undertaken at high luminosities.

A study was carried out within the ATLAS full simulation framework, using topological clustering and local hadron calibration, where samples with up to 200 pileup events per crossing (with both 50ns and 25ns bunch structure) were used. Topoclusters are an attempt to reconstruct three-dimensional energy deposits in the calorimeter and are built using a nearest-neighbor algorithm that clusters calorimeter cells with energy significance ($|E_{cell}|/\sigma$) > 4 for the seed, > 2 for neighbors, and > 0 at the boundary. E_{cell} is calibrated using information derived from test beam and detailed GEANT4 simulations (EM scale) and σ is the sum in quadrature of the electronic and expected pileup noise, as described in Sec. 10.5.2 of Ref. [173]. Topoclusters can be further calibrated using local information (LCW) as described in Ref. [174].

Figure 1-27 shows an example of an event where hard jets are embedded in a background of soft energy resulting from multiple minimum bias events. An effective density ρ can be determined on an event-by-event basis [175] based on energy depositions outside hard jets. The corrected jet transverse momentum can be calculated by subtracting the contribution due to pileup ρA^{jet}, where A^{jet} is the active area of the jet. The technique works since the pileup density depends linearly on the number of interactions up to very high values of the average number of pileup events. As can be seen in Fig. 1-27, the optimization of σ pileup noise during topocluster formation is critical to suppress pileup contributions at high luminosity. When the pileup noise used in topoclustering is chosen to match the pileup conditions, a significant reduction on the event p_T density is achieved. Although the event-by-event pileup subtraction accounts for global pileup fluctuations from one event to another, it is not sensitive to local fluctuations. A residual correction is necessary to account for the higher occupancy inside jets and for out-of-time pileup effects.

The jet calibration scheme has been shown to work well up to very high luminosities. The pileup subtraction technique restores the jet energy response to that of jets in the presence of no pileup. The pileup subtraction also significantly reduces the number of fake (pileup) events per jet, as shown in Fig. 1-28. There are approximately 3 (0.5) pileup jets with $p_T > 20$ (40) GeV per event, with approximately 140 additional interactions per crossing. Further improvements can be expected using tracking and vertexing information.

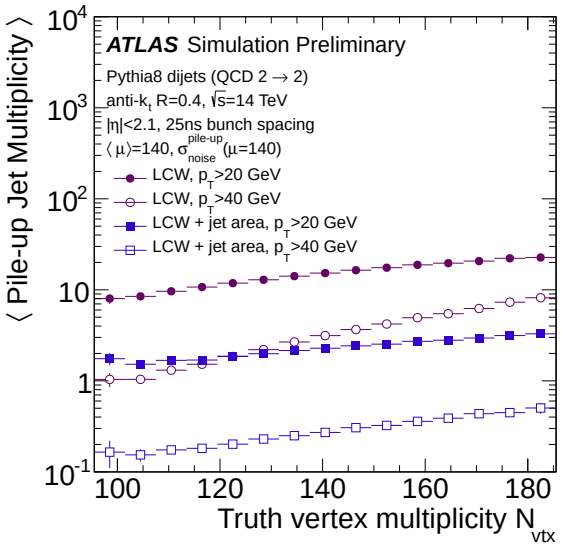


Figure 1-28. *The mean pileup jet multiplicity as a function of the number of truth vertices N_{vtx} in events with an average number of interactions per bunch crossing, $\langle\mu\rangle = 140$. A pileup-jet is defined as a reconstructed jet that is not closely matched in ΔR to a truth jet.*

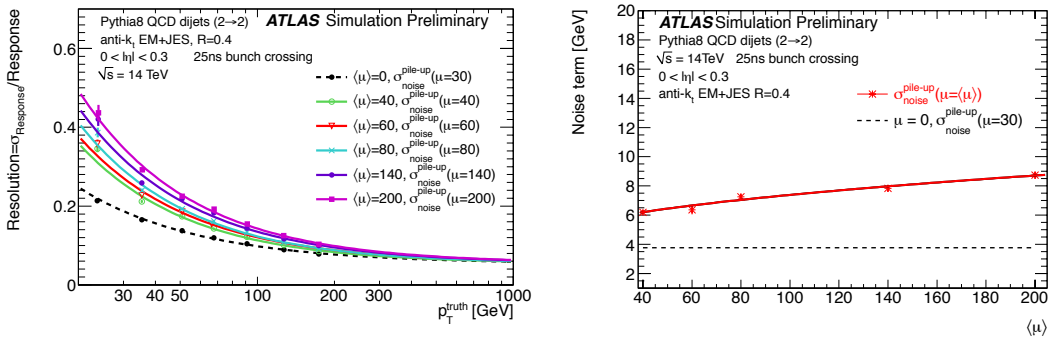


Figure 1-29. *The fractional jet energy resolution as a function of jet p_T for different values of the mean number of interactions per bunch crossing (left) and the noise term of the jet energy resolution as a function of $\langle\mu\rangle$ (right).*

The jet energy resolution at low jet transverse momentum degrades in the presence of pileup; there are local pileup fluctuations within events, not captured by the global event-by-event energy density used in the calibration. The result is an effective noise term whose magnitude increases as the square root of the average number of additional interactions. A reduction of local pileup fluctuations may be possible using tracking information and advanced subtraction techniques using more local information. Figure 1-29 shows the dependence of the fractional jet energy resolution and the noise term on an average number of interactions per bunch crossing, $\langle\mu\rangle$. The square root dependence of the noise term indicates that the degradation in resolution is due to pileup fluctuations and there are no additional contributions from no-linear effects of topoclustering or local hadron calibration.

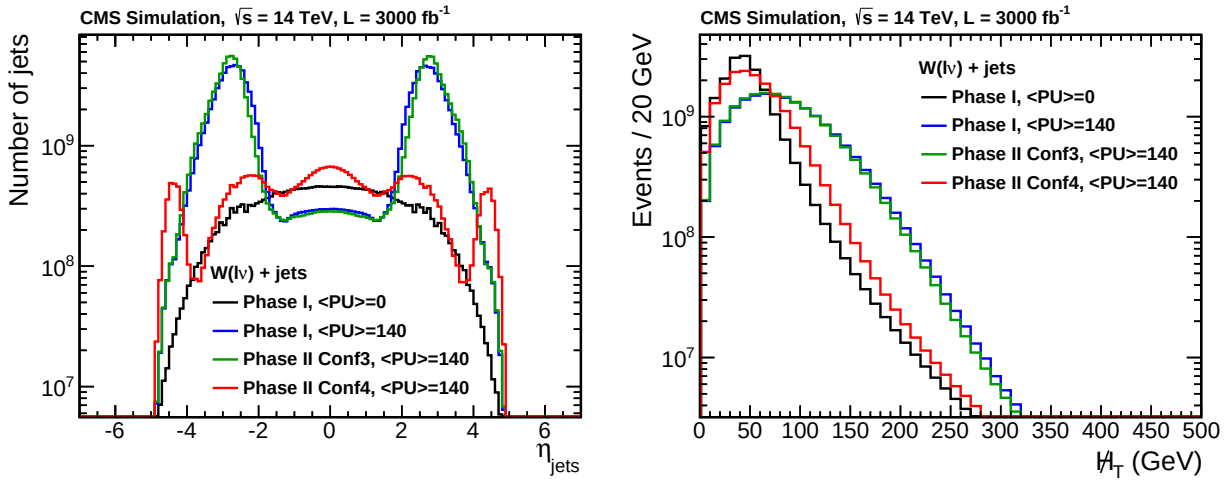


Figure 1-30. *Pseudorapidity distributions for jets with $p_T > 30$ GeV (left) and $\not{H}_T$ distributions (right) for various pileup and detector configurations in $W(\to \ell\nu)$ + jets events (left). The Phase II configuration 4 (Conf4) corresponds to the detector design which includes a tracker extended up to $|\eta| = 4$, while the Phase I and Phase II configuration 3 (Conf3) detector has a tracker covering only up to $|\eta| = 2.5$.*

In addition to the optimization in event reconstruction, the proper detector upgrade will be important to deal with high pileup environment. CMS uses the particle-flow event reconstruction [176], and pileup charged hadron subtraction can removes a large fraction of pileup charged particles on a particle-by-particle basis in the region covered by a tracking system. As shown in Fig. 1-30, an extension of the tracking detector to forward region is expected to help reducing pileup jets substantially in the forward region and improve missing E_T ($\not{H}_T$) resolution [177] in events with $\langle\mu\rangle = 140$ expected during high luminosity LHC (HL-LHC).

Jet substructure is a key technique for the reconstruction of boosted objects. Grooming algorithms significantly reduce the sensitivity to pileup, due to the reduced jet area. The original jet mass can be recovered, with reasonably low degradation of mass resolution. Figure 1-31 shows the jet mass distribution in $Z' \to t\bar{t}$ events before and after the application of trimming, for increasing values of $\langle\mu\rangle$. Trimming is implemented by re-clustering the jet into subjets of radius $R = 0.3$. The clusters belonging to subjets that carry at least 5% of the original jet p_T are kept, and those clusters in subjets with less than 5% of the original jet p_T are discarded.

Finally, we conclude with a statement about the increased level of activity expected as the energy of a pp collider increases. The total inelastic cross section, 74.7 ± 1.7 mb at 8 TeV [178] is expected to grow to 80 mb at 13 TeV, 90 mb at 33 TeV, and 105 mb at 100 TeV. Inelastic events with at least one track in the central region have a central track density ($\Delta\eta \times \Delta\phi$) of 1.0 at 8 TeV and will have a central charged track density of 1.1 ± 0.1 at 13 TeV, growing to 1.33 ± 0.14 at 30 TeV and 1.8 ± 0.4 at 100 TeV. The transverse energy for inelastic events deposited per unit ΔR^2 in the central region of the detector has been measured at ~ 0.8 GeV at 8 TeV, and will grow to 1.0 ± 0.15 GeV at 13 TeV, 1.25 ± 0.2 GeV at 30 TeV, and 1.9 ± 0.35 GeV at 100 TeV. The larger inelastic cross sections and the increased activity found in each inelastic event as the center-of-mass energy increases will add to the difficulty for carrying out precision physics measurements.

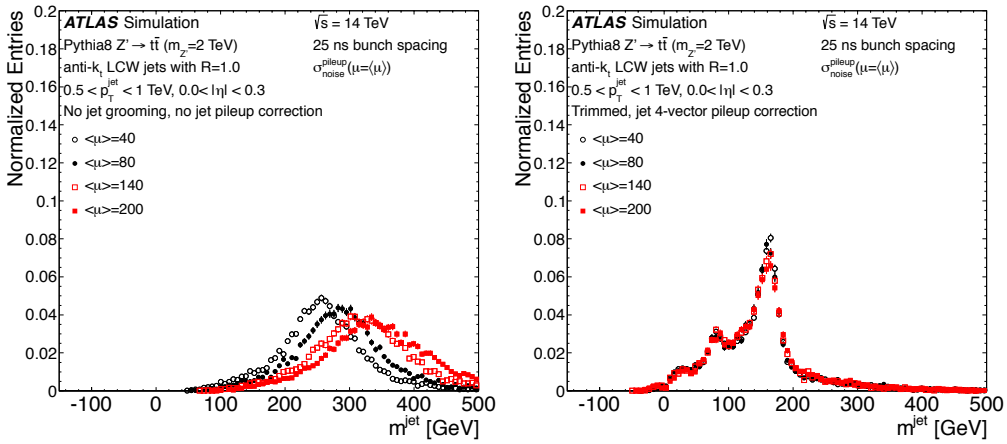


Figure 1-31. *The jet mass distribution before (left) and after (right) trimming in $Z' \to t\bar{t}$ events, for $m(Z') = 2$ TeV and anti-k_T jets with $R = 1.0$. The mean number of interactions per bunch crossing is 40 (open circles), 80 (closed circles), 140 (open squares) and 200 (closed squares). The value of the pileup noise (σ) used in the topoclustering is optimized for each value of pileup, except in the case of $\langle\mu\rangle = 40$ where the value of σ is optimized for $\langle\mu\rangle = 30$, as in 2012 data.*

1.11 Conclusions

We summarize here the main conclusions of our report, with an emphasis on where advances in our understanding of QCD are needed to fully explore the electroweak scale at run 2 of the LHC and at future machines. We divide our conclusions below into four broad categories.

1. Parton distribution functions for precision and discovery physics:

   - Improvements in our current understanding of PDFs are needed in the 'precision region.' For example, the differences between the CT, MSTW and NNPDF gluon PDFs are large exactly in the range relevant for Higgs studies. Efforts are underway to understand the source of the differences between the three global PDF groups, and this will hopefully result in a reduction of the total PDF uncertainty for Higgs production in 8 and 14 TeV proton-proton collisions. Collider data may also help to reduce the uncertainties in this precision region, but a future electron-hadron collider, such as the LHeC, would be the ultimate machine to provide PDFs for precision HL-LHC physics.
   - Improvement in our current understanding of PDFs is needed in the 'discovery region.' The optimal use of current and future LHC data in global PDf fits is needed to reduce the uncertainties in order to facilitate high-mass discoveries.
   - Photon-induced reactions will become an increasingly large contribution to scattering processes at future high-energy colliders. Further work is needed to constrain the photon distribution function from LHC data. Photon PDFs and their uncertainties need to be available from all PDF groups.

2. The frontiers of perturbation theory:

   - Higher precision calculations combining QCD at NNLO and beyond, together with EW corrections at NLO, are needed to fully realize the potential of future high energy pp collisions. The capability

to perform an NNLO calculation for any $2 \to 2$ process and selected $2 \to 3$ processes is desired, and seems within reach.

- Should QCD and electroweak corrections be combined additively or multiplicatively? Does either prescription correctly reproduce the result of an exact calculation? Calculations of mixed corrections are needed to check how to perform this combination, and to develop an intuition about when each method is appropriate.
- The battle for precision must be fought on several fronts. Progress on both fixed-order calculations and on the resummation of large logarithms is crucial. It will remain so at future colliders, where the larger phase space available will lead to increasingly larger ratios between the available scales. The full realization of the potential of future proton-proton machines to unravel the identity of the Higgs boson requires advances in our QCD calculational abilities.
- Achieving a theoretical precision at the 1% level will require a detailed understanding of possible corrections to the typically-assumed factorization picture, and a re-examination of assumptions such as the universality of PDFs and fragmentation functions.

3. The Sudakov zone:

   - At high energies, electroweak corrections became as large as, or larger than, QCD corrections. The inclusion of electroweak corrections into theoretical simulation programs is mandatory for physics studies at future high energy proton-proton colliders.
   - Electroweak corrections are technically challenging for high-multiplicity final states. In many common kinematic situations these corrections are dominated by Sudakov logarithms. Continued attention should be devoted to assessing frameworks for their approximate inclusion into Monte Carlo simulations.

4. The determination of fundamental constants:

   - The current errors on α_s, m_b and m_c induce sizable parametric uncertainties in predictions for Higgs boson decay rates. Lattice and continuum extraction methods both feature smaller errors than used in coupling extractions, and have consistent central values. The error assumptions in future Higgs coupling analyses should be revisited.
   - Improvements in lattice calculations, data from LHeC, and data from future e^+e^- colliders could reduce the error on α_s to 0.1%.

The rapid progress in QCD and EW phenomenology that has been observed in the recent past, along with that expected in the near future, will, along with the data taken at the LHC, allow for full exploitation of the discovery and precision-measurement capability of the LHC and subsequent colliders.

ACKNOWLEDGEMENTS

L. Barzè is supported by the ERC Grant 291377.

T. Becher and X.Garcia i Tormo are supported by the Swiss National Science Foundation (SNF) under grant 200020-140978 and the Sinergia grant number CRSII2 141847 1.

G. Bodwin and R. Boughezal are supported by the U.S. Department of Energy under Contract No. DE-AC02-06CH11357.

J. M. Campbell, P. Mackenzie and R. Van de Water are supported by the U.S. Department of Energy under Contract No. DE-AC02-06CH11359.

S. Carrazza and S. Forte are supported by an Italian PRIN 2010 and by a European EIBURS grant.

M. Chiesa, G. Montagna, M. Moretti, O. Nicrosini and F. Piccinini are supported by the italian PRIN project 2010YJ2NYW and by the Research Executive Agency (REA) of the European Union under the Grant Agreement number PITN-GA-2010-264564 (LHCPhenoNet).

S. Hoeche is supported by the U.S. Department of Energy under Contract No. DE-AC02-76SF00515.

F. Petriello is supported by the U.S. Department of Energy under Grant No. DE-SC0010143.

J. Rojo is supported by a Marie Curie Intra–European Fellowshipa of the European Community's 7th Framework Programme under contract number PIEF-GA-2010-272515.

F. Tramontano is supported by the italian PRIN project 2010YJ2NYW.

References

[1] S. Dawson, A. Gritsan, H. Logan, J. Qian, C. Tully, R. Van Kooten, *et al.* (2013).

[2] J. Beringer *et al.* (Particle Data Group), Phys. Rev. D **86**, 010001 (2012).

[3] K. Hikasa *et al.* (Particle Data Group), Phys. Rev. D **45**, S1 (1992).

[4] G. Dissertori, "α_s at an e^+e^- Z factory," presentation at the Snowmass energy frontier meeting, Seattle, July 2013.

[5] S. Bethke, Nucl. Phys. Proc. Suppl. **234**, 229 (2013), 1210.0325.

[6] S. Schael *et al.* (ALEPH, DELPHI, L3, OPAL, and SLD Collaborations, the LEP Electroweak Working Group, the SLD Electroweak and Heavy Flavour Groups), Phys. Rept. **427**, 257 (2006), hep-ex/0509008.

[7] S. Bethke, Nucl. Phys. Proc. Suppl. **135**, 345 (2004), hep-ex/0407021.

[8] P. Baikov, K. Chetyrkin, and J. H. Kuhn, Phys. Rev. Lett. **101**, 012002 (2008), 0801.1821.

[9] P. Baikov, K. Chetyrkin, J. Kuhn, and J. Rittinger, Phys. Rev. Lett. **108**, 222003 (2012), 1201.5804.

[10] G. Gomez-Ceballos, M. Klute, M. Zanetti, P. Lenzi, M. Bachtis, *et al.* (2013), 1308.6176.

[11] H. Flacher, M. Goebel, J. Haller, A. Hocker, K. Monig, *et al.*, Eur. Phys. J. C **60**, 543 (2009), 0811.0009.

[12] S. Schael *et al.* (ALEPH, DELPHI, L3, and OPAL Collaborations, LEP Electroweak Working Group) (2013), 1302.3415.

[13] G. Altarelli, PoS **Corfu2012**, 002 (2013), 1303.6065.

[14] M. Davier, S. Descotes-Genon, A. Hocker, B. Malaescu, and Z. Zhang, Eur. Phys. J. C **56**, 305 (2008), 0803.0979.

[15] A. Pich, PoS **ConfinementX**, 022 (2012), 1303.2262.

[16] T. Affolder *et al.* (CDF Collaboration), Phys. Rev. Lett. **88**, 042001 (2002), hep-ex/0108034.

[17] V. M. Abazov *et al.* (D0 Collaboration), Phys. Rev. D **80**, 111107 (2009), 0911.2710.

[18] B. Malaescu and P. Starovoitov, Eur. Phys. J. C **72**, 2041 (2012), 1203.5416.

[19] V. M. Abazov *et al.* (D0 Collaboration), Phys. Lett. B **718**, 56 (2012), 1207.4957.

[20] S. Chatrchyan *et al.* (CMS Collaboration) (2013), 1304.7498.

[21] S. Chatrchyan *et al.* (CMS Collaboration) (2013), 1307.1907.

[22] A. G.-D. Ridder, T. Gehrmann, E. Glover, and J. Pires, Phys. Rev. Lett. **110**, 162003 (2013), 1301.7310.

[23] J. Abelleira Fernandez *et al.* (LHeC Study Group), J. Phys. G **39**, 075001 (2012), 1206.2913.

[24] J. Abelleira Fernandez *et al.* (LHeC Study Group) (2012), 1211.5102.

[25] O. Bruening and M. Klein, Mod. Phys. Lett. A **28**, 1330011 (2013), 1305.2090.

[26] A. Denner, S. Heinemeyer, I. Puljak, D. Rebuzzi, and M. Spira, Eur. Phys. J. C **71**, 1753 (2011), 1107.5909.

[27] G. Dissertori, A. Gehrmann-De Ridder, T. Gehrmann, E. Glover, G. Heinrich, *et al.*, JHEP **0908**, 036 (2009), 0906.3436.

[28] G. Dissertori, A. Gehrmann-De Ridder, T. Gehrmann, E. Glover, G. Heinrich, *et al.*, Phys. Rev. Lett. **104**, 072002 (2010), 0910.4283.

[29] M. Baak, M. Goebel, J. Haller, A. Hoecker, D. Kennedy, *et al.*, Eur. Phys. J. C **72**, 2205 (2012), 1209.2716.

[30] J. Gao, M. Guzzi, J. Huston, H.-L. Lai, Z. Li, *et al.* (2013), 1302.6246.

[31] S. Alekhin, J. Blumlein, and S. Moch, Phys. Rev. D **86**, 054009 (2012), 1202.2281.

[32] R. D. Ball, V. Bertone, L. Del Debbio, S. Forte, A. Guffanti, *et al.*, Phys. Lett. B **707**, 66 (2012), 1110.2483.

[33] A. Martin, W. Stirling, R. Thorne, and G. Watt, Eur. Phys. J. C **64**, 653 (2009), 0905.3531.

[34] M. Czakon, P. Fiedler, and A. Mitov, Phys. Rev. Lett. **110**, 252004 (2013), 1303.6254.

[35] C. McNeile, C. Davies, E. Follana, K. Hornbostel, and G. Lepage, Phys. Rev. D **82**, 034512 (2010), 1004.4285.

[36] E. Shintani, S. Aoki, H. Fukaya, S. Hashimoto, T. Kaneko, *et al.*, Phys. Rev. D **82**, 074505 (2010), 1002.0371.

[37] K. Maltman, D. Leinweber, P. Moran, and A. Sternbeck, Phys. Rev. D **78**, 114504 (2008), 0807.2020.

[38] P. Mackinzie *et al.*, "m_c, m_b, and α_s: Lattice status and prospects," presentation at the Snowmass meeting, Minneapolis, August 2013.

[39] K. Chetyrkin, J. Kuhn, A. Maier, P. Maierhofer, P. Marquard, *et al.*, Phys. Rev. D **80**, 074010 (2009), 0907.2110.

[40] I. Allison *et al.* (HPQCD Collaboration), Phys. Rev. D **78**, 054513 (2008), 0805.2999.

[41] S. Aoki *et al.* (PACS-CS Collaboration), JHEP **0910**, 053 (2009), 0906.3906.

[42] B. Blossier, P. Boucaud, M. Brinet, F. De Soto, X. Du, *et al.*, Phys. Rev. Lett. **108**, 262002 (2012), 1201.5770.

[43] S. Forte and G. Watt (2013), 1301.6754.

[44] A. De Roeck and R. Thorne, Prog. Part. Nucl. Phys. **66**, 727 (2011), 1103.0555.

[45] E. Perez and E. Rizvi, Rep. Prog. Phys. **76**, 046201 (2013), 1208.1178.

[46] G. Bozzi, J. Rojo, and A. Vicini, Phys. Rev. D **83**, 113008 (2011), 1104.2056.

[47] V. Radescu (H1 and ZEUS Collaborations), PoS **ICHEP2010**, 168 (2010).

[48] A. Cooper-Sarkar (ZEUS and H1 Collaborations), PoS **EPS-HEP2011**, 320 (2011), 1112.2107.

[49] A. Martin, W. Stirling, R. Thorne, and G. Watt, Eur. Phys. J. C **63**, 189 (2009), 0901.0002.

[50] R. D. Ball, V. Bertone, S. Carrazza, C. S. Deans, L. Del Debbio, *et al.*, Nucl. Phys. B **867**, 244 (2013), 1207.1303.

[51] R. D. Ball, S. Carrazza, L. Del Debbio, S. Forte, J. Gao, *et al.*, JHEP **1304**, 125 (2013), 1211.5142.

[52] A. Martin, R. Roberts, W. Stirling, and R. Thorne, Eur. Phys. J. C **39**, 155 (2005), hep-ph/0411040.

[53] S. Carrazza (2013), 1307.1131.

[54] S. Carrazza (2013), 1305.4179.

[55] R. D. Ball *et al.* (NNPDF Collaboration) (2013), 1308.0598.

[56] A. Bierweiler, T. Kasprzik, H. Kuhn, and S. Uccirati, JHEP **1211**, 093 (2012), 1208.3147.

[57] G. Aad *et al.* (ATLAS Collaboration), Phys. Rev. D **86**, 014022 (2012), 1112.6297.

[58] S. Chatrchyan *et al.* (CMS Collaboration), Phys. Rev. D **87**, 112002 (2013), 1212.6660.

[59] G. Aad *et al.* (ATLAS Collaboration), Eur. Phys. J. C **73**, 2509 (2013), 1304.4739.

[60] M. L. Mangano and J. Rojo, JHEP **1208**, 010 (2012), 1206.3557.

[61] G. Altarelli, R. D. Ball, and S. Forte, Nucl. Phys. B **799**, 199 (2008), 0802.0032.

[62] K. Melnikov and F. Petriello, Phys. Rev. D **74**, 114017 (2006), hep-ph/0609070.

[63] R. Gavin, Y. Li, F. Petriello, and S. Quackenbush, Comput. Phys. Commun. **182**, 2388 (2011), 1011.3540.

[64] S. Catani, L. Cieri, G. Ferrera, D. de Florian, and M. Grazzini, Phys. Rev. Lett. **103**, 082001 (2009), 0903.2120.

[65] Y. Li and F. Petriello, Phys. Rev. D **86**, 094034 (2012), 1208.5967.

[66] C. Bernaciak and D. Wackeroth, Phys. Rev. D **85**, 093003 (2012), 1201.4804.

[67] L. Barze, G. Montagna, P. Nason, O. Nicrosini, F. Piccinini, *et al.*, Eur. Phys. J. C **73**, 2474 (2013), 1302.4606.

[68] M. Czakon, M. L. Mangano, A. Mitov, and J. Rojo (2013), 1303.7215.

[69] D. d'Enterria and J. Rojo, Nucl. Phys. B **860**, 311 (2012), 1202.1762.

[70] L. Carminati, G. Costa, D. D'Enterria, I. Koletsou, G. Marchiori, *et al.*, EPL **101**, 61002 (2013), 1212.5511.

[71] S. A. Malik and G. Watt (2013), 1304.2424.

[72] W. Stirling and E. Vryonidou, Phys.Rev.Lett. **109**, 082002 (2012), 1203.6781.

[73] ATLAS Collaboration, ATLAS-CONF-2013-045 (2013), `http://cds.cern.ch/record/1546800`.

[74] S. Chatrchyan *et al.* (CMS Collaboration) (2013), 1310.1138.

[75] F. Aaron *et al.* (H1 and ZEUS Collaborations), JHEP **1001**, 109 (2010), 0911.0884.

[76] F. Aaron *et al.* (H1 Collaboration), Eur. Phys. J. C **64**, 561 (2009), 0904.3513.

[77] F. James and M. Roos, Comput. Phys. Commun. **10**, 343 (1975).

[78] G. Azuelos *et al.*, "New Physics with the LHeC", Poster submitted to EPS, Stockholm, July 2013.

[79] J. M. Campbell and R. K. Ellis, Phys. Rev. D **60**, 113006 (1999), hep-ph/9905386.

[80] J. M. Campbell, R. K. Ellis, and C. Williams, JHEP **1107**, 018 (2011), 1105.0020.

[81] See web-page: `https://twiki.cern.ch/twiki/bin/view/LHCPhysics/HiggsEuropeanStrategy2012`.

[82] G. Aad *et al.* (ATLAS Collaboration), New J. Phys. **15**, 033038 (2013), 1301.6872.

[83] J. R. Andersen and J. M. Smillie, JHEP **1001**, 039 (2010), 0908.2786.

[84] J. R. Andersen and J. M. Smillie, JHEP **1106**, 010 (2011), 1101.5394.

[85] J. Andersen *et al.* (SM and NLO Multileg Working Group) (2010), 1003.1241.

[86] Z. Bern, L. Dixon, F. Febres Cordero, S. Hoeche, H. Ita, *et al.*, Phys. Rev. D **88**, 014025 (2013), 1304.1253.

[87] M. Rubin, G. P. Salam, and S. Sapeta, JHEP **1009**, 084 (2010), 1006.2144.

[88] D. Matre and S. Sapeta (2013), 1307.2252.

[89] F. Campanario and S. Sapeta, Phys. Lett. B **718**, 100 (2012), 1209.4595.

[90] S. Hoeche, F. Krauss, M. Schonherr, and F. Siegert, JHEP **1304**, 027 (2013), 1207.5030.

[91] S. Hoche, L. Reina, M. Wobisch, C. Bauer, Z. Bern, *et al.* (2013), 1309.3598.

[92] S. Frixione and B. R. Webber, JHEP **0206**, 029 (2002), hep-ph/0204244.

[93] P. Nason, JHEP **0411**, 040 (2004), hep-ph/0409146.

[94] S. Frixione, P. Nason, and C. Oleari, JHEP **0711**, 070 (2007), 0709.2092.

[95] S. Hoeche, F. Krauss, M. Schonherr, and F. Siegert, Phys. Rev. Lett. **110**, 052001 (2013), 1201.5882.

[96] S. Alioli, S. Moch, and P. Uwer, JHEP **1201**, 137 (2012), 1110.5251.

[97] R. Frederix and S. Frixione, JHEP **1212**, 061 (2012), 1209.6215.

[98] S. Catani, F. Krauss, R. Kuhn, and B. Webber, JHEP **0111**, 063 (2001), hep-ph/0109231.

[99] L. Lönnblad, JHEP **0205**, 046 (2002), hep-ph/0112284.

[100] M. L. Mangano, M. Moretti, and R. Pittau, Nucl. Phys. B **632**, 343 (2002), hep-ph/0108069.

[101] N. Lavesson and L. Lönnblad, JHEP **0812**, 070 (2008), 0811.2912.

[102] L. Lönnblad and S. Prestel, JHEP **1303**, 166 (2013), 1211.7278.

[103] S. Hoeche, J. Huang, G. Luisoni, M. Schoenherr, and J. Winter, Phys. Rev. D **88**, 014040 (2013), 1306.2703.

[104] Z. Nagy and D. E. Soper, JHEP **0709**, 114 (2007), 0706.0017.

[105] S. Hoeche, F. Krauss, M. Schonherr, and F. Siegert, JHEP **1209**, 049 (2012), 1111.1220.

[106] S. Platzer and M. Sjodahl, JHEP **1207**, 042 (2012), 1201.0260.

[107] S. Alioli, C. W. Bauer, C. J. Berggren, A. Hornig, F. J. Tackmann, *et al.* (2012), 1211.7049.

[108] S. Alioli, C. W. Bauer, C. Berggren, A. Hornig, F. J. Tackmann, *et al.* (2013), 1305.5246.

[109] J. R. Andersen, L. Lönnblad, and J. M. Smillie, JHEP **1107**, 110 (2011), 1104.1316.

[110] N. Kidonakis and J. F. Owens, Phys. Rev. D **63**, 054019 (2001), hep-ph/0007268.

[111] R. D. Ball, M. Bonvini, S. Forte, S. Marzani, and G. Ridolfi, Nucl. Phys. B **874**, 746 (2013), 1303.3590.

[112] M. Bonvini, S. Forte, and G. Ridolfi, Phys. Rev. Lett. **109**, 102002 (2012), 1204.5473.

[113] D. de Florian and M. Grazzini, Phys. Lett. B **718**, 117 (2012), 1206.4133.

[114] S. Catani, D. de Florian, M. Grazzini, and P. Nason, JHEP **0307**, 028 (2003), hep-ph/0306211.

[115] S. Buehler and A. Lazopoulos (2013), 1306.2223.

[116] S. Forte, private communication.

[117] R. Boughezal, F. Caola, K. Melnikov, F. Petriello, and M. Schulze, JHEP **1306**, 072 (2013), 1302.6216.

[118] C. Anastasiou, R. Boughezal, and F. Petriello, JHEP **0904**, 003 (2009), 0811.3458.

[119] S. Dittmaier, A. Huss, C. Schwinn, in preparation.

[120] K. Mishra, T. Becher, L. Barze, M. Chiesa, S. Dittmaier, *et al.* (2013), 1308.1430.

[121] CMS Collaboration, CMS-PAS-SMP-12-012 (2013), `https://cds.cern.ch/record/1547589`.

[122] S. Dittmaier, A. Huss, and C. Speckner, JHEP **1211**, 095 (2012), 1210.0438.

[123] ATLAS Collaboration, ATLAS-CONF-2013-017 (2013), `http://cds.cern.ch/record/1525524`.

[124] CMS Collaboration, CMS-PAS-EXO-12-060 (2013), `http://cds.cern.ch/record/1522476`.

[125] T. Becher and X. G. i. Tormo, Phys. Rev. D **88**, 013009 (2013), 1305.4202.

[126] G. Aad *et al.* (ATLAS Collaboration), Phys. Rev. D **85**, 092002 (2012), 1201.1276.

[127] G. Aad *et al.* (ATLAS Collaboration), Phys. Rev. D **85**, 032009 (2012), 1111.2690.

[128] ATLAS Collaboration, ATLAS-CONF-2013-056 (2013), `http://cds.cern.ch/record/1557773`.

[129] S. Chatrchyan *et al.* (CMS Collaboration), JHEP **1201**, 010 (2012), 1110.3226.

[130] S. Chatrchyan *et al.* (CMS Collaboration), JHEP **1206**, 126 (2012), 1204.1643.

[131] CMS Collaboration, CMS-PAS-SMP-12-026 (2013), `https://cdsweb.cern.ch/record/1537320`.

[132] A. Denner, S. Dittmaier, T. Kasprzik, and A. Muck, JHEP **0908**, 075 (2009), 0906.1656.

[133] A. Denner, S. Dittmaier, T. Kasprzik, and A. Muck, JHEP **1106**, 069 (2011), 1103.0914.

[134] A. Denner, S. Dittmaier, T. Kasprzik, and A. Mck, Eur. Phys. J. C **73**, 2297 (2013), 1211.5078.

[135] ATLAS Collaboration, ATLAS-CONF-2013-067 (2013), `http://cds.cern.ch/record/1562879`.

[136] CMS Collaboration, CMS-PAS-HIG-13-008 (2013), `http://cds.cern.ch/record/1546778`.

[137] J. Baglio, L. D. Ninh, and M. M. Weber (2013), 1307.4331.

[138] J. H. Kuhn, A. Kulesza, S. Pozzorini, and M. Schulze, Nucl. Phys. B **727**, 368 (2005), hep-ph/0507178.

[139] J. H. Kuhn, A. Kulesza, S. Pozzorini, and M. Schulze, Nucl. Phys. B **797**, 27 (2008), 0708.0476.

[140] E. Maina, S. Moretti, M. R. Nolten, and D. A. Ross, Phys. Lett. B **570**, 205 (2003), hep-ph/0307021.

[141] E. Maina, S. Moretti, and D. A. Ross, Phys. Lett. B **593**, 143 (2004), hep-ph/0403050.

[142] S. Moretti, M. R. Nolten, and D. A. Ross, Nucl. Phys. B **759**, 50 (2006), hep-ph/0606201.

[143] S. Actis, A. Denner, L. Hofer, A. Scharf, and S. Uccirati, JHEP **1304**, 037 (2013), 1211.6316.

[144] P. Ciafaloni and D. Comelli, Phys. Lett. B **446**, 278 (1999), hep-ph/9809321.

[145] M. Beccaria, P. Ciafaloni, D. Comelli, F. Renard, and C. Verzegnassi, Phys. Rev. D **61**, 073005 (2000), hep-ph/9906319.

[146] M. Ciafaloni, P. Ciafaloni, and D. Comelli, Phys. Rev. Lett. **84**, 4810 (2000), hep-ph/0001142.

[147] M. Ciafaloni, P. Ciafaloni, and D. Comelli, Nucl. Phys. B **589**, 359 (2000), hep-ph/0004071.

[148] M. Ciafaloni, P. Ciafaloni, and D. Comelli, Phys. Rev. Lett. **87**, 211802 (2001), hep-ph/0103315.

[149] A. Denner and S. Pozzorini, Eur. Phys. J. C **18**, 461 (2001), hep-ph/0010201.

[150] A. Denner and S. Pozzorini, Eur. Phys. J. C **21**, 63 (2001), hep-ph/0104127.

[151] J. H. Kuhn, A. Kulesza, S. Pozzorini, and M. Schulze, Phys. Lett. B **609**, 277 (2005), hep-ph/0408308.

[152] J. H. Kuhn, A. Kulesza, S. Pozzorini, and M. Schulze, JHEP **0603**, 059 (2006), hep-ph/0508253.

[153] J. H. Kuhn, A. Kulesza, S. Pozzorini, and M. Schulze, Phys. Lett. B **651**, 160 (2007), hep-ph/0703283.

[154] E. Accomando, A. Denner, and S. Pozzorini, JHEP **0703**, 078 (2007), hep-ph/0611289.

[155] M. Chiesa, G. Montagna, L. Barze', M. Moretti, O. Nicrosini, *et al.* (2013), 1305.6837.

[156] M. L. Mangano, M. Moretti, F. Piccinini, R. Pittau, and A. D. Polosa, JHEP **0307**, 001 (2003), hep-ph/0206293.

[157] G. Aad *et al.* (ATLAS Collaboration), Phys. Lett. B **710**, 67 (2012), 1109.6572.

[158] S. Chatrchyan *et al.* (CMS Collaboration), JHEP **1108**, 155 (2011), 1106.4503.

[159] S. Chatrchyan *et al.* (CMS Collaboration), Phys. Rev. Lett. **109**, 171803 (2012), 1207.1898.

[160] G. Aad *et al.* (ATLAS Collaboration), Phys. Lett. B **716**, 62 (2012), 1206.0756.

[161] S. Chatrchyan *et al.* (CMS Collaboration), Phys. Lett. B **710**, 91 (2012), 1202.1489.

[162] A. Banfi, G. P. Salam, and G. Zanderighi, JHEP **1206**, 159 (2012), 1203.5773.

[163] T. Becher and M. Neubert, JHEP **1207**, 108 (2012), 1205.3806.

[164] F. J. Tackmann, J. R. Walsh, and S. Zuberi, Phys. Rev. D **86**, 053011 (2012), 1206.4312.

[165] A. Banfi, P. F. Monni, G. P. Salam, and G. Zanderighi, Phys. Rev. Lett. **109**, 202001 (2012), 1206.4998.

[166] T. Becher, M. Neubert, and L. Rothen (2013), 1307.0025.

[167] I. W. Stewart, F. J. Tackmann, J. R. Walsh, and S. Zuberi (2013), 1307.1808.

[168] X. Liu and F. Petriello, Phys. Rev. D **87**, 014018 (2013), 1210.1906.

[169] X. Liu and F. Petriello, Phys. Rev. D **87**, 094027 (2013), 1303.4405.

[170] C. F. Berger, C. Marcantonini, I. W. Stewart, F. J. Tackmann, and W. J. Waalewijn, JHEP **1104**, 092 (2011), 1012.4480.

[171] G. Ferrera, M. Grazzini, and F. Tramontano, Phys.Rev.Lett. **107**, 152003 (2011), 1107.1164.

[172] G. T. Bodwin, E. Braaten, E. Eichten, S. L. Olsen, T. K. Pedlar, *et al.* (2013), 1307.7425.

[173] G. Aad *et al.* (ATLAS Collaboration), JINST **3**, S08003 (2008).

[174] C. Cojocaru *et al.* (ATLAS Liquid Argon EMEC/HEC Collaboration), Nucl. Instrum. Meth. A **531**, 481 (2004), physics/0407009.

[175] M. Cacciari and G. P. Salam, Phys. Lett. B **659**, 119 (2008), 0707.1378.

[176] CMS Collaboration, CMS-PAS-PFT-09-001 (2009), `http://cdsweb.cern.ch/record/1194487`.

[177] CMS Collaboration, CMS-PAS-FTR-13-014 (2013), `http://cds.cern.ch/record/1607141`.

[178] G. Antchev *et al.* (TOTEM Collaboration), Phys. Rev. Lett. **111**(1), 012001 (2013).